AN IMPLEMENTATION OF THE BOUNDARY-INTEGRAL TECHNIQUE FOR PLANAR PROBLEMS IN ELASTICITY AND ELASTO-PLASTICITY

Peter C. Riccardella

Report SM-73-10 April 1973

Submitted in partial fulfillment of the
requirements for the degree of
Doctor of Philosophy at Carnegie-Mellon University

Department of Mechanical Engineering
Carnegie Institute of Technology
Carnegie-Mellon University
Pittsburgh, Pennsylvania

Carnegie-Mellon University

CARNEGIE INSTITUTE OF TECHNOLOGY

AND

MELLON INSTITUTE OF SCIENCE

THESIS

SUBMITTED IN PARTIAL FULFILLMENT OF THE REQUIREMENTS

FOR THE DEGREE OF Doctor of Philosophy

TITLE An Implementation of the Boundary-Integral Technique for Planar Problems of Elasticity and Elasto-Plasticity

PRESENTED BY Peter C. Riccardella

ACCEPTED BY THE DEPARTMENT OF Mechanical Engineering

Thomas Kline Jr. — MAJOR PROFESSOR — 27 April 1973 — DATE

Milton C. Shaw — DEPARTMENT HEAD — April 30, 1973. — DATE

APPROVED BY THE COLLEGE COUNCIL

C. Warren — DEAN — 5/1/73 — DATE

ACKNOWLEDGEMENTS

The author wishes to express his sincere gratitude to his co-advisors, Drs. J. L. Swedlow and T. A. Cruse, the former for his instruction and assistance in the plasticity aspects of this research, and the latter for his patient tutorship on the boundary-integral technique. Thanks are also due to the other members of the thesis committee, Drs. W. W. Feng and W. VanBuren. The author acknowledges the financial support provided by the U.S. Army Research Office (Durham) under Research Grant DA-ARO-D-31-124-72-G3. Finally, the author is grateful to his wife, Susan, for her patience and understanding during the course of the research, and for her meticulous stenographic assistance in the preparation of this document.

ABSTRACT

The subject of this dissertation is the extension of the boundary-integral technique to problems exhibiting non-linear material behavior (elasto-plasticity). As the first step in implementing the elasto-plastic procedure, an advanced elastic implementation is developed. This advanced implementation is shown to offer substantial improvement in numerical accuracy over previous elastic implementations. A method for incorporating the effects of material non-linearity into the boundary-integral technique is then developed and implemented, and several sample problems are presented which illustrate both the applicability of the implementation and some of its limitations.

Both implementations are evaluated with regard to their degree of realization of the potential advantages of the boundary-integral technique through application to real engineering problems. The elastic implementation represents a second generation implementation of an approach which has been available in the literature for several years. Therefore, as should be expected, this implementation is highly efficient and possesses to a large extent all of the potential advantages of the boundary-integral technique. On the other hand, the elasto-plastic boundary-integral solution technique represents the very first attempt at implementation of this approach for elasto-plastic problems. While the results are not as convincing as those for the second generation elastic implementation, they are encouraging.

An Implementation of the Boundary-Integral Technique
for Planar Problems of Elasticity and Elasto-Plasticity by
Peter C. Riccardella - Dept. of Mechanical Engineering
Carnegie-Mellon University

The boundary-integral technique offers the potential to be a very powerful, general purpose tool for the solution of linear and non-linear problems in the area of solid mechanics. As greater computational capability becomes available, the advantages of the boundary-integral technique should become even more consequential since the technique inherently tends to increase the portion of problem solving effort performed by the computer and to decrease the effort required of the analyst.

TABLE OF CONTENTS

CHAPTER I - INTRODUCTION

With the advent of the large scale digital computer for scientific analysis, a great amount of emphasis in engineering has been placed upon the development of efficient numerical solution techniques to take maximum advantage of this increased computing capability. A great many problems of real engineering interest were virtually unsolvable prior to the age of the computer, and could only be formulated in the most general of terms. Many of the "classic" problem solutions, which represent major efforts of the great mathematicians of the past, have been reduced to trivial exercises through expeditious use of the computer. In the field of solid mechanics, the solution method which has received the most attention, and thus is the most highly developed, is the finite element technique.

The groundwork for the finite element technique was laid almost twenty years ago by several investigators [1,2].* Basically, the method consists of subdividing the body to be analyzed into a number of discrete elements, and then characterizing the behavior of the body by a large stiffness matrix which is constructed through summation of the behavior of the individual elements. Advanced developments of this basic method have been achieved in recent years which include non-linear capability, both in material behavior [3,4,5,6] and in geometric behavior (finite deformation) [7,8,9,10]; and large scale general purpose

*Numbers in brackets refer to references listed in the bibliography.

capability (static and dynamic) [11,12,13,14]. The finite element technique possesses some inherent advantages, not the least of which are simplicity of formulation and relatively general applicability. However, the method also has its disadvantages. Anyone who has performed the tedious job of setting up a finite element mesh for a large scale problem is well aware of one of the major disadvantages of the method: difficulty in modelling. Another, although related, disadvantage of the finite element technique is that it is characteristically inefficient for problems involving large stress or strain gradients.

While advancements in the field of finite elements have been progressing rapidly, another numerical solution method for solid mechanics problems which is potentially more powerful than the finite element technique has received comparatively little attention. This method is a surface integral equation approach which has come to be known as the boundary-integral technique. The method derives its foundations from the vast backlog of experience in scalar potential theory [15]. The initial applications of boundary-integral equations to solid mechanics problems have taken place within the past ten years [16,17,18,19,20]. Basically, the method combines a reciprocal theorem and a suitable singular solution to the governing differential equations to construct a relationship between relevant boundary values in a well-posed problem. Several advantages of the

method are obvious. Since the method involves discretization of the boundary of the body only, the dimensionality of the problem is reduced by one in comparison to the finite element technique. Thus, the method is characteristically more efficient than finite elements from a modelling standpoint. Furthermore, the method has been shown to exhibit a high degree of resolution in problems with large stress and strain gradients [21]. However, the boundary-integral technique is also not without disadvantages. The formulation of the method, and thus the necessary computer coding, are relatively complex. Secondly, the method does not appear to offer as much generality as the finite element approach. For instance, finite element simulations of large, non-linear structures containing multiple element types, and under complex dynamic loading conditions have appeared recently [22]; and at this time, extension of the boundary-integral technique to problems of this type is not foreseen.

The subject of this dissertation is the extension of the boundary-integral technique to problems exhibiting non-linear material behavior (elasto-plasticity). As the first step in implementing the boundary-integral technique for two dimensional elasto-plastic problems, an advanced elastic implementation was developed. This advanced implementation offers a substantial improvement in numerical accuracy over previous elastic implementations. The development, formulation, and demonstration of this implementation

constitute the subject matter of Chapter II of this dissertation. The two dimensional elasto-plastic implementation is discussed in Chapter III. A method for incorporating the effects of material non-linearity into the boundary-integral technique is developed and implemented, and several example problems are presented which illustrate both the applicability of the implementation, and some of its limitations.

CHAPTER II - IMPROVED ELASTIC IMPLEMENTATION

A. *INTRODUCTORY REMARKS*

The boundary-integral technique has been demonstrated to be a powerful numerical tool for use in solving problems of two and three dimensional elasticity. Numerical boundary-integral solutions to several problems of engineering importance have been presented in the literature [16,21,23,24]. One advantage of the method is that numerical discretization occurs only on the boundary of the body being analyzed, thus reducing by one the dimension of the numerical equations which must be solved. Many problems which are extremely expensive or even prohibitive in terms of computer time and storage using conventional numerical techniques can be solved relatively inexpensively using the boundary-integral technique. Other advantages of the method include relative ease of modelling to the analyst, and high resolution of field quantities in regions of high gradients.

In checking out the boundary-integral technique by solving problems with known solutions [25], it has been discovered that the implementations of the technique developed to date, while demonstrating an ability to predict overall trends in a problem, are not as accurate as would be desired with regard to details of the stress and deformation fields. These implementations approximate the

boundary of the body to be analyzed by a series of discrete elements over which the displacements and tractions are assumed to be constant. The constant boundary value assumption limits the accuracy with which non-uniform boundary conditions can be modelled. A new implementation of the boundary-integral technique for problems of two dimensional elasticity is presented in this chapter. Linearly varying (rather than constant value) displacements and tractions are assumed over the discretized elements of the boundary. This linear boundary value approach is shown to yield a substantial improvement in numerical accuracy over the constant boundary value approach, while requiring little or no increase in computer running times and storage requirements. Thus the engineering usefulness of the boundary-integral technique for elastic problems is enhanced significantly.

The general development of the boundary-integral technique is reviewed in Section B of this Chapter, and the linear boundary value implementation is developed in Section C. The numerical accuracy of the linear boundary value implementation is evaluated by comparison with exact solutions for a broad range of problems in Section D of this Chapter. Comparisons with results from the constant boundary value approach are included where such results are available. Appendices A and B give detailed mathematical derivations which are required for the development of the linear boundary value approach, and Appendix C gives a detailed description (including input in-

structions) of the computer program BITE which was used in developing the numerical results.

B. DEVELOPMENT OF BOUNDARY-INTEGRAL EQUATIONS FOR ELASTICITY

The development of the boundary-integral technique for two and three dimensional elasticity is well documented in the literature [16, 23]. A summary of this development is included here for completeness.

The surface tractions and displacements associated with any two solutions to the governing equations of elasticity in a region R can be related through Betti's theorem of elastic reciprocity [26]. In the absence of body forces, Betti's theorem is stated as follows

$$\int_S t_j^* u_j \, dS = \int_S u_j^* t_j \, dS, \tag{2-1}$$

where S represents the surface of the region R. The development of the boundary integral approach proceeds by setting the starred quantities in equation (2-1) equal to the displacements and tractions associated with the well-known solution to Kelvin's problem of a concentrated unit load in an infinite body

$$\begin{aligned} u_j^*(x) &= U_{ij}(x,\xi)e_i \\ t_j^*(x) &= T_{ij}(x,\xi)e_i, \end{aligned} \tag{2-2a}$$

where for two dimensions (plane strain)

$$\begin{aligned} U_{ij} &= -\frac{1}{8\pi\mu(1-\nu)}\left[\delta_{ij}(3-4\nu)\ln r - r_{,i}r_{,j}\right] \\ T_{ij} &= -\frac{1}{4\pi(1-\nu)}\left(\frac{1}{r}\right)\left(\frac{\partial r}{\partial n}\right)\Big\{\left[\delta_{ij}(1-2\nu) + 2r_{,i}r_{,j}\right] \\ &\qquad - (1-2\nu)(r_{,i}n_j - r_{,j}n_i)\Big\}, \end{aligned} \tag{2-2b}$$

and where μ is the elastic shear modulus, ν is Poisson's ratio, δ_{ij} is the Kronecker delta, r is the distance between the field point x and the load point ξ as shown in Figure 2-1, and the commas denote differentiation with respect to x_i. The case of plane stress can be handled through the use of an effective Poisson's ratio given by $[\nu/(1+\nu)]$.

Substituting equations (2-2) into (2-1) leads to the Somigliana identity [26]

$$u_i(\xi) + \int_S u_j(x)T_{ij}(x,\xi)dS(x) = \int_S t_j(x)U_{ij}(x,\xi)dS(x), \qquad (2\text{-}3)$$

where $u_i(\xi)$ is the displacement vector at an arbitrary internal point ξ (defined by the vector ξ_i), and the vectors $u_j(x)$ and $t_j(x)$ are the displacement and traction vectors at a surface point x (defined by the vector x_i). A small circular region of radius ε surrounding the point ξ has been eliminated from the region R due to the singular nature of the Kelvin problem at that point. The $u_i(\xi)$ term in equation (2-3) results from taking the limit of the surface integrals as ε approaches zero.

The essence of the boundary-integral technique is to allow the internal point ξ to pass to an arbitrary surface point z, yielding a set of integral equations which can be solved for the unknown boundary tractions and displacements in a well-posed boundary value problem. It should be noted that the kernels of the integrals in equation (2-3) exhibit singularities as ξ approaches S, so that the resulting set of

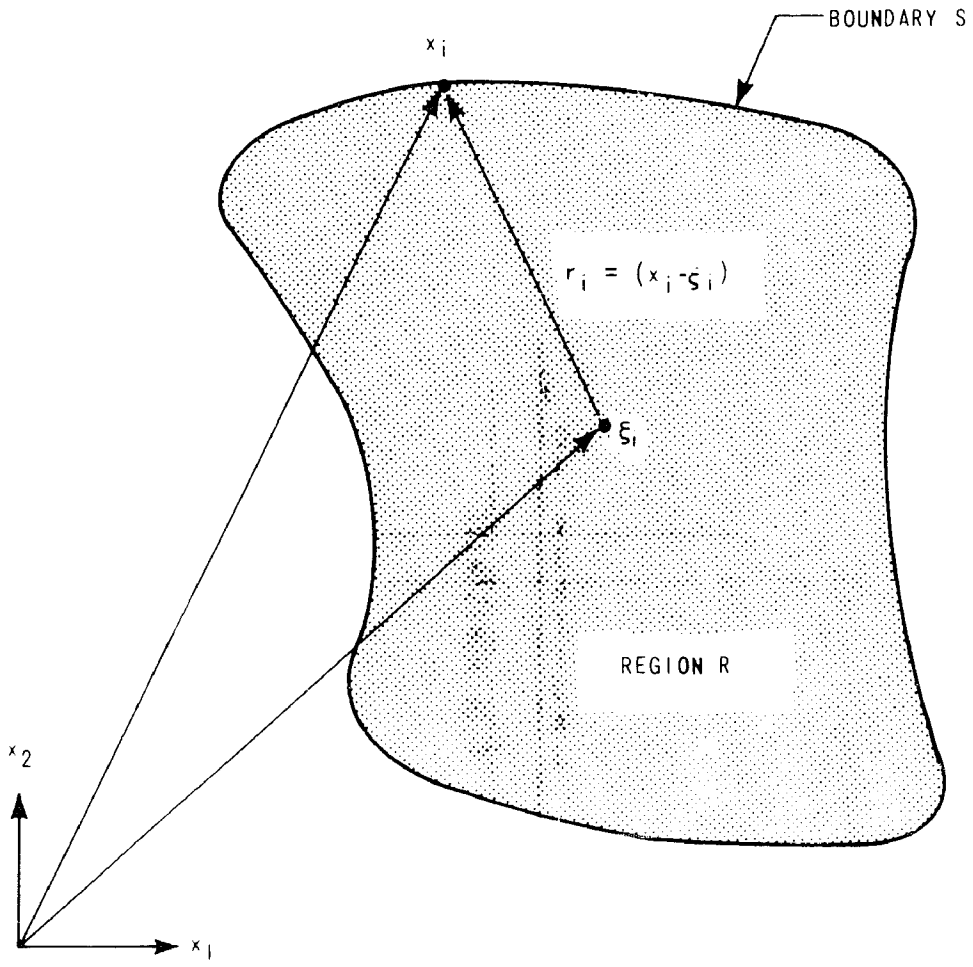

Figure 2-1. Geometric Definitions

integral equations will be singular. Further, the value of the first integral in equation (2-3) is discontinuous as ξ passes through the surface, so that a jump term arises in the limiting procedure.

In the solution methods presented to date [21,23] the boundary is approximated by a number of straight (or flat) segments over which the tractions and displacements are assumed to be constant. The nodal points to which the constant values of traction and displacement refer are located at the center of each segment. Thus the boundary points can be assumed to lie on flat portions of the boundary rather than at corners. The limiting procedure for ξ approaching a flat portion of the boundary is illustrated schematically in Figure 2-2(a). The results of this limit for the individual terms of equation (2-3) are as follows

$$\begin{aligned}
&\lim_{\xi \to z} u_i(\xi) = u_i(z) \\
&\lim_{\xi \to z} \int_S u_j(x) T_{ij}(x,\xi) dS(x) = -\frac{1}{2} u_i(z) + \int_{(S-S^*)} u_j(x) T_{ij}(x,z) dS(x) \qquad (2\text{-}4) \\
&\lim_{\xi \to z} \int_S t_j(x) U_{ij}(x,\xi) dS(x) = \int_{(S-S^*)} t_j(x) U_{ij}(x,z) dS(x).
\end{aligned}$$

The integrals over (S-S*) are to be evaluated as Cauchy principal values, letting the surface S* shrink to zero, and hereafter will be denoted only as integrals on S for brevity. Note that the jump term for this case is $-\frac{1}{2} u_i(z)$.

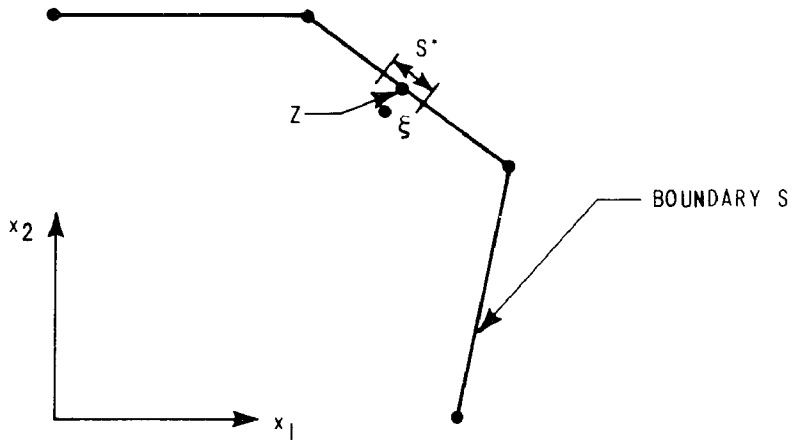

a) LIMITING PROCEDURE FOR ξ APPROACHING FLAT BOUNDARY

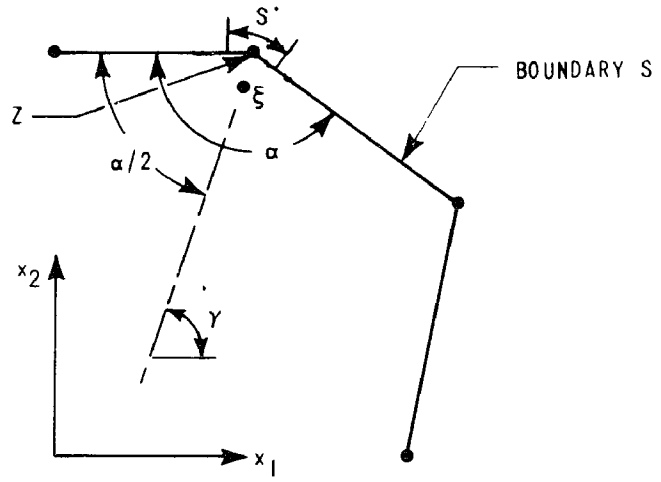

b) LIMITING PROCEDURE FOR ξ APPROACHING BOUNDARY CORNER OF INCLUDED ANGLE α

Figure 2-2. Limiting Procedures for Passing Internal Point ξ to a Surface Node Z

Substituting these limits into equation (2-3) yields the boundary constraint equation for two dimensions

$$\frac{1}{2}\, u_i(z) + \int_S u_j(x) T_{ij}(x,z)\, dS(x) = \int_S t_j(x) U_{ij}(x,z)\, dS(x). \tag{2-5}$$

Since the boundary has been assumed to be broken down into a number (NSEG) of straight segments, the base point z can be allowed to lie at the center of a particular segment (N), yielding an equation for the displacements of segment N in terms of the surface integrals of the tractions and displacements over the whole boundary

$$\frac{1}{2}\, u_i(z_N) + \int_S u_j(x) T_{ij}(x,z_N)\, dS(x) = \int_S t_j(x) U_{ij}(x,z_N)\, dS(x). \tag{2-6}$$
$$(N = 1, \ldots, NSEG)$$

The integrals in equation (2-6) can be broken down into sums of the integrals over each segment since the tractions and displacements have been assumed to be constant on the boundary segments

$$\frac{1}{2}\, u_i(z_N) + \sum_{M=1}^{NSEG} u_j(x_M) \int_{\Delta S_M} T_{ij}(x_M, z_N)\, dS(x_M) = \sum_{M=1}^{NSEG} t_j(x_M) \int_{\Delta S_M} U_{ij}(x_M, z_N)\, dS(x_M), \tag{2-7}$$

where

$x_M = x_1, x_2, \ldots x_{NSEG}$

ΔS_M = length of segment M.

The integrals in equation (2-7) are evaluated in closed form as a function of the coordinates of x_M and z_M. Introducing the short notation

$$\begin{aligned}
\Delta T_{ij}(M,N) &= \int_{\Delta S_M} T_{ij}(x_M, z_N)\, dS(x_M) \\
\Delta U_{ij}(M,N) &= \int_{\Delta S_M} U_{ij}(x_M, z_N) dS(x_M) \\
u_i(N) &= u_i(z_N) \\
u_j(M) &= u_j(x_M) \\
t_j(M) &= t_j(x_M),
\end{aligned} \tag{2-8}$$

equations (2-7) can be cast in the following matrix form

$$\left[A_{ij}(M,N) \right] \left\{ u_j(M) \right\} = \left[B_{ij}(M,N) \right] \left\{ t_j(M) \right\}, \tag{2-9}$$

where the matrices A and B are given by

$$\begin{aligned}
A_{ij}(M,N) &= \Delta T_{ij}(M,N) - I(M,N)/2 \\
B_{ij}(M,N) &= \Delta U_{ij}(M,N).
\end{aligned} \tag{2-10}$$

I(M,N) in equation(2-10)is the identity matrix. For a well posed boundary value problem, half of the total number of components of tractions and displacements at a point are specified and the other half are unknown. Thus equations (2-9) represent a set of (2x NSEG) linear simultaneous equations in (2x NSEG) unknowns which can be solved to yield the unknown boundary values.

Once the boundary solution has been obtained, the Somigliana identity (2-1) can be used to evaluate displacements at any point in the body by simple quadrature. The Somigliana identity can also be differentiated with respect to ξ_k to yield an expression for displacement gradients as follows

$$u_{i,k}(\xi) + \int_S u_j(x) T_{ij,k}(x,\xi) dS(x) = \int_S t_j(x) U_{ij,k}(x,\xi) dS(x), \qquad (2\text{-}11)$$

where for two dimensions (plane strain)

$$U_{ij,k} = \frac{-1}{8\pi\mu(1-\nu)} \left(\frac{1}{r}\right) \left[\delta_{ij}(3-4\nu) r_{,k} - \delta_{jk} r_{,i} + 2r_{,i} r_{,j} r_{,k}\right]$$

$$T_{ij,k} = \frac{-1}{4\pi(1-\nu)} \left(\frac{1}{r}\right)^2 \Big\{ \left[-2(1-2\nu)\delta_{ij} r_{,k} + 2\delta_{jk} r_{,i} - 8r_{,i} r_{,j} r_{,k}\right] \left(\frac{\partial r}{\partial n}\right) \qquad (2\text{-}12)$$

$$+ (1-2\nu)\left[n_k \delta_{ij} + n_i \delta_{jk} - n_j \delta_{ik} - 2n_i r_{,j} r_{,k} + 2n_j r_{,i} r_{,k}\right]$$

$$+ 2n_k r_{,i} r_{,j} \Big\} .$$

The case of plane stress is again handled through the use of an effective Poisson's ratio. This expression can be used in conjunction with Hooke's law to calculate stresses at any desired point within the body. Thus the complete internal stress and deformation field can be obtained by simple quadrature at as many internal points as is desired from the boundary solution of equation (2-9).

The procedure for three dimensional problems is similar [23], except the number of equations and unknowns becomes (3x NSEG), and evaluation of the coefficients involves surface integrals over flat surface elements

rather than line integrals over straight line segments. It has been demonstrated [16,21,23,24] that the above procedure, when automated, can be used to generate useful solutions to problems of engineering importance. However, this constant boundary value approach requires a relatively large number of boundary segments to yield accurate solutions to problems with high stress and strain gradients. In order to improve the relative accuracy of the technique, a linear boundary value approach is developed and demonstrated in the remaining sections of this chapter.

C. *FORMULATION OF IMPROVED NUMERICAL SOLUTION TECHNIQUE*

It has been posited that a more accurate solution would result if linearly varying (rather than constant value) displacements and tractions were assumed on the boundary segments. The advantage of this approach is the ability to model non-uniform boundary conditions more accurately.

In the model now being reported, values of tractions and displacements are assigned to nodes located at the intersections of the boundary segments rather than at their centerpoints. Continuity of displacements is assured since two adjacent segments share one common node. Two difficulties become immediately apparent:

(1) Since the nodes now lie at intersections between segments, the possibility exists for nodes to occur at corners rather than on flat portions of the boundary, and the limiting procedure which led to equations (2-4) must be revised to accommodate this.

(2) While the theory of elasticity requires continuity of displacements, it admits step changes in boundary tractions. Step changes in traction occurred as a matter of course when the boundary equations were formulated in terms of segment centerpoints; however,

they require special consideration when the equations are formulated in terms of nodes between segments.

The limiting procedure for ξ approaching a corner point of included angle α is illustrated schematically in Figure 2-2(b). The results of this limit for the individual terms of equation (2-3) are as follows

$$\begin{aligned}
&\lim_{\xi \to z} u_i(\xi) = u_i(z) \\
&\lim_{\xi \to z} \int_S u_j(x) T_{ij}(x,\xi) dS(x) = -C_{ij} u_j(z) + \int_{(S-S^*)} u_j(x) T_{ij}(x,z) dS(x) \qquad (2\text{-}13) \\
&\lim_{\xi \to z} \int_S t_j(x) U_{ij}(x,\xi) dS(x) = \int_{(S-S^*)} t_j(x) U_{ij}(x,z) dS(x).
\end{aligned}$$

Again the integrals on (S-S*) are to be evaluated as Cauchy principal values and will be denoted as integrals on S hereafter. The jump term is given in terms of the tensor C_{ij} which can be expressed as follows

$$\begin{aligned}
C_{11} &= \left[1 - \frac{\alpha}{2\pi} - \frac{\cos(2\gamma)\,\sin(\alpha)}{4\pi\,(1-\nu)} \right] \\
C_{12} &= C_{21} = \left[\frac{\sin(2\gamma)\,\sin(\alpha)}{4\pi\,(1-\nu)} \right] \qquad (2\text{-}14) \\
C_{22} &= \left[1 - \frac{\alpha}{2\pi} + \frac{\cos(2\gamma)\,\sin(\alpha)}{4\pi\,(1-\nu)} \right],
\end{aligned}$$

where α is the included angle of the corner and γ is the angle between the bisector of α and the x_1 coordinate axis as shown in Figure 2-2(b). Note that for the degenerate case of $\alpha = \pi$, C_{ij} reduces to a diagonal tensor with values of 1/2 as would be expected from equation (2-4).

Substituting these limits into the Somigliana identity (2-3) yields the boundary constraint equation for linear boundary value segments in two dimensions

$$(\delta_{ij}-C_{ij})u_j(z) + \int_S u_j(x)T_{ij}(x,z)dS(x) = \int_S t_j(x)U_{ij}(x,z)dS(x). \tag{2-15}$$

Considering z to lie at a particular boundary node (N), and considering the integrals to be sums of the integrals over each segment (P) as before yields

$$(\delta_{ij}-C_{ij})u_j(z_N) + \sum_{P=1}^{NSEG} \int_{\Delta S_P} u_j(x_P)T_{ij}(x_P,z_N)dS(x_P) = \sum_{P=1}^{NSEG} \int_{\Delta S_P} t_j(x_P)U_{ij}(x_P,z_N)dS(x_P), \tag{2-16}$$

where ΔS_P refers to the length of segment P. Note that the $u_j(x_P)$ and $t_j(x_P)$ terms have not been factored out of the integrals as they were in the constant boundary value case given by equation (2-7). Using the linear representation of boundary displacements and tractions given in Figure 2-3, and utilizing the short notation introduced by equations (2-8), equation (2-16) can be rewritten in the following form

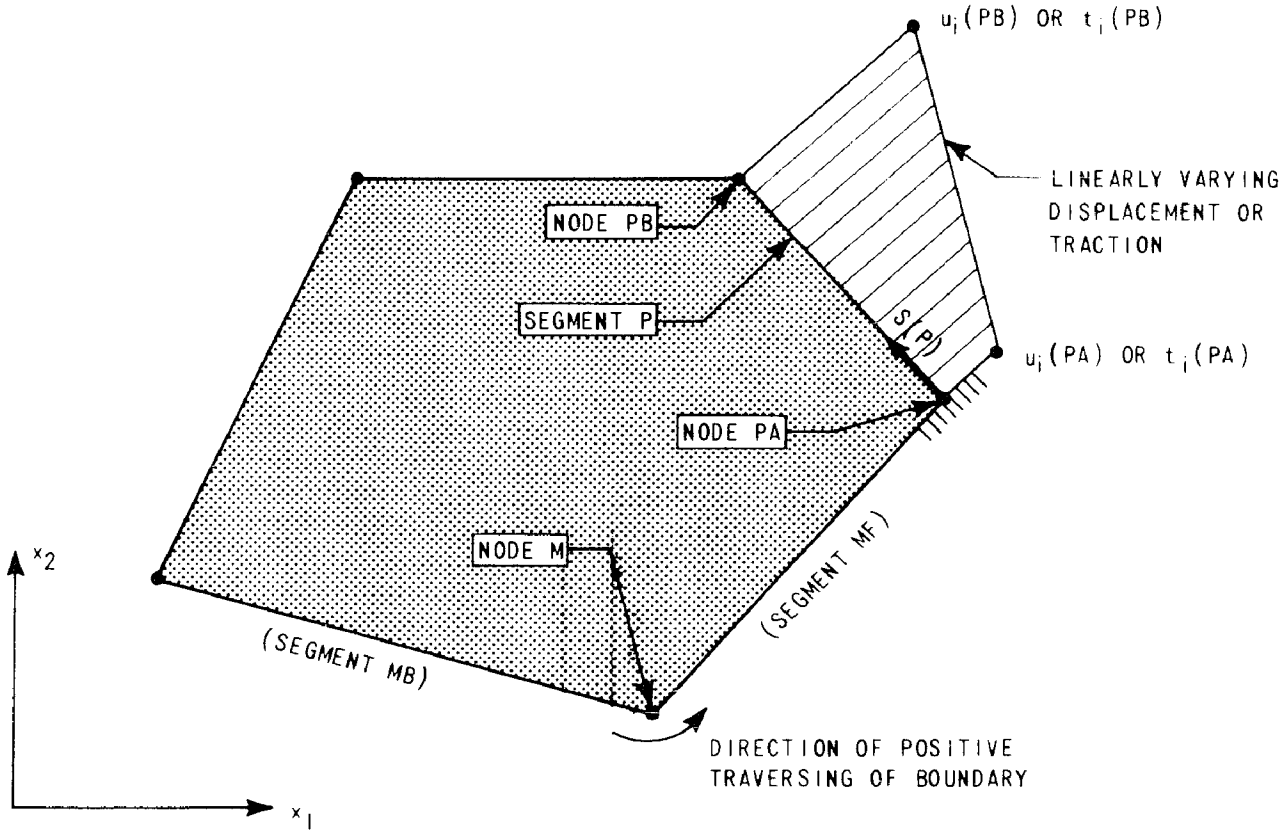

ASSUMED DISPLACEMENTS AND TRACTIONS ON SEGMENT P:

$$u_i = \frac{u_i(PB) - u_i(PA)}{\Delta S(P)} S(P) + u_i(PA)$$

$$t_i = \frac{t_i(PB) - t_i(PA)}{\Delta S(P)} S(P) + t_i(PA)$$

WHERE $\Delta S(P)$ = LENGTH OF SEGMENT P
$S(P)$ = TANGENTIAL LENGTH PARAMETER FOR SEGMENT P

Figure 2-3. Linear Representation of Displacements and Tractions on a Boundary Segment

$$(\delta_{ij}-C_{ij})u_j(N) + \sum_{P=1}^{NSEG}\left\{\left[\frac{u_j(PB)-u_j(PA)}{\Delta S_P}\right]\int_{\Delta S_P} T_{ij}(N,P)S(P)dS(P)\right.$$

$$\left. + u_j(PA)\int_{\Delta S_P} T_{ij}(P,M)dS(P)\right\} = \sum\left\{\left[\frac{t_j(PB)-t_j(PA)}{\Delta S_P}\right]\right. \qquad (2\text{-}17)$$

$$\left.\int_{\Delta S_P} U_{ij}(N,P)S(P)dS(P) + t_j(PA)\int_{\Delta S_P} U_{ij}(N,P)dS(P)\right\}.$$

PA denotes the node preceding segment P and PB denotes the node following it, where the boundary is considered to be traversed positively in the counterclockwise direction as shown in Figure 2-3. Since the reference values of displacement and traction are at the nodes, it is convenient to eliminate reference to segment P before putting equation (2-17) in matrix form. Letting the segment behind a boundary node M be denoted MB, and the segment in front of node M be denoted MF, as the boundary is traversed in the positive direction, equation (2-17) can be rewritten in terms of summations over the nodes as follows

$$(\delta_{ij}-C_{ij})u_j(N) + \sum_{M=1}^{NNOD} u_j(M)\left[\frac{1}{\Delta S_{MB}}\int_{\Delta S_{MB}} T_{ij}(N,MB)S(MB)dS(MB)\right.$$

$$\left. - \frac{1}{\Delta S_{MF}}\int_{\Delta S_{MF}} T_{ij}(N,MF)S(MF)dS(MF) + \int_{\Delta S_{MF}} T_{ij}(N,MF)dS(MF)\right] \qquad (2\text{-}18)$$

$$= \sum_{M=1}^{NNOD} t_j(M)\left[\frac{1}{\Delta S_{MB}}\int_{\Delta S_{MB}} U_{ij}(N,MB)S(MB)dS(MB)\right.$$

$$\left. - \frac{1}{\Delta S_{MF}}\int_{\Delta S_{MF}} U_{ij}(N,MF)S(MF)dS(MF) + \int_{\Delta S_{MF}} U_{ij}(N,MF)dS(MF)\right],$$

where NNOD is the number of nodes.

The integrals in equation (2-18) have been evaluated in closed form in terms of the coordinates of nodes N and M and segments MB and MF, and the results are tabulated in Appendix A. The following short notation can be introduced

$$
\begin{aligned}
\Delta T^{B}_{ij}(M,N) &= \frac{1}{\Delta S_{MB}} \int_{\Delta S_{MB}} T_{ij}(N,MB)S(MB)dS(MB) \\
\Delta T^{F}_{ij}(M,N) &= \frac{1}{\Delta S_{MF}} \int_{\Delta S_{MF}} T_{ij}(N,MF)S(MF)dS(MF) \\
\Delta T^{F}_{ij}(M,N) &= \int_{\Delta S_{MF}} T_{ij}(N,MF)dS(MF) \\
\Delta U^{B}_{ij}(M,N) &= \frac{1}{\Delta S_{MB}} \int_{\Delta S_{MB}} U_{ij}(N,MB)S(MB)dS(MB) \\
\Delta U^{F}_{ij}(M,N) &= \frac{1}{\Delta S_{MF}} \int_{\Delta S_{MF}} U_{ij}(N,MF)S(MF)dS(MF) \\
\Delta U^{F}_{ij}(M,N) &= \int_{\Delta S_{MF}} U_{ij}(N,MF)dS(MF),
\end{aligned}
\tag{2-19}
$$

where the superscripts F and B refer to the elements in front of or in back of Node M.

Equation (2-18) can be put into the following matrix form

$$
\left[A_{ij}(M,N) \right] \left\{ u_j(M) \right\} = \left[B_{ij}(M,N) \right] \left\{ t_j(M) \right\}, \tag{2-20}
$$

where the terms of the A and B matrices are given by

$$A_{ij}(M,N) = (\delta_{ij}-C_{ij})I(M,N) + \Delta T^{B}_{ij}(M,N) - \Delta T^{F}_{ij}(M,N) + \Delta T^{F}_{ij}(M,N)$$
$$B_{ij}(M,N) = \Delta u^{B}_{ij}(M,N) - \Delta u^{F}_{ij}(M,N) + \Delta U^{F}_{ij}(M,N), \qquad (2\text{-}21)$$

and where I(M,N) is the identity matrix. Equations (2-20) then represent a set of (2x NNOD) linear simultaneous equations in (2x NNOD) unknowns which can be solved to yield the unknown displacements and tractions at the nodes as before.

The difficulty associated with step changes in traction boundary conditions could be handled during modelling by simply placing two nodes very close to each other and assigning different traction values to each. This would effect a very rapid linear change in boundary traction which approaches a step change as the nodes, and thus the node displacements become the same. To avoid the numerical difficulties which may be encountered for very small segments and the modelling inconveniences which would be introduced by the above procedure, the concept of adding very short segments for step type boundary conditions has been formalized and automated in the following manner. The integrals for the linear boundary value segments (equation 2-19 and Appendix A) have been reformulated in terms of segment length ΔS, and the limit of each integral as ΔS approaches zero has been evaluated. This limiting process is outlined in Appendix B, and the results indicate that the net contribution to the set of

simultaneous equations (2-20) due to a zero-length segment is null. Thus zero-length segments can be added at any point where a step change in boundary conditions occurs, and zero values can be assigned to the integrals associated with these zero-length segments.

Another modelling convenience can be introduced into the boundary-integral method for problems which are symmetric with respect to one or both coordinate axes. Figure 2-4(a) shows a problem which exhibits one degree of symmetry. For this problem, the tractions and displacements of nodes in the second and third quadrants are equal in magnitude to those of the corresponding nodes in the first and fourth quadrants. Since the symmetry shown is about the x_1 axis, x_2 components retain the same sign and x_1 components undergo a sign reversal. This correspondence can be used to reduce the number of the simultaneous equations (2-20) by combining terms in the coefficient matrices A and B which operate upon equal valued displacements and tractions, after making the necessary sign changes. Thus only the shaded portion of Figure 2-4(a) need be modelled, and the size of the problem is reduced by a factor of two. Similar arguments apply to problems which exhibit two degrees of symmetry such as that illustrated in Figure 2-4(b). In the doubly-symmetric case, only the first quadrant (shaded region in Figure 2-4(b)) must be modelled, and the size of the problem is reduced by a factor of four.

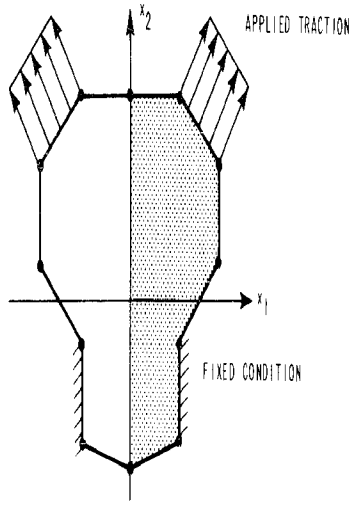

a) SYMMETRY ABOUT ONE COORDINATE AXIS (ONE DEGREE OF SYMMETRY)

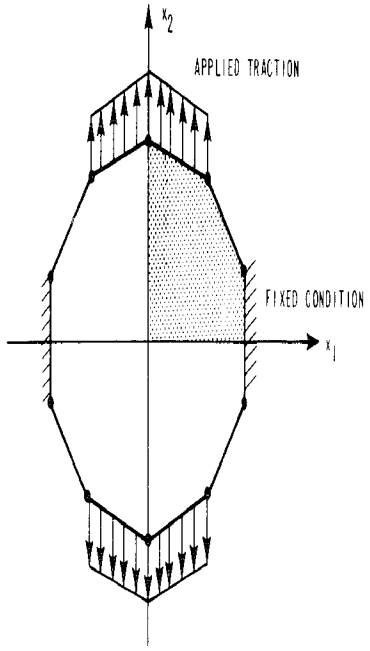

b) SYMMETRY ABOUT TWO COORDINATE AXES (TWO DEGREES OF SYMMETRY)

Figure 2-4. Illustration of Symmetry Conditions

Once the boundary constraint equations (2-20) are solved for the unknown boundary tractions and displacements, the results can be used to evaluate displacements at any internal point I, using the Somigliana identity with the boundary-integrals discretized in the same manner as equation (2-18)

$$
\begin{aligned}
u_i(I) = -\sum_{M=1}^{NNOD} u_j(M) \Bigg[& \frac{1}{\Delta S_{MB}} \int_{\Delta S_{MB}} T_{ij}(I,MB)S(MB)dS(MB) \\
& - \frac{1}{\Delta S_{MF}} \int_{\Delta S_{MF}} T_{ij}(I,MF)S(MF)dS(MF) + \int_{\Delta S_{MF}} T_{ij}(I,MF)dS(MF) \Bigg] \\
& + \sum_{M=1}^{NNOD} t_j(M) \Bigg[\frac{1}{\Delta S_{MB}} \int_{\Delta S_{MB}} U_{ij}(I,MB)S(MB)dS(MB) \\
& - \frac{1}{\Delta S_{MF}} \int_{\Delta S_{MF}} U_{ij}(I,MF)S(MF)dS(MF) + \int_{\Delta S_{MF}} U_{ij}(I,MF)dS(MF) \Bigg],
\end{aligned}
\tag{2-22}
$$

where the kernels T_{ij} and U_{ij} are evaluated with respect to the internal point I. The boundary values $u_j(M)$ and $t_j(M)$ are known, so that the summations can be carried out directly.

Displacement gradients at any internal point (I) can be evaluated by differentiating equation (2-22) as follows

$$
\begin{aligned}
u_{i,k}(I) = -\sum_{M=1}^{NNOD} u_j(M) \Bigg[& \frac{1}{\Delta S_{MB}} \int_{\Delta S_{MB}} T_{ij,k}(I,MB)S(MB)dS(MB) \\
& - \frac{1}{\Delta S_{MF}} \int_{\Delta S_{MF}} T_{ij,k}(I,MF)S(MF)dS(MF) + \int_{\Delta S_{MF}} T_{ij,k}(I,MF)dS(MF) \Bigg] \\
& + \sum_{M=1}^{NNOD} t_j(M) \Bigg[\frac{1}{\Delta S_{MB}} \int_{\Delta S_{MB}} U_{ij,k}(I,MB)S(MB)dS(MB) \\
& - \frac{1}{\Delta S_{MF}} \int_{\Delta S_{MF}} U_{ij,k}(I,MF)S(MF)dS(MF) + \int_{\Delta S_{MF}} U_{ij,k}(I,MF)dS(MF) \Bigg],
\end{aligned}
\tag{2-23}
$$

where the differentiated kernels are given, as before, by equations (2-12).

The integrals in equation (2-23) have been evaluated in closed form in terms of the coordinates of node M and internal point I, and the segments MB and MF. These integrations are also tabulated in Appendix A. Introducing the additional short notation

$$\begin{aligned} \Delta D_{ijk} &= \int_{\Delta S} U_{ij,k} dS \\ \Delta \mathcal{D}_{ijk} &= \frac{1}{\Delta S} \int_{\Delta S} U_{ij,k} S dS \\ \Delta S_{ijk} &= \int_{\Delta S} T_{ij,k} dS \\ \Delta \mathcal{S}_{ijk} &= \frac{1}{\Delta S} \int_{\Delta S} T_{ij,k} S dS , \end{aligned} \tag{2-24}$$

equation (2-23) can be rewritten

$$\begin{aligned} u_{i,k}(I) = &- \sum_{M=1}^{NNOD} u_j(M)[\Delta \mathcal{D}_{ijk}(MB) - \Delta \mathcal{D}_{ijk}(MF) + \Delta D_{ijk}(MF)] \\ &+ \sum_{M=1}^{NNOD} t_j(M)[\Delta \mathcal{S}_{ijk}(MB) - \Delta \mathcal{S}_{ijk}(MF) + \Delta S_{ijk}(MF)]. \end{aligned} \tag{2-25}$$

The summations in equation (2-25) can be carried out directly, and combined with Hooke's law to yield stresses at as many internal points (I) as desired. Thus the complete internal stress and deformation field can be generated from the boundary solution with a high degree of resolution.

Equations (2-20) and (2-25) represent a discrete solution to problems of two dimensional elasticity using the boundary integral technique with linear boundary value segments. As in the constant boundary value case, the solution lends itself quite readily to automation. The present procedure involves two unknowns at each boundary node, while the constant boundary value procedure involves two unknowns at each boundary segment. However, in a connected two dimensional region, the number of boundary nodes will be equal to the number of boundary segments, so that the linear boundary value approach does not require any additional storage or solution time for a given degree of model refinement. The linear boundary value approach does require slightly more setup time than the constant boundary value approach since the individual terms in the matrices are more complex.

A computer program (BITE) has been written to automate the solution procedure described in this Section. A flow chart and a set of input instructions for this program are given in Appendix C. A maximum of eighty boundary segments is allowed, and up to two degrees of symmetry can be considered. The program requires approximately 120,000 octal words of core to execute, and has been used successfully on UNIVAC 1108 and CDC 6600/7600 computers.

D. NUMERICAL RESULTS

In order to demonstrate the range and accuracy of the solution technique developed in Section C, a series of examples is presented in this Section, ranging from simple problems of unit squares to relatively difficult problems which contain large stress and strain gradients. Closed form solutions are available for all of the problems chosen, and in each case the accuracy of the method has been evaluated as a function of number of boundary segments used in modelling. Comparisons to results from the constant boundary value approach (Section B) are given where such results are available.

1. Unit Square Problems - As a basic check of the operation of the computer program, a unit square under uniaxial tension ($\sigma = 10^6$ psi) was analyzed using the model shown in Figure 2-5(a). Since the problem exhibits two degrees of symmetry the model requires only two segments in the first quadrant. A zero-length segment is added between nodes 2 and 3 since the x_2-traction undergoes a step change from zero to σ at that point. The resulting boundary solution is tabulated in Figure 2-6. The boundary displacements are accurate to within the accuracy of the computer. Internal stresses at the six points indicated in Figure 2-5(a) are listed in Figure 2-6, and they are also within machine accuracy.

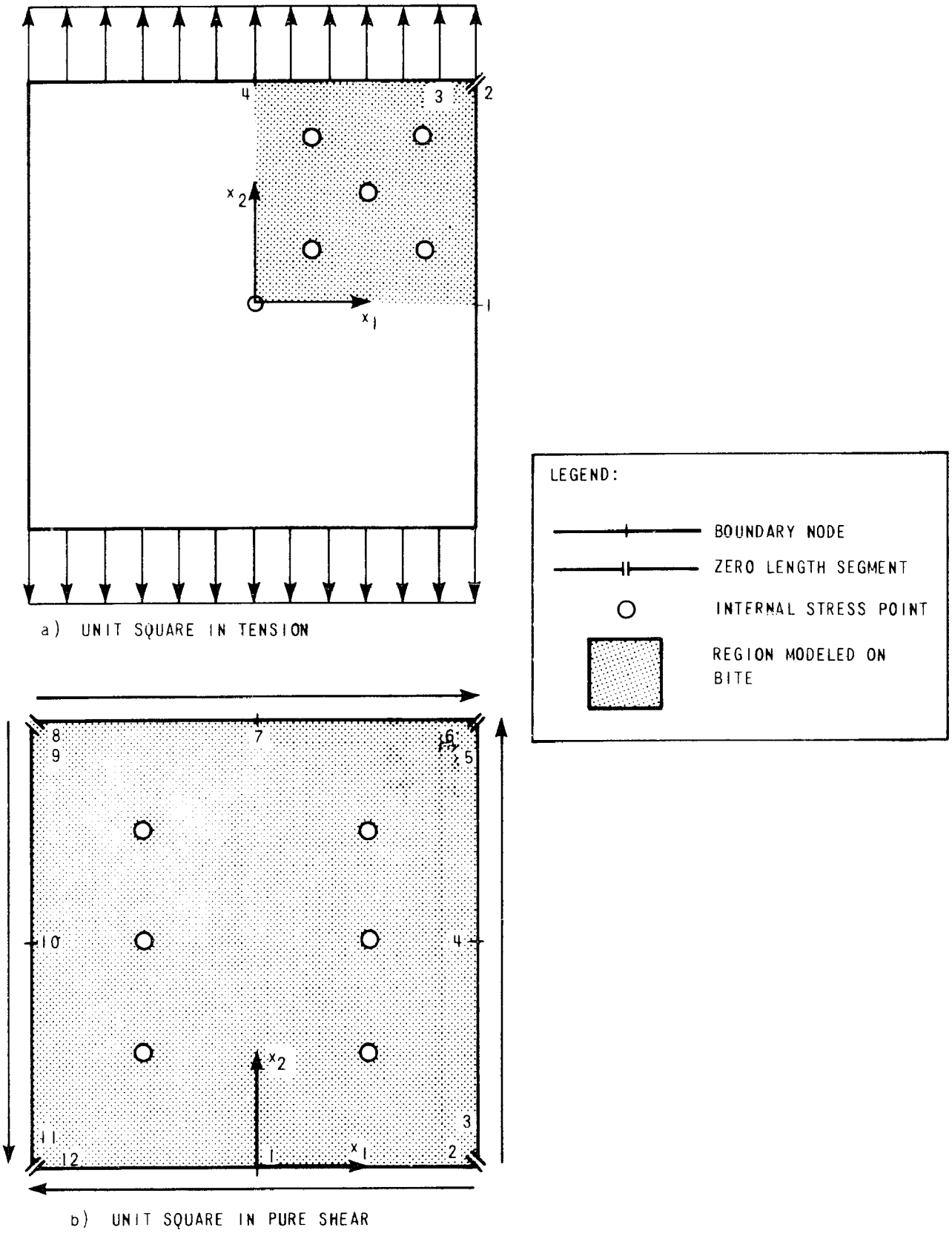

Figure 2-5. Boundary Integral Models for Unit Square Problems

SAMPLE PROBLEM 1 - UNIT SQUARE IN TENSION (NSYM= 2)

BOUNDARY SOLUTION						
	X1 COORDINATE DIRECTION			X2 COORDINATE DIRECTION		
NODE	KNOWN	X1-TRAC	X1-DISP	KNOWN	X2-TRAC	X2-DISP
1	TRAC	0.000	-.005000000	TRAC	0.000	-.000000000
2	TRAC	0.000	-.005000000	TRAC	0.000	.016666667
3	TRAC	0.000	-.005000000	TRAC	1000000.000	.016666667
4	TRAC	0.000	.000000000	TRAC	1000000.000	.016666667

INTERNAL STRESS SOLUTION

N	X1	X2	X1-STRESS PRINC-1	X2-STRESS PRINC-2	X12-SHEAR STRESS TOCT	X3-STRESS ANGLE
1	0.0000	0.0000	.000 1000000.001	1000000.001 .000	-.000 471404.521	0.000 -90.000
2	.1250	.1250	.000 1000000.001	1000000.001 .000	.000 471404.521	0.000 90.000
3	.3750	.1250	.000 1000000.002	1000000.002 .000	.000 471404.522	0.000 90.000
4	.2500	.2500	-.000 1000000.001	1000000.001 -.000	.000 471404.521	0.000 90.000
5	.1250	.3750	-.000 1000000.001	1000000.001 -.000	.000 471404.521	0.000 90.000
6	.3750	.3750	-.000 1000000.002	1000000.002 -.000	.000 471404.522	0.000 90.000

Figure 2-6. Computer Results for Unit Square in Tension

As a second basic check problem, the same unit square was analyzed for pure shear loading ($\tau = 10^6$ psi) using the model illustrated in Figure 2-5(b). Since this case exhibits no symmetry, eight segments are required for modelling. Zero-length segments are added at all four corners since step type boundary conditions occur there. The resulting boundary and internal solutions are tabulated in Figure 2-7, and again the solutions are within machine accuracy.

It should be pointed out that the high degree of accuracy with relatively few boundary segments demonstrated in the previous two problems is to be expected since linear variation of boundary tractions and displacements represents an exact solution for these problems. No generalizations should be made from these results concerning the accuracy of the method in problems for which the model is an approximate solution. These two problems were intended only as a verification of the basic functioning of the program. The remaining sample problems in this Section serve to demonstrate the accuracy of the technique in the presence of stress and strain gradients.

2. *Beam Bending Problems* - The second set of problems chosen to evaluate the program is the bending of a beam due to an applied end moment and shear force. These problems are significantly more

SAMPLE PROBLEM 2 - UNIT SQUARE IN PURE SHEAR (NSYM = 0)

BOUNDARY SOLUTION

	X1 COORDINATE DIRECTION			X2 COORDINATE DIRECTION		
NODE	KNOWN	X1-TRAC	X1-DISP	KNOWN	X2-TRACC	X2-DISP
1	DISP	-1000000.001	0.000000000	DISP	.000	0.000000000
2	DISP	-1000000.002	-0.000000000	TRAC	-0.000	.029328154
3	TRAC	-0.000	-.000000000	TRAC	1000000.000	.029328154
4	TRAC	0.000	.014005179	TRAC	1000000.000	.029328154
5	TRAC	-0.000	.028010359	TRAC	1000000.000	.029328154
6	TRAC	1000000.000	.028010359	TRAC	-0.000	.029328154
7	TRAC	1000000.000	.028010359	TRAC	0.000	-.000000000
8	TRAC	1000000.000	.028010359	TRAC	-0.000	-.029328154
9	TRAC	-0.000	.028010359	TRAC	-1000000.000	-.029328154
10	TRAC	0.000	.014005179	TRAC	-1000000.000	-.029328154
11	TRAC	-0.000	-.000000000	TRAC	-1000000.000	-.029328154
12	DISP	-1000000.002	-0.000000000	TRAC	-0.000	-.029328154

INTERNAL STRESS SOLUTION

N	X1	X2	X1-STRESS PRINC-1	X2-STRESS PRINC-2	X12-SHEAR STRESS TOCT	X3-STRESS ANGLE
1	.2500	.2500	.000 1000000.002	-.000 -1000000.002	1000000.002 816496.582	0.000 45.000
2	.2500	.5000	-.000 1000000.002	-.000 -1000000.002	1000000.002 816496.582	0.000 45.000
3	.2500	.7500	.000 1000000.002	-.000 -1000000.002	1000000.002 816496.582	0.000 45.000
4	-.2500	.2500	-.000 1000000.002	.000 -1000000.002	1000000.002 816496.582	0.000 45.000
5	-.2500	.5000	.000 1000000.002	.000 -1000000.002	1000000.002 816496.582	0.000 45.000
6	-.2500	.7500	-.000 1000000.002	.000 -1000000.002	1000000.002 816496.582	0.000 45.000

Figure 2-7. Computer Results for Unit Square in Pure Shear

difficult than the unit square problems from the standpoint of numerical modelling. A beam with a length to depth ratio of five to one was analyzed using three models with 24, 48, and 72 boundary segments as shown in Figure 2-8. In one case the left end of the beam was fixed and a transverse load was applied to the right end. In the second case the left end was again fixed and a bending moment was applied to the right end. The convergence of both cases as a function of number of boundary segments is shown in Figure 2-9 for both maximum deflection and reaction moment at the fixed end. Reasonable convergence is indicated in both cases, considering that beam bending problems are extremely difficult to solve using numerical modelling techniques.

An important distinction between the boundary-integral and finite element techniques can be inferred from the data in Figure 2-9. In the boundary integral results, both displacements and reaction forces converge at the same rate with increasing model refinement. Thus for non-convergent boundary integral solutions, equilibrium is not assured. Finite element results, on the other hand, will always give force equilibrium, regardless of how crude the model. In one respect, this distinction can be interpreted as an advantage to the analyst using the boundary-integral technique. That is, an equilibrium check can be employed as one means of establishing a sufficiently refined model.

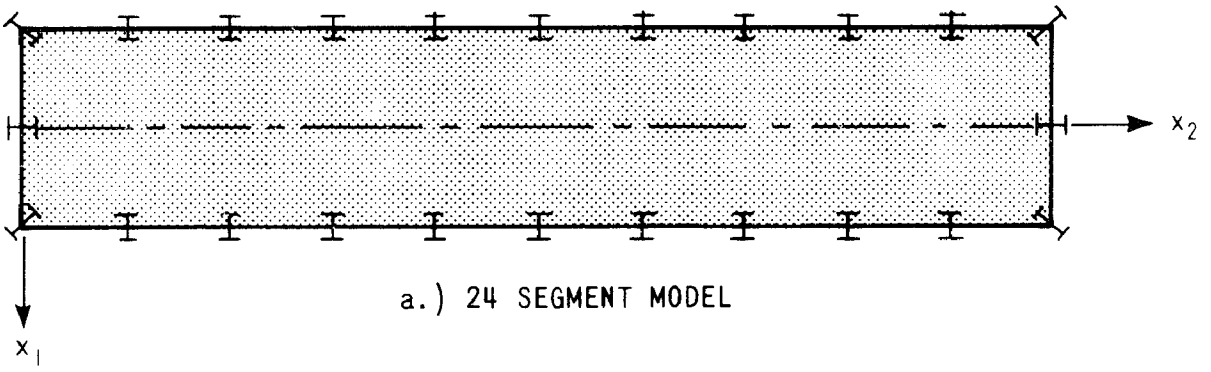

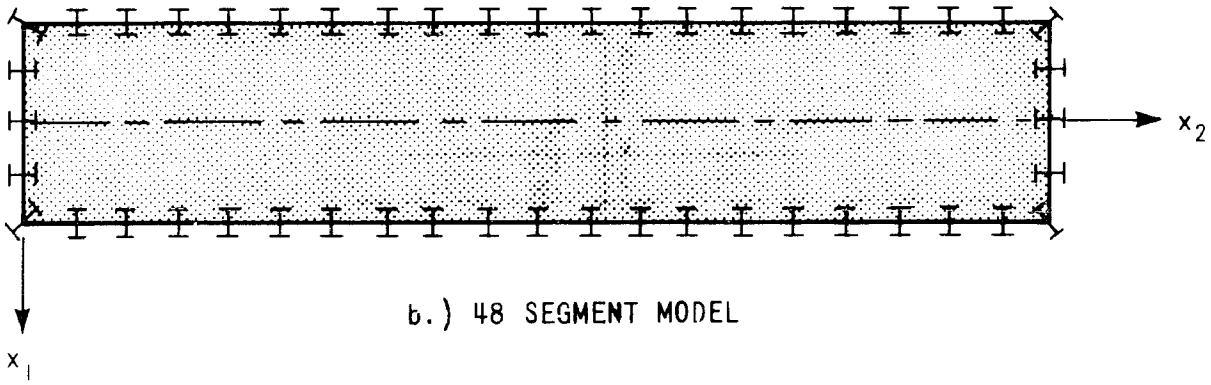

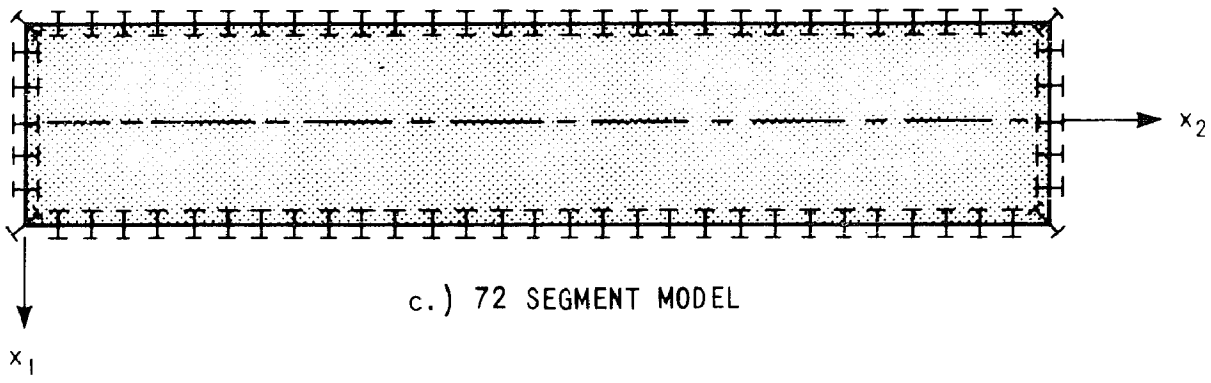

Figure 2-8. Boundary Integral Models for Beam Bending Problem

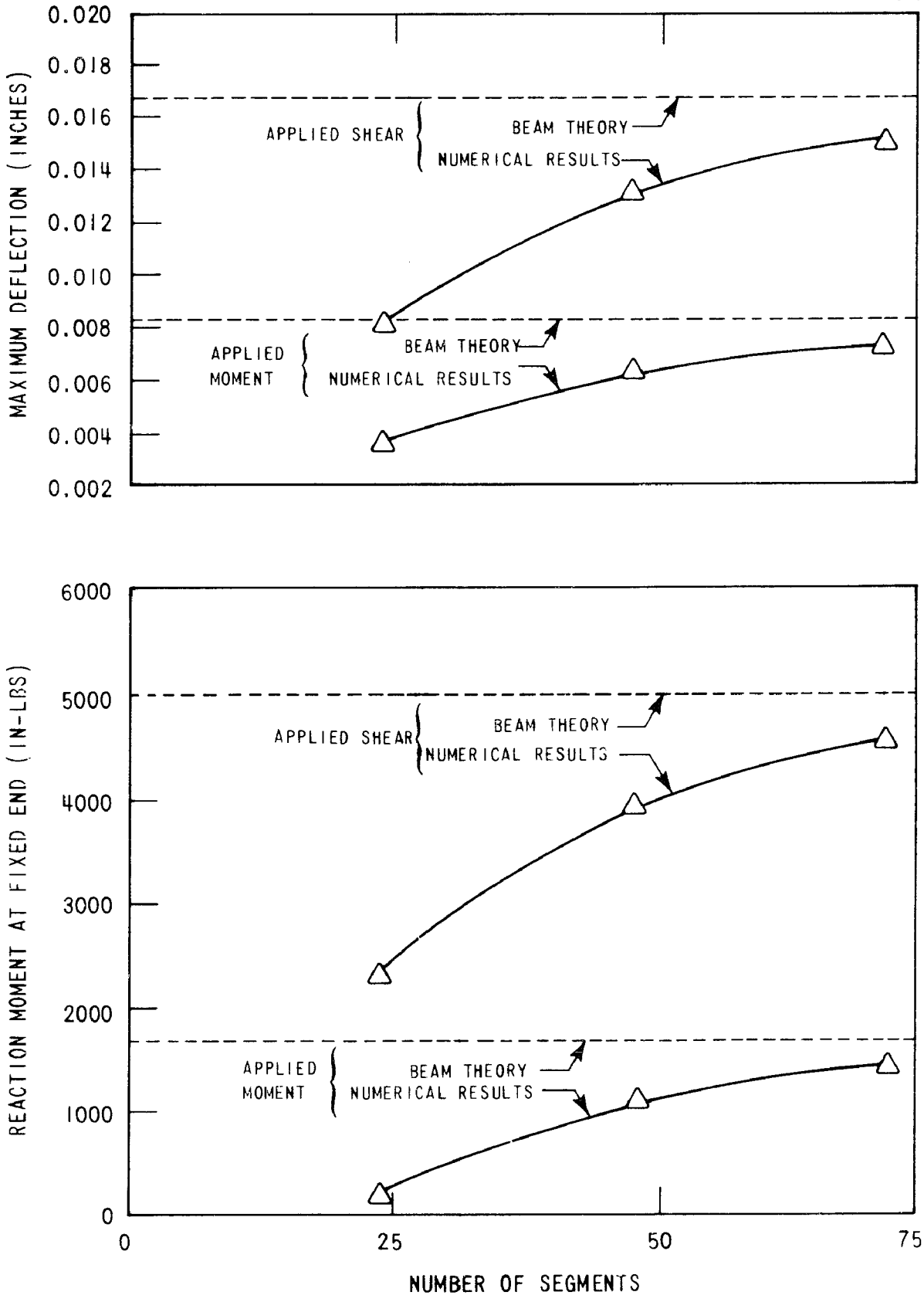

Figure 2-9. Results of Beam Bending Problems

Running times for these beam problems on CDC 6600 and CDC 7600 computers are given in Table I below. While the accuracy of the approach is not nearly as great here as it was for the unit square problems, the running times in Table I compare favorably with what would be required for similar solutions using conventional numerical techniques such as the finite element method. Beam flexure problems are particularly difficult to model numerically without using specially adapted discretization procedures. The real advantages of the boundary-integral technique are better realized in continuum problems with large stress and strain concentrations such as those considered in the next two sets of sample problems.

TABLE I - RUNNING TIMES FOR BEAM PROBLEMS

Number of Segments	CDC 6600	CDC 7600
24	2.9 sec.	
48	9.75 sec.	
72		1.65 sec.

3. *Cutout Problems* - In order to demonstrate the ability of the program to solve problems with high stress gradients a series of problems of large plates in uniaxial tension with circular and elliptical cutouts has been run. When analyzing this type of problem, the superposition technique illustrated in Figure 2-10 can be used to good advantage. For the problem shown in Figure 2-10(a), the portion of the boundary at infinity need not be modelled since it is traction free. The loading is represented by an applied x_2-traction on the surface of the cutout equal to the scalar product of the remote tension and the unit normal to the cutout surface. The results for the problem shown in Figure 2-10(c) are then computed by adding the results of Figure 2-10(a) to those of the problem shown in Figure 2-10(b), which are trivial. Thus when using this superposition technique, cutout problems can be solved without modelling the remote boundary.

The circular cutout problem was analyzed using the model shown in Figure 2-11. Twenty-five segments per quadrant were used, and only the first quadrant was modelled since the problem is doubly-symmetric. Internal stresses were computed at a series of points along the x_1 axis, and the results are compared to the closed form solution to the problem [27] in Figure 2-12. The results of a similar analysis using constant boundary value segments [25] are also given. Figure 2-12 gives stress concentration factors as a function of normalized distance from the cutout surface X, where

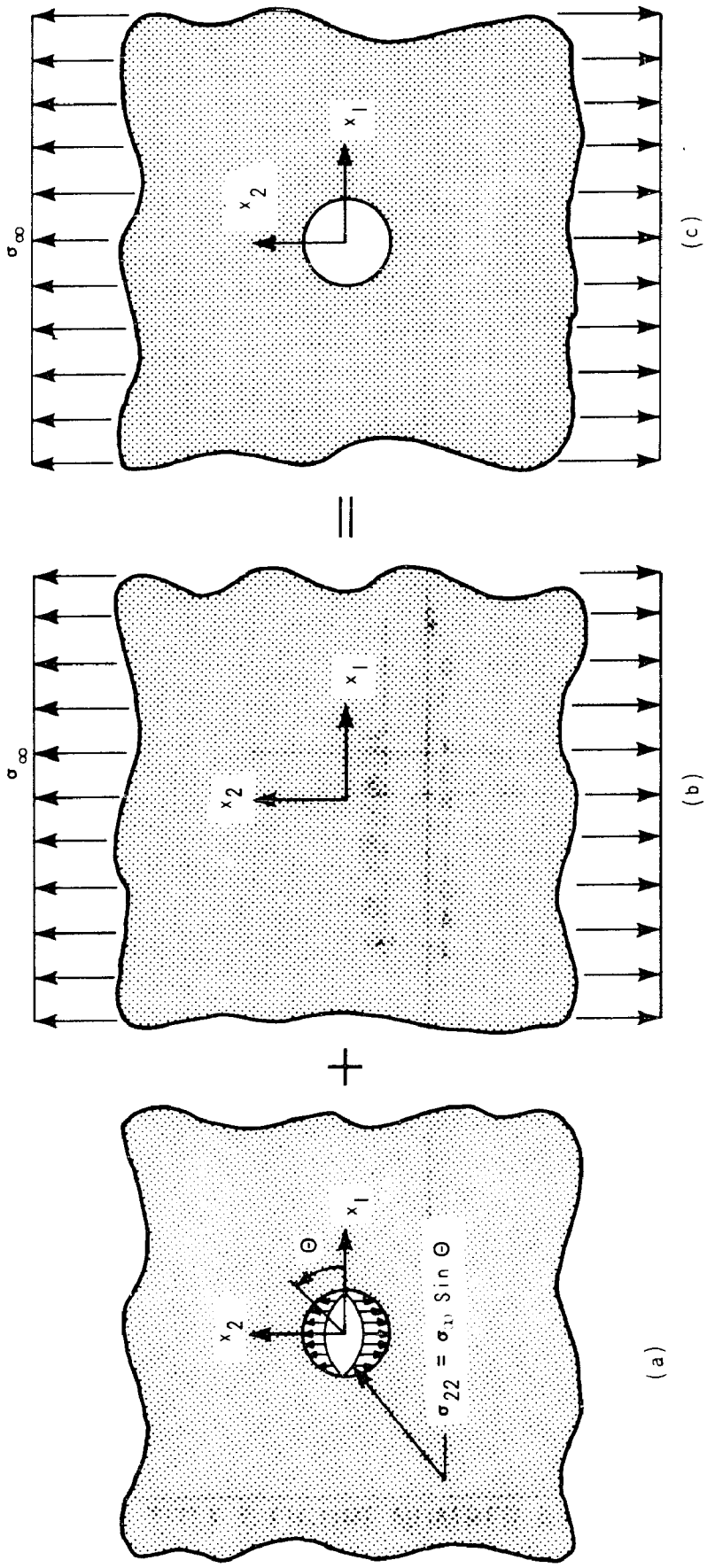

Figure 2-10. Superposition Technique for Cutout Problems

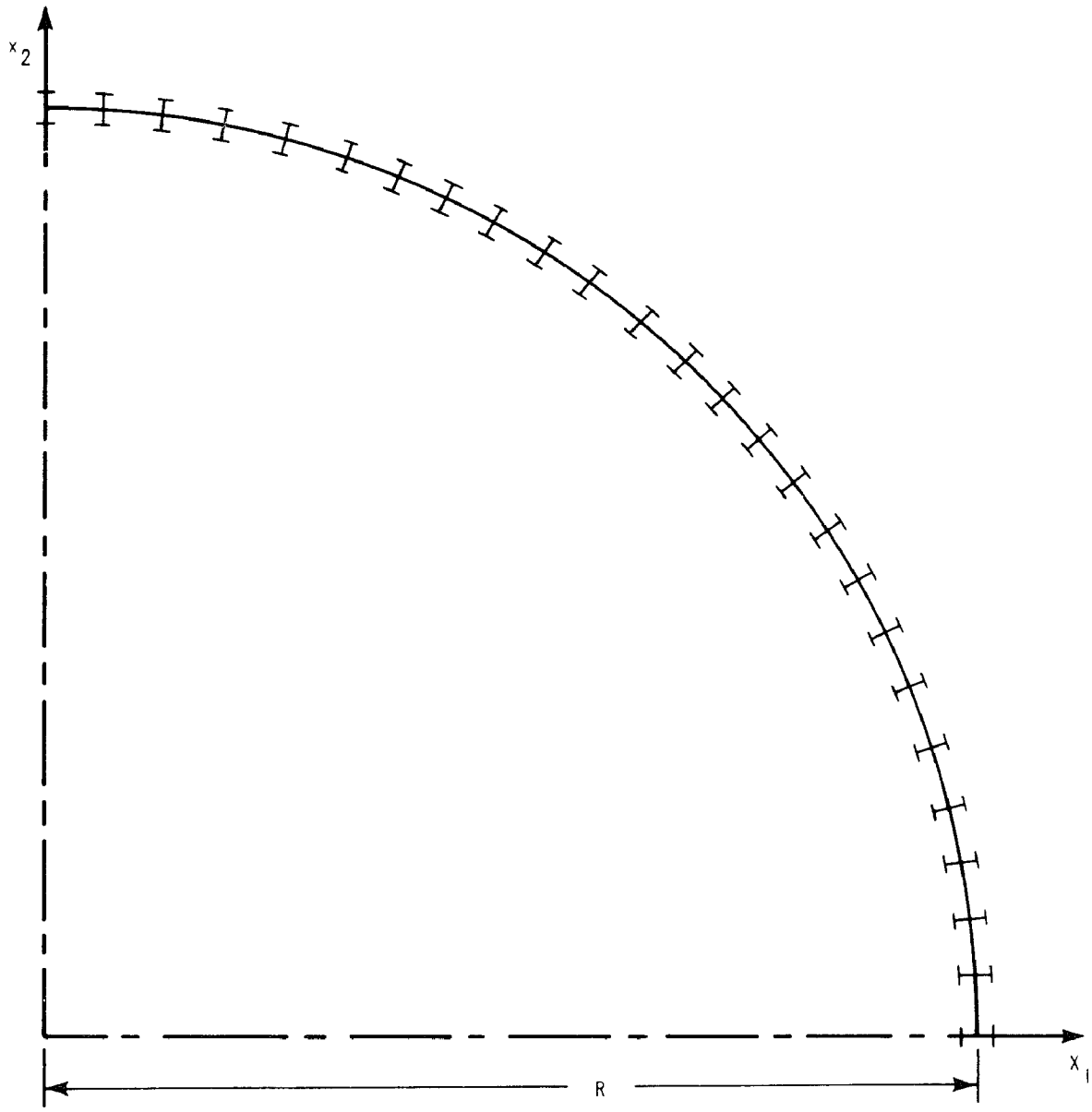

Figure 2-11. Twenty-Five Segment Model Used for Circular Cutout Problem

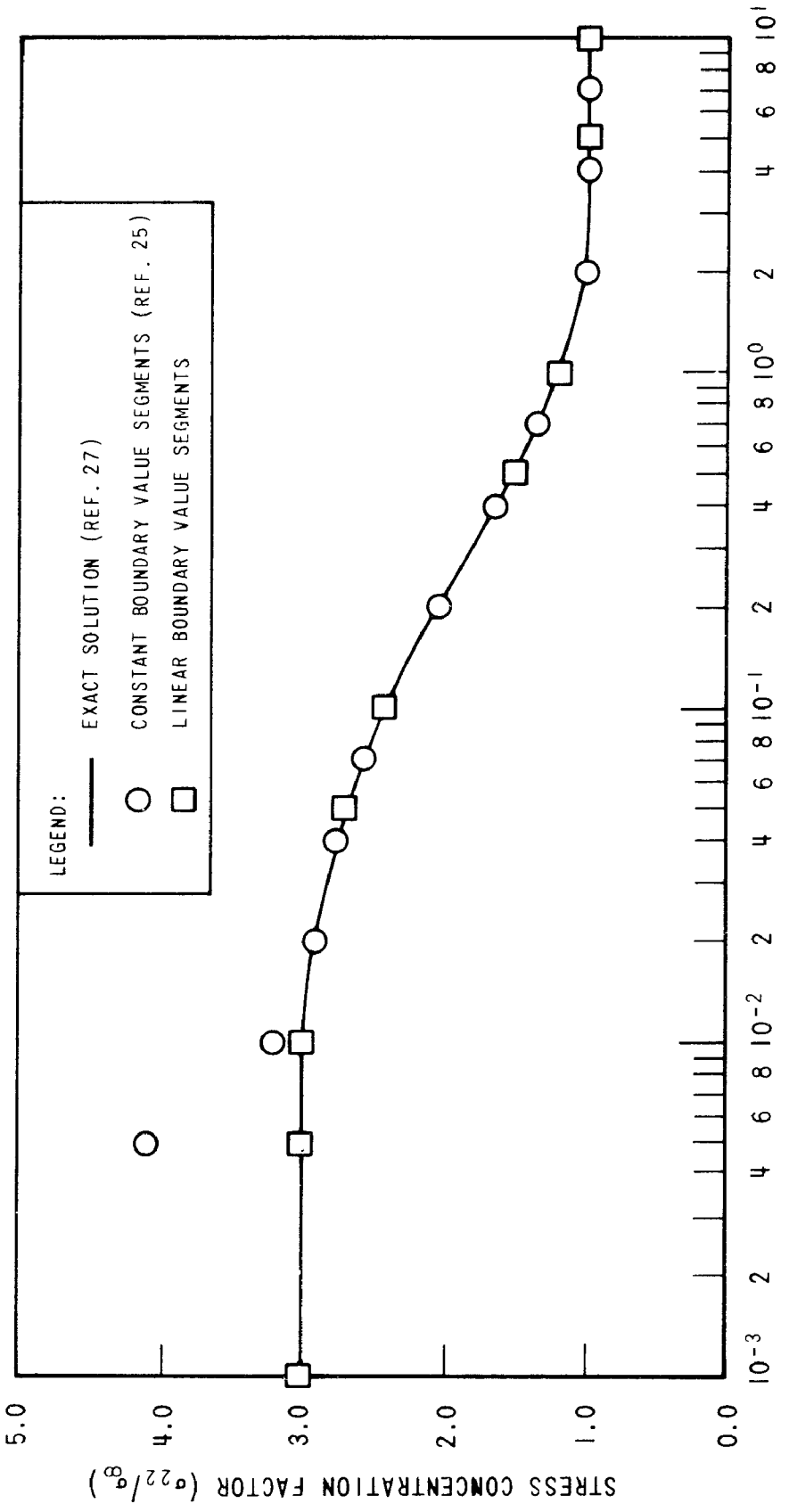

Figure 2-12. Results of Boundary Integral Solutions to Circular Cutout Problem

$$X = \frac{x_1 - R}{R} \quad \text{(normalized distance along } x_1 \text{ axis)}$$
$$R = \text{radius of circle} \tag{2-26}$$

The results of the current analysis show good agreement with the exact solution for X as small as 0.001, while the constant boundary value results diverged from the exact solution at X approximately equal to 0.01. Thus the use of linear rather than constant boundary value segments improved the resolution by at least an order of magnitude for the circular cutout problem.

The problem of an elliptical cutout in an infinite plate was first solved by Inglis [28]. For remote uniaxial tension transverse to the major axis of the ellipse, the maximum stress occurs on the surface of the ellipse at the major axis, and is given by

$$\sigma_{max} = (1 + 2\frac{a}{b})\ \sigma_\infty \tag{2-27}$$

where σ_∞ is the applied remote tension and a and b are the semi-major and minor axes of the ellipse respectively (See Figure 2-13).

The elliptical cutout problem presents an additional modelling difficulty because for a given number of segments it is not obvious how to distribute those segments for maximum accuracy. Since the closed form solution gives very high stress and displacement gradients in the vicinity of the tips of the ellipse, it is obvious that a greater segment density is required there. However, experimentation

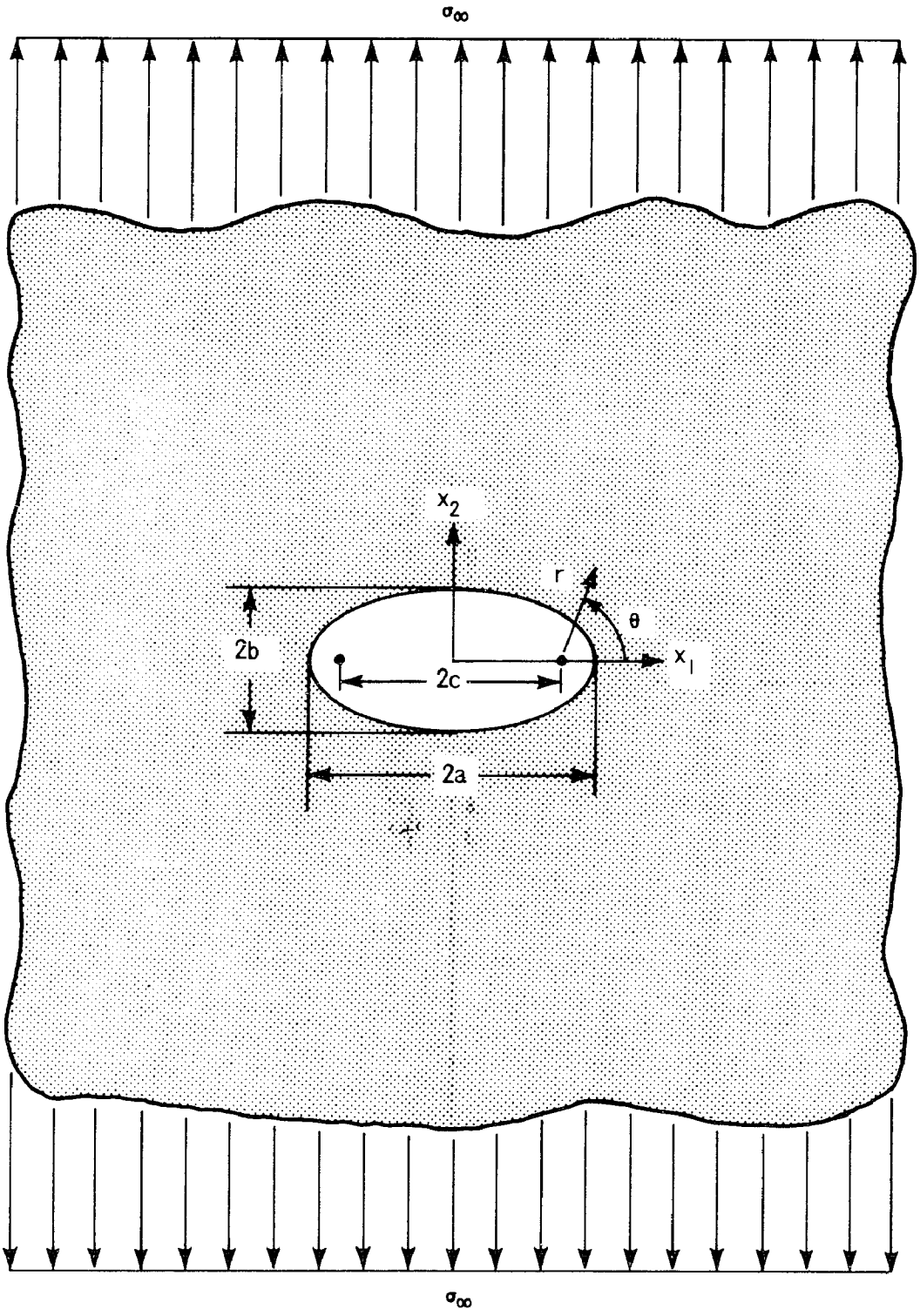

Figure 2-13. Inglis Ellipse Problem

with various types of models has indicated that it is possible to over-concentrate the number of segments at the tips of the ellipse and thus lose accuracy for a given number of segments. A model study was carried out in which several modelling schemes were investigated with respect to their accuracy as a function of number of segments, and the most efficient scheme of those studies was used for the results presented here.

Elliptical cutouts with aspect ratios $(\frac{a}{b})$ of 4.5, 9.5, 19.5, 49.5, and 99.5 have been analyzed using the linear boundary integral program. According to equation (2-27) these aspect ratios correspond to theoretical stress concentration factors of 10, 20, 40, 100, and 200 respectively. The results of the numerical analyses are compared to the closed form solution to the problems [29] in Figures 2-14, -15, -16, -17, and -18. These figures give theoretical and numerical values of stresses in the x_1 and x_2 directions as a function of normalized distance (r/a) from the focal points of the ellipses, where

r = distance from focal point
a = semi major axis of ellipse. (See Figure 2-13)

Several models with increasing numbers of segments were run for each aspect ratio, and the convergence of the solution technique is evident in Figures 2-14 through 2-18. The convergence is essentially uniform. That is, both the x_1- and x_2 stresses converge at

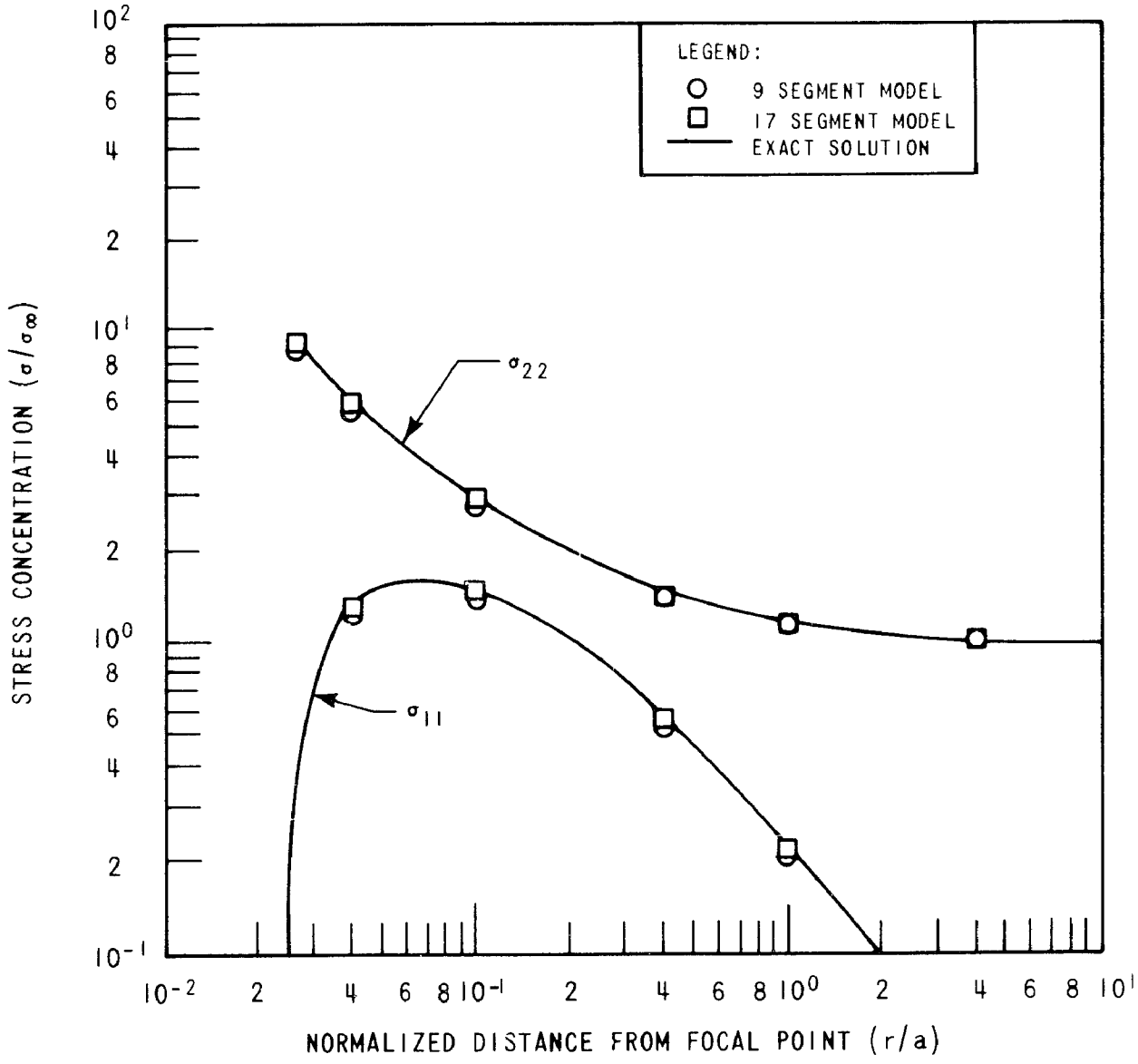

Figure 2-14. Numerical Solution to Inglis Ellipse Problem (Aspect Ratio = 4.5)

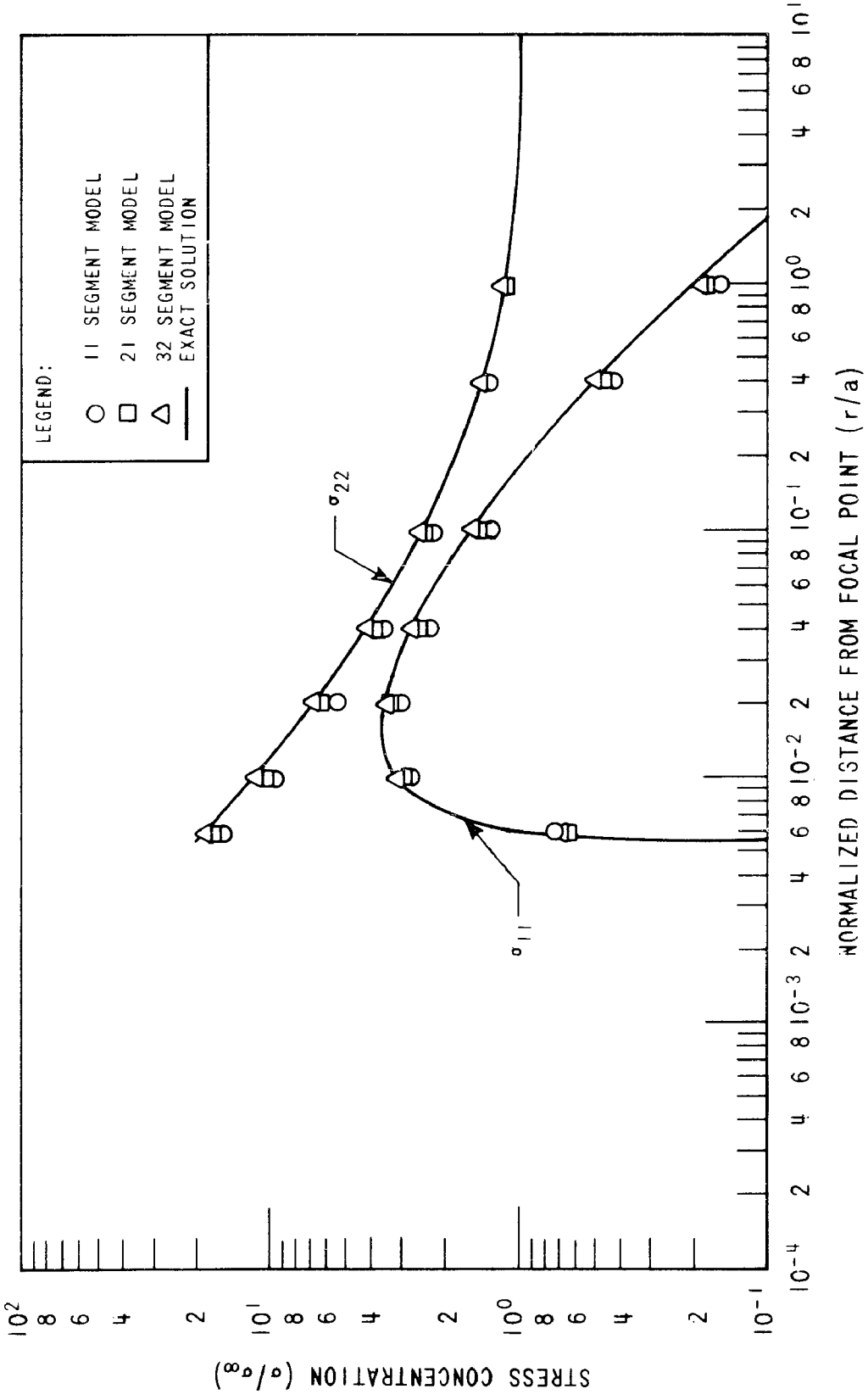

Figure 2-15. Numerical Solution to Inglis Ellipse Problem (Aspect Ratio 9.5)

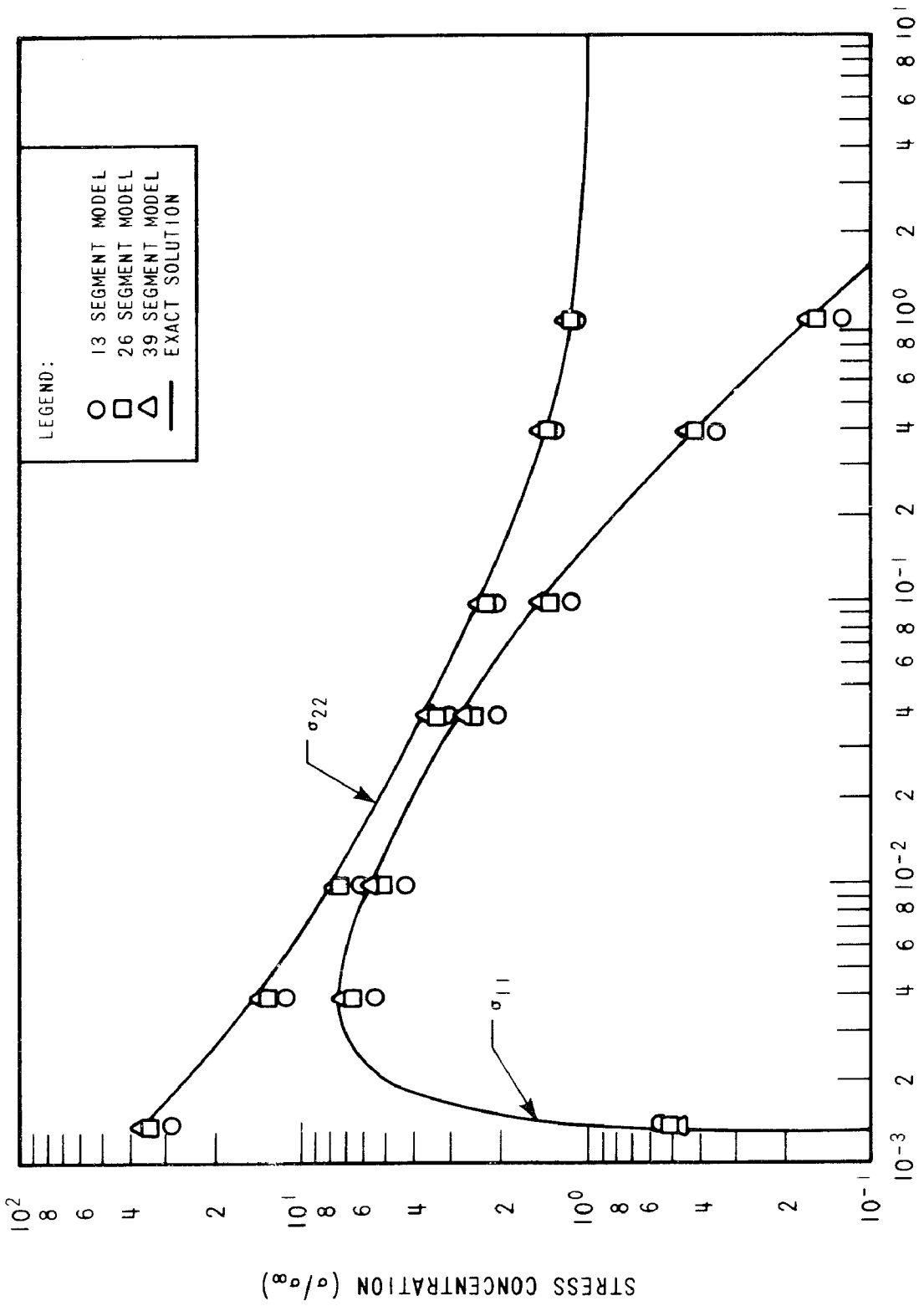

Figure 2-16. Numerical Solution to Inglis Ellipse Problem (Aspect Ratio 19.5)

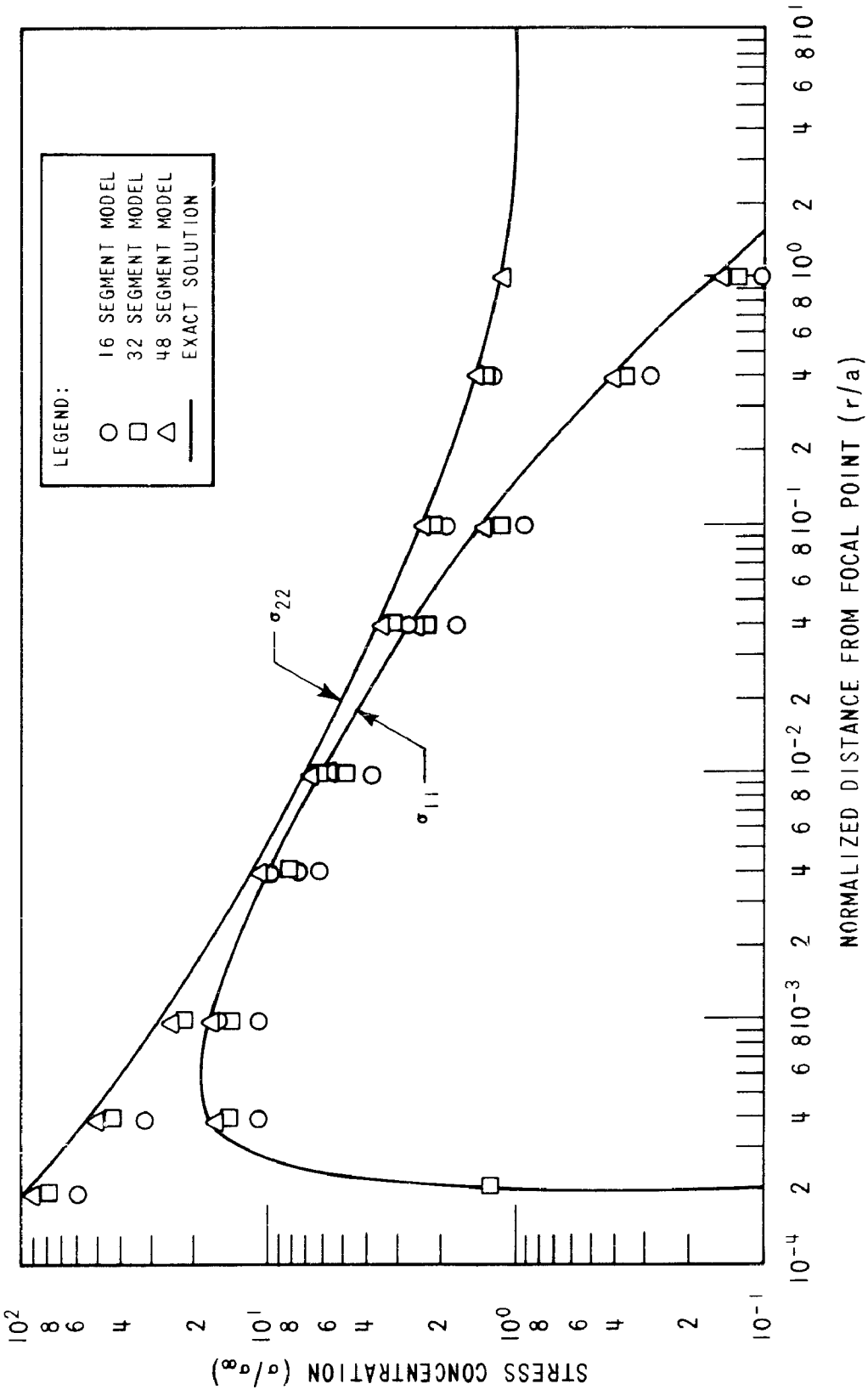

Figure 2-17. Numerical Solution to Inglis Ellipse Problem (Aspect Ratio 49.5)

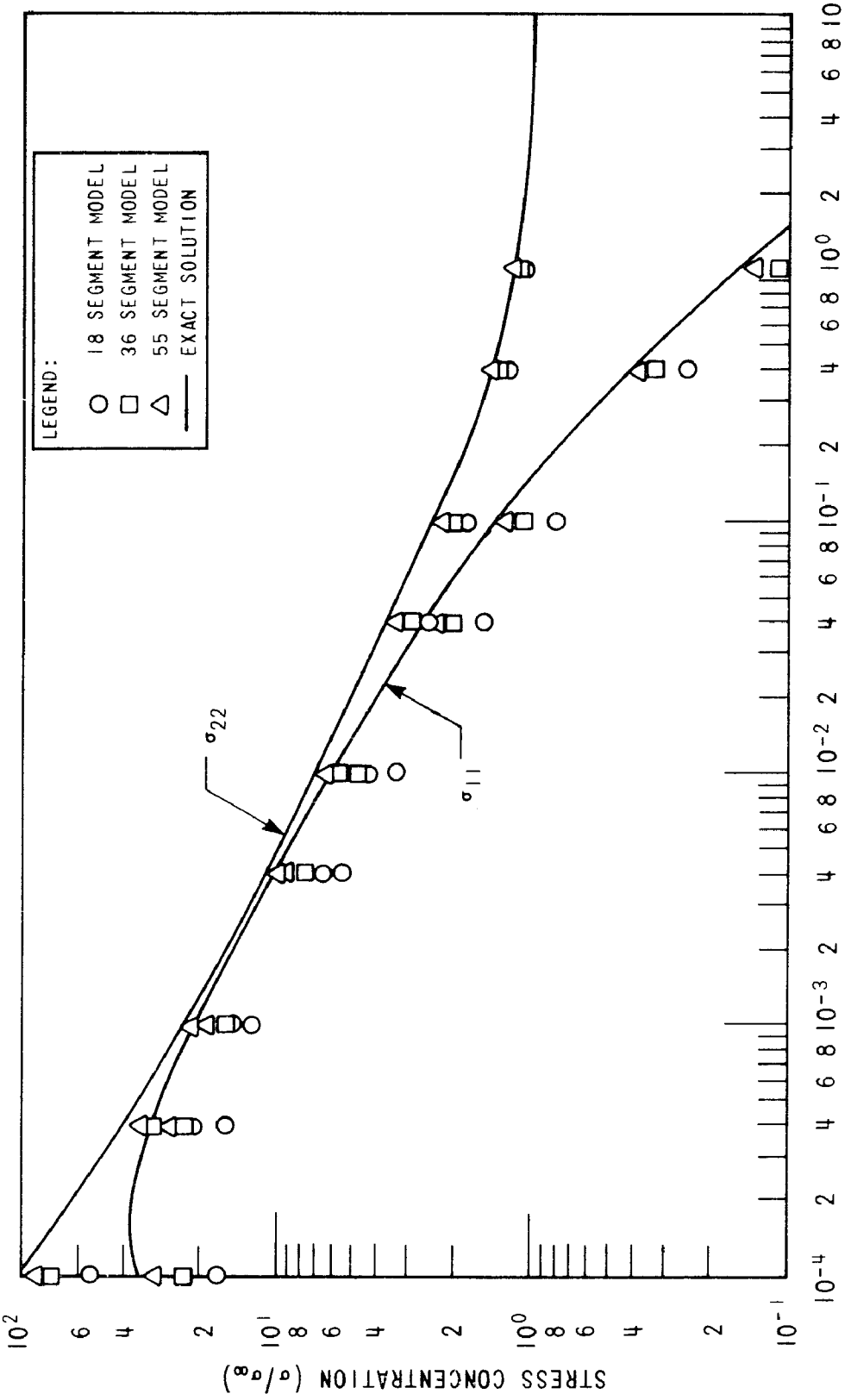

Figure 2-18. Numerical Solution to Inglis Ellipse Problem (Aspect Ratio 99.5)

approximately the same rate at all points in the body. The only exception is the x_2-direction stress at large distances from the ellipse, which always seems to fall very close to the exact solution, regardless of how crude the model. Figure 2-19 shows the relative accuracy of the solution technique for all six aspect ratios for the uniformly convergent parts of the stress distributions as a function of number of segments. It is apparent that the higher the aspect ratio (and thus the stress concentration), the more segments are required to achieve the same level of accuracy. These results demonstrate, however, that the solution technique has the ability to accurately predict very high stress concentrations with relatively simple models.

An analysis of the same elliptical cutout problem was performed using the boundary integral technique with constant boundary value segments [25], and a comparison of the results indicates a significant improvement in numerical accuracy by using linear boundary value segments. The relative accuracy of the two techniques as a function of number segments is given in Figure 2-20. Note that the linear boundary value solution converges from low side of the actual solution while the constant boundary value solution converges from the high side. This difference in convergence behavior is to be expected due to basic differences in the two numerical schemes.

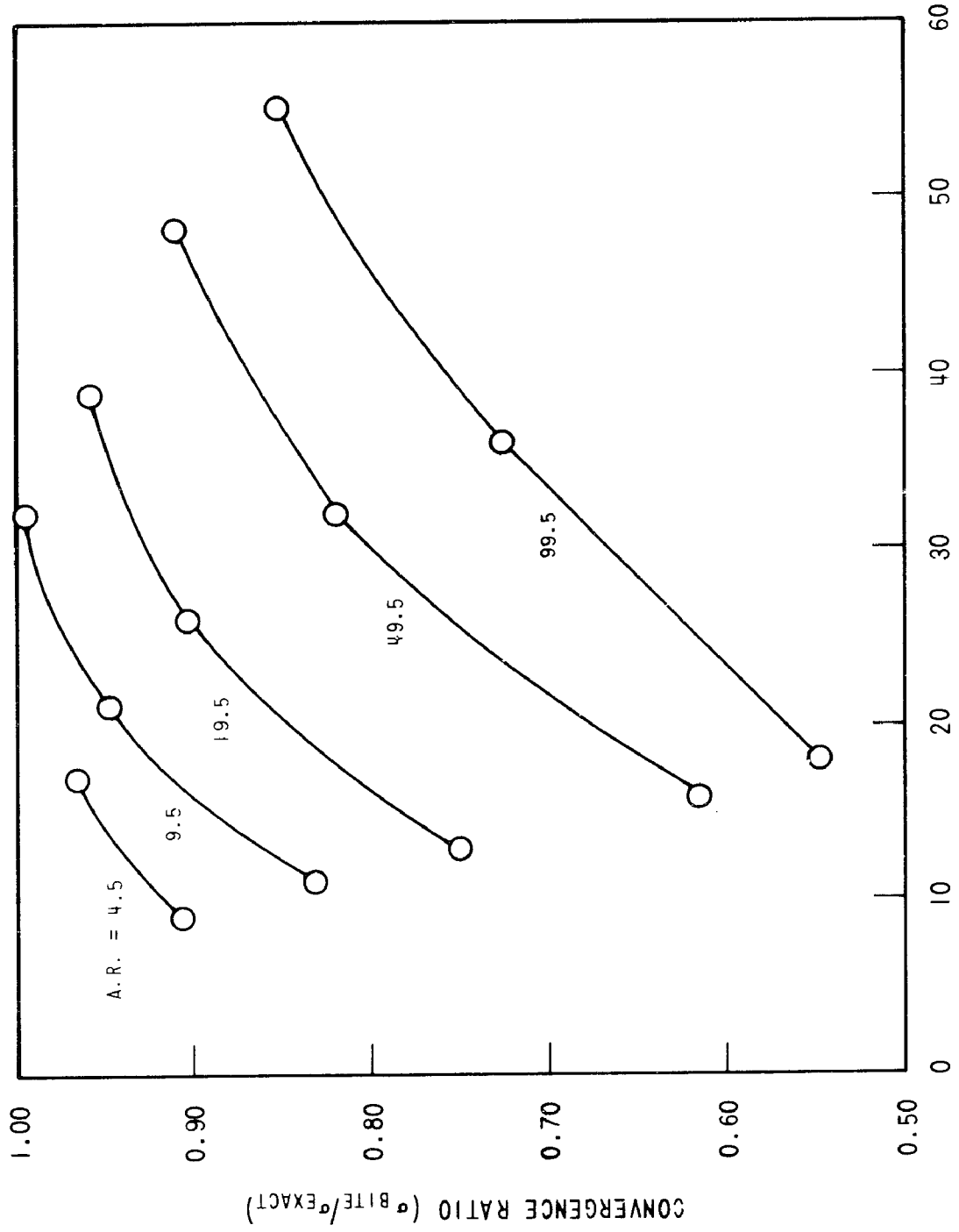

Figure 2-19. Convergence of Numerical Solution to Inglis Ellipse Problem for Various Aspect Ratios

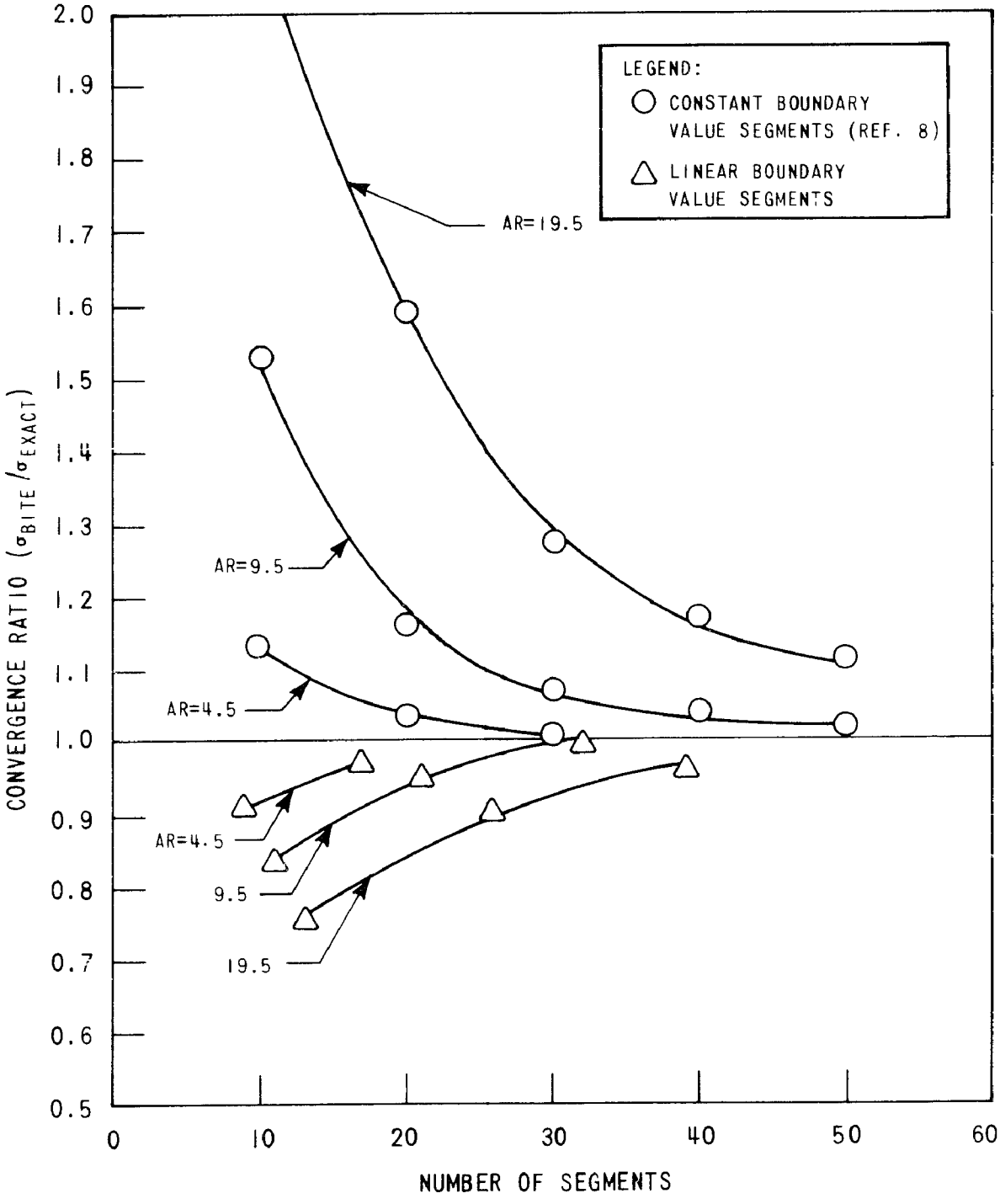

Figure 2-20. Relative Convergence of Two Boundary Integral Techniques for Inglis Ellipse Problem

4. Crack Problems - The reason for performing such an extensive study of the Inglis ellipse problem was to develop an efficient modelling scheme for crack problems. The nature of the numerics of the boundary-integral technique produces a singular matrix when an ideal mathematical crack (or slit) is modelled, since one or more rows of the coefficient matrix become identical in that case. This problem can be circumvented by modelling cracks as ellipses, or other types of finite cutouts. As the opening of the cutout is reduced, the solution of the cutout problem approaches that of the mathematical crack. By choosing a cutout with a sufficiently fine opening, the solution to the mathematic crack problem can be reproduced with sufficient resolution to yield the elastic singularity while at the same time avoiding the singular matrix difficulty.

Figure 2-21 gives the x_1 and x_2 direction stresses from the closed form solution to the Inglis ellipse problem as a function of normalized distance (r/a) from the focal points of the ellipses. As the aspect ratio increases the solution approaches that of a mathematical crack (aspect ratio = ∞), and the focal points of the ellipse become the crack tips. Ranges of the distance coordinate (r/a) in Figure 2-21 are labeled according to the effects which are considered important in those ranges in linear elastic fracture problems [30]. The middle decade of the plot ($0.01 < r/a < 0.1$)

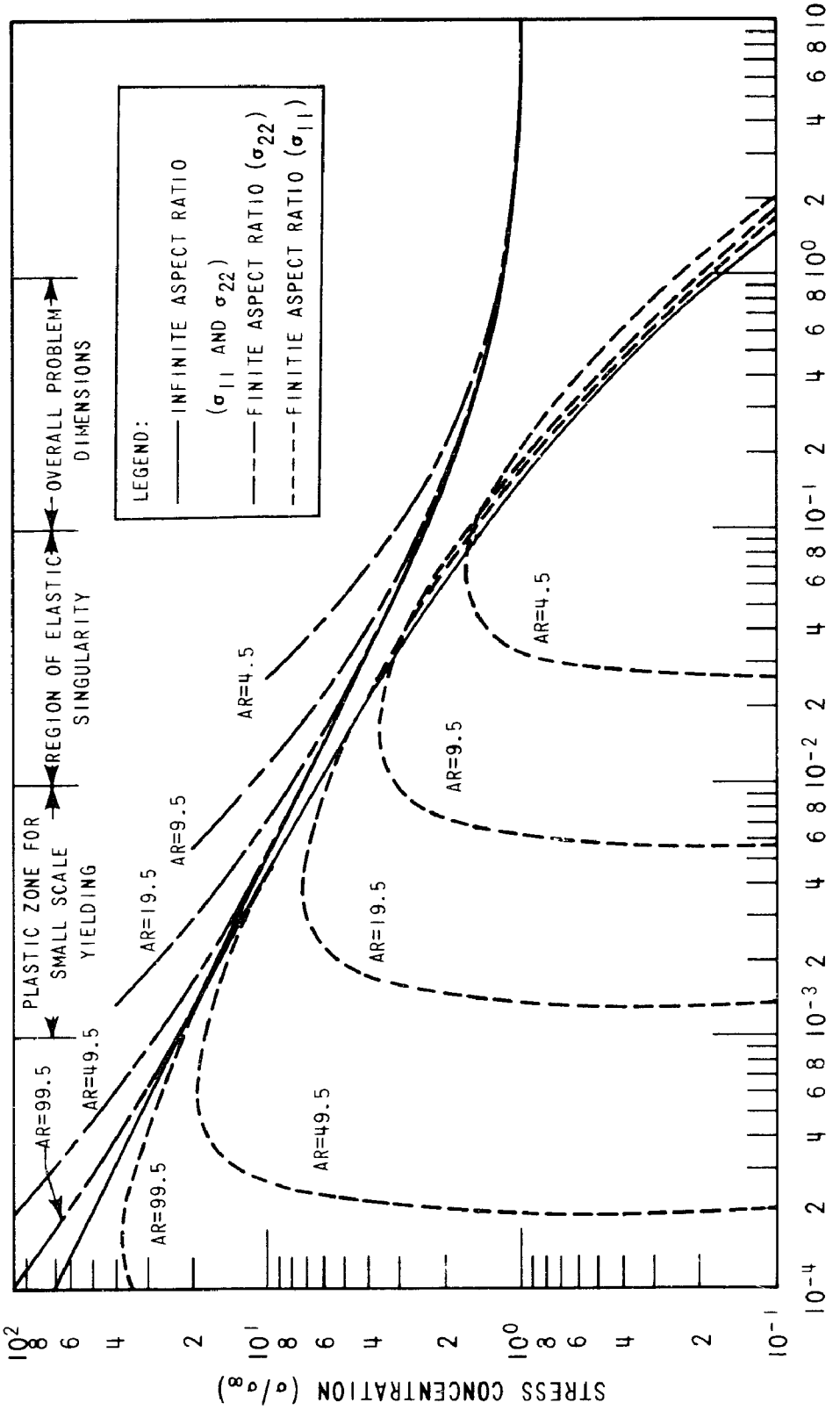

Figure 2-21. Exact Solution to Inglis Ellipse Problem for Various Aspect Ratios

is the region in which the elastic singularity is dominant. In the next smaller decade ($0.001 < r/a < 0.01$), small scale yielding occurs in real materials, and the stresses are not well represented by the elastic singularity. Thus, to numerically predict the elastic singularity in a real problem, it is only necessary to accurately describe the mathematical crack solution down to a resolution of $(r/a) = 0.01$.

Since in the previous study it was determined that it is more difficult to numerically model higher aspect ratio ellipses (Figure 2-19), it is desirable to use as low an aspect ratio ellipse as possible for crack problems from the standpoint of minimizing number of segments. Inspection of Figure 2-21 indicates that an elliptical cutout with an aspect ratio of 19.5 adequately describes the elastic singularity in the important region. In Figure 2-16, it can be seen that the 19.5 aspect ratio ellipse can be modelled with about a 10 percent underestimate using a 26 segment model. However, since the x_2-direction stresses from the closed form solution to the 19.5 aspect ratio ellipse tend to overestimate the elastic singularity by about 7 percent, the net error should only be about 3 percent if the x_2-direction stresses from the 26 segment model are used to predict stress intensity factors in crack problems. The 26 segment model for a 19.5 aspect ratio ellipse is shown in detail in Figure 2-22. This model has been

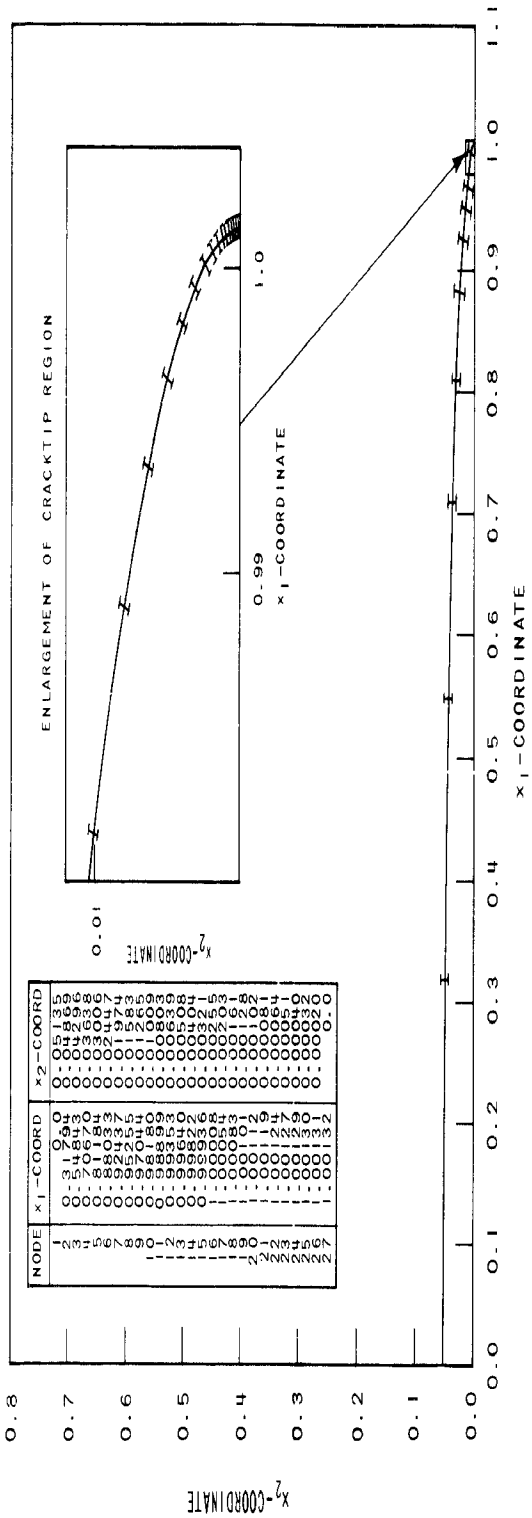

Figure 2-22. Twenty-Six Segment Model of 19.5 Aspect Ratio Ellipse (Used for all Crack Problems)

used, in conjunction with the outer boundary models shown in Figure 2-23, to analyze four familiar crack problems taken from reference [31].

Values of stress intensity factor can be estimated from numerical results by using a curve fitting procedure to determine the first two terms of the series expansion of the crack tip stress field along the x_1 axis, given by

$$\sigma_{22} = \frac{K_I}{\sqrt{2\pi r}} + C \qquad (2\text{-}28)$$

where K_I is the opening mode stress intensity factor, and C is an arbitrary constant. Multiplying both sides of equation (2-28) by $\sqrt{2\pi r}$

$$\sigma_{22}\sqrt{2\pi r} = K_I + C\sqrt{2\pi r} \qquad (2\text{-}29)$$

In Figure 2-24 the x_2-direction stresses from the numerical results for the four crack problems of Figure 2-23 have been multiplied by $\sqrt{2\pi r}$ and plotted against $\sqrt{2\pi r}$. Only stress points in the elastic singularity region ($0.01 < r/a < 0.1$) were chosen since outside of that range equation (2-29) is not expected to apply. By plotting a best fit straight line through the numerical data, and extrapolating that straight line back to $r = 0$, an estimate of K_I can be obtained.

K_I estimates for the four crack problems of Figure 2-23, determined by this curve fitting technique, are listed in Table II.

a.) CENTER CRACKED PLATE

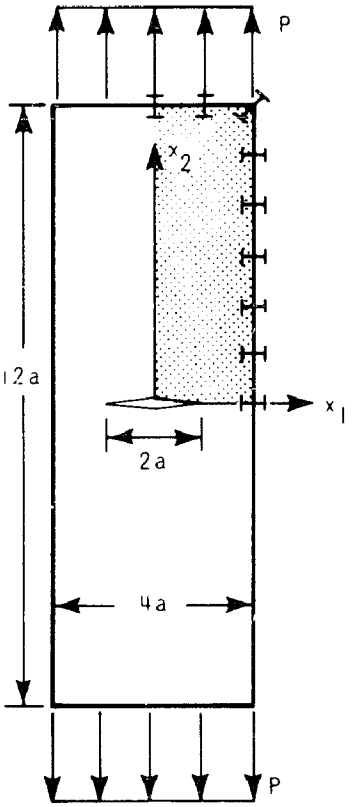

b.) COMPACT CRACKLINE LOADED SPECIMEN

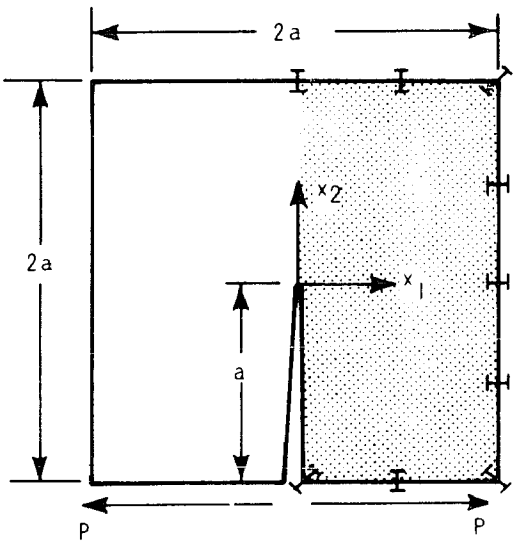

c.) SINGLE EDGE CRACKED PLATE (TENSION)

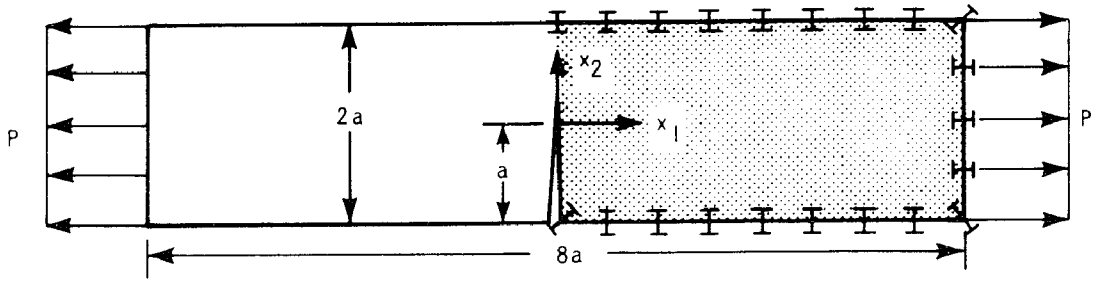

d.) SINGLE EDGE CRACKED PLATE (BENDING)

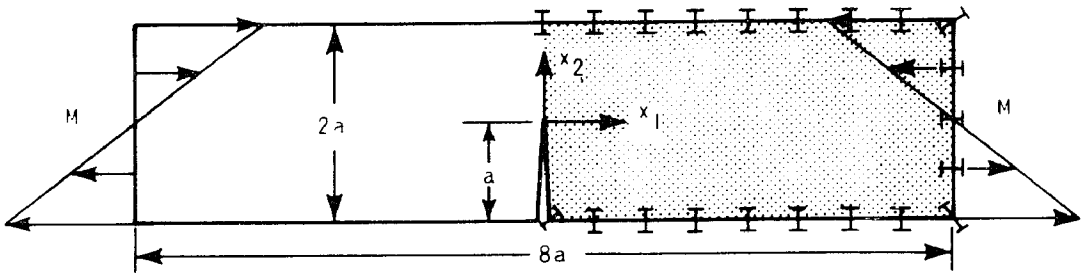

Figure 2-23. Boundary Integral Models for Crack Problems

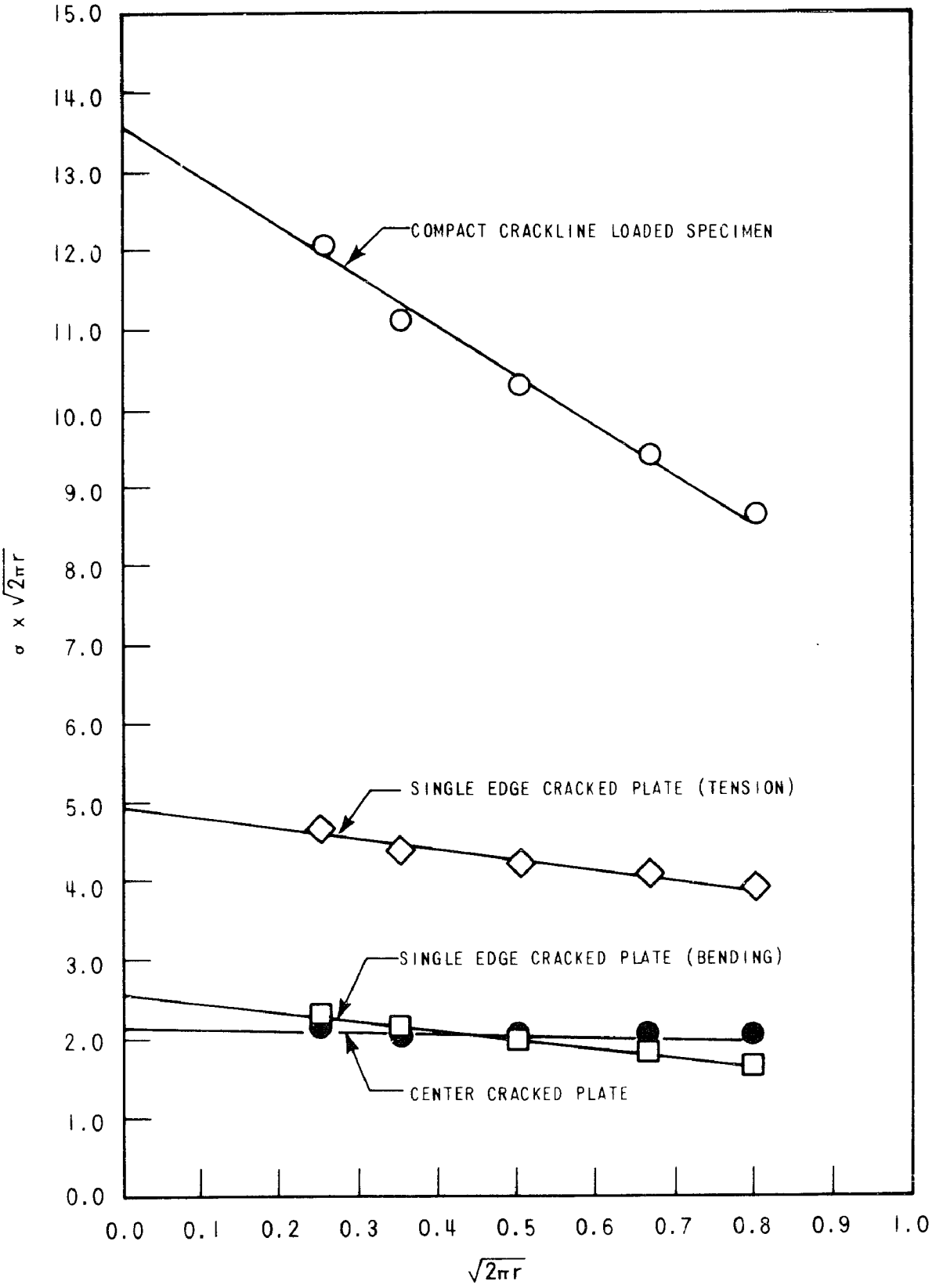

Figure 2-24. Estimation of Stress Intensity Factors from Numerical Results for Crack Problems

This table also gives the accepted solutions from the literature for these problems [31]. The agreement between the two sets of data shows a maximum deviation of 5% for the compact crackline loaded specimen, with the other three problems showing even better agreement. Table II also gives total model size and running times on a CDC-6600 computer. It is evident from the data listed in Table II that the boundary-integral technique with linear boundary value segments has the ability to accurately estimate stress intensity factors for two dimensional crack problems using very small amounts of computer time in comparison to other numerical solution techniques. Furthermore, the amount of work required to set up the boundary-integral models for these problems is trivial in comparison to what would be required for the same problems using a conventional numerical technique such as finite elements.

TABLE II - RESULTS OF CRACK PROBLEMS

	K_{IA} (Boundary Integral Technique)	K_{IB} (Reference 31)	RATIO (K_{IA}/K_{IB})	MODEL Total Number of Segments	COMPUTER TIME CDC-6600
Center Cracked Plate	2.15	2.10	1.02	34	18 sec
Compact Crackline Loaded Specimen	13.5	14.26	.95	34	11 sec
Single Edge Cracked Plate (Tension)	4.95	5.0	.99	46	17 sec
Single Edge Cracked Plate (Bending)	2.6	2.65	.98	46	17 sec

E. SUMMARY

The boundary-integral technique for two dimensional elasticity has been covered in detail in this chapter. The fundamentals of the technique are derived for completeness, and the implementations of the technique presented to date are discussed. An advanced implementation, which utilizes linearly varying (rather than constant value) displacements and tractions over discretized segments of the boundary is developed. Finally, a series of sample problems is presented which demonstrates the improved range and accuracy of the new implementation.

This chapter is intended to serve as a stepping stone to the more complex implementation of the boundary-integral technique for elasto-plastic problems. The fundamental relations derived herein are drawn upon heavily in the elasto-plastic development of the next chapter. Many of the steps in the development are merely repeated in the next chapter with modifications for plasticity. Nevertheless, the improved elastic implementation does represent a significant contribution in itself, since it yields a substantial improvement in accuracy over previous implementations of the boundary-integral technique, and since it can be used to solve important engineering problems, such as crack problems, with relative ease in comparison to other numerical solution techniques.

CHAPTER III - ELASTO-PLASTIC IMPLEMENTATION

A. *INTRODUCTORY REMARKS*

A natural question arises from the foregoing elastic work as to whether the boundary integral technique can be extended to solve problems of elasto-plasticity. If the same advantages in computer time and storage carry over into the elasto-plastic case, the method would represent a significant improvement over conventional numerical techniques in this field, since computer time and storage are usually very critical for elasto-plastic problems. Furthermore, the other advantages of high stress and strain field resolution and relative ease of modelling are also expected to apply in the elasto-plastic case.

Boundary-integral equations have been formulated for the elasto-plastic problem [32], however, the equations have not been implemented into a numerical solution technique to date. Implementation of the boundary integral technique is more complex for elasto-plastic problems than it was for elasticity due to the fact that the governing equations are no longer linear. This chapter presents a numerical implementation of the boundary-integral technique for problems of two-dimensional elasto-plasticity. The material non-linearity is handled by considering the loading and unloading of the body to take place in small increments, over which the governing equations are assumed to be linear [33]. A further complication is introduced due to the

fact that the boundary-integral equations, when used for elasto-plastic problems, are not strictly boundary equations; they require a volume integration over the plastic strain increments at each load step. A procedure is developed for numerical evaluation of this volume integral, and the overall solution technique is automated in the form of a digital computer program. As in the elastic case, the viability of the program is demonstrated through example problems.

The general development of the boundary-integral technique for elasto-plasticity is reviewed in Section B of this Chapter, and the numerical implementation is developed in Section C. The potential and limitations of the numerical implementation are evaluated in Section D by presenting a series of sample problems, and comparing them to known solutions (either exact where available or numerical). Appendices D and E give detailed mathematical developments of the volume integration scheme and elasto-plastic flow rule required for the procedure, and Appendix F gives a detailed description (including input instructions) of the computer program BITEP which was used in developing the numerical results.

B. DEVELOPMENT OF BOUNDARY-INTEGRAL EQUATIONS FOR ELASTO-PLASTICITY

A formulation of a set of boundary-integral equations for problems of elasto-plastic flow has been reported in the literature [32]. The development of these equations is summarized here for completeness. An elasto-plastic form of Betti's reciprocal work theorem can be formulated in terms of stress and elastic strain rates for a work hardening material

$$\int_R \sigma^*_{ij}\dot{\varepsilon}^e_{ij}dV = \int_R \varepsilon^*_{ij}\dot{\sigma}_{ij}dV, \tag{3-1}$$

where $\dot{\sigma}_{ij}$ and $\dot{\varepsilon}^e_{ij}$ are the stress and elastic strain rates for the elasto-plastic problem, and σ^*_{ij} and ε^*_{ij} are the stresses and strains for an arbitrary elastic problem. The work hardening restriction is necessary to insure ellipticity of the governing equations [33] so that the divergence theorem applies, and so that equation (3-1) can be cast in terms of surface integrals over the boundary traction and displacement rates ($\dot{t}_i$ and $\dot{u}_i$) and a volume integral over the plastic strain rates ($\dot{\varepsilon}^p_{ij}$)

$$\int_S t^*_i\dot{u}_i dS - \int_R \sigma^*_{ij}\dot{\varepsilon}^p_{ij}dV = \int_S u^*_i\dot{t}_i dS\,. \tag{3-2}$$

Choosing, as before, the solution to Kelvin's problem of a concentrated unit load in an infinite body for the starred quantities leads to an elasto-plastic version of the Somigliana identity

$$\dot{u}_i(\xi) + \int_S \dot{u}_j(x) T_{ij}(x,\xi) dS(x) = \int_S \dot{t}_j(x) U_{ij}(x,\xi) dS(x) + \int_R \Sigma_{ijk}(x,\xi) \dot{\varepsilon}^p_{jk}(x) dV(x), \tag{3-3}$$

where the tensors $U_{ij}(x,\xi)$ and $T_{ij}(x,\xi)$ are defined as previously (equations 2-2), and $\Sigma_{jik}(x,\xi)$ defines the stress field which would exist at a point x in an infinite body subjected to a unit point load at ξ in the direction defined by the base vectors e_i

$$\sigma_{jk} = \Sigma_{ijk}(x,\xi) e_i \, . \tag{3-4}$$

For two dimensions (plane strain)

$$\Sigma_{ijk} = - \frac{1}{4\pi(1-\nu)} \left(\frac{1}{r}\right) \left[\delta_{ij}(1-2\nu) r_{,k} + \delta_{ik}(1-2\nu) r_{,j} - \delta_{jk}(1-2\nu) r_{,i} + 2 r_{,i} r_{,j} r_{,k}\right], \tag{3-5}$$

where ν is Poisson's ratio, δ_{ij} is the Kronecker delta, and the geometric quantities are defined, as before, in Figure 2-1. The case of plane stress is again handled through the use of an effective Poisson's ratio. Equation (3-5) is to be expanded in two dimensions only, however, in the case of plane strain the volume integral in (3-3) must include the effect of the third direction. This effect is easily incorporated through the use of Hooke's law and the assumption of incompressible plastic strains.

The quantities S and R are again chosen to exclude the region immediately surrounding the load point ξ due to the singular nature of the Kelvin problem at that point. The $\dot{u}_i(\xi)$ term in equation (3-3) results from taking the limit of the surface integrals as this region shrinks to zero, while the contribution of this region to the volume integral disappears in the limit. Note that in the absence of yielding ($\dot{\varepsilon}^p_{ij} = 0$), equation (3-3) reduces to the familiar Somigliana identity for elasticity (2-3).

Development of the boundary-integral technique proceeds, as before, by allowing the internal point ξ to pass to an arbitrary surface point z, yielding a set of integral equations which involve surface integrals over the boundary traction and displacement rates, and a volume integral of the plastic strain rate. The limiting procedure for the boundary integrals can be carried out exactly as in the elastic case (Figure 2-2 and equation 2-13), and the volume integral remains well-behaved in the limit, yielding the boundary constraint equation for elasto-plastic flow

$$(\delta_{ij}-C_{ij})\dot{u}_j(z) + \int_S \dot{u}_j(x)T_{ij}(x,z)dS(x) = \int_S \dot{t}_j(x)U_{ij}(x,z)dS(x) + \int_R \Sigma_{ijk}(x,z)\dot{\varepsilon}^p_{jk}(x)dV(x) \qquad (3\text{-}6)$$

The C_{ij} jump term results from the discontinuity in the value of the first integral in equation (3-3) as ξ passes to the surface, and is given by equation (2-14). In the case of no yielding ($\dot{\varepsilon}^p_{ik} = 0$)

equation (3-6) reduces to the elastic boundary constraint equation (2-15).

The elasto-plastic Somigliana identity (3-3) can be differentiated with respect to ξ_1 to yield an expression for displacement gradient at any point in the body

$$\dot{u}_{i,1} + \int_S \dot{u}_j(x) T_{ij,1}(x,\xi) dS(x) = \int_S \dot{t}_j(x) U_{ij,1}(x,\xi) dS(x) + \frac{\partial}{\partial \xi_1} \int_R \Sigma_{ijk}(x,\xi) \dot{\varepsilon}^p_{jk}(x) dV(x) \tag{3-7}$$

where the differentiated kernels $T_{ij,1}$ and $U_{ij,1}$ are defined as before (equation 2-12). The differentiation has not been carried inside of the volume integral in (3-7) because to do so would result in a non-integrable singularity. This equation also reduces to the standard elastic form (2-11) in the absence of plasticity.

Due to the effects of plasticity, the boundary constraint equation (3-6) is no longer strictly a boundary equation. Furthermore, the volume integration in (3-6) includes an unknown of the problem ($\dot{\varepsilon}^p_{ij}$), thereby negating the applicability of the Fredholm theorems of existence and uniqueness which apply to the singular integral equations of the elastic boundary-integral technique. For this reason, the only means for demonstrating the potential of the technique to give correct solutions to physical problems is through numerical implementation.

C. FORMULATION OF NUMERICAL SOLUTION TECHNIQUE

In order to obtain numerical solutions to the integral equations developed in the previous section, the boundary of the body is again approximated by a number of straight line segments, and the volume of the body is approximated by a number of multi-lateral elements (See Figure 3-1). Assuming that the boundary traction and displacement rates vary linearly over the boundary segments, the boundary integrals in equations (3-6) and (3-7) can be replaced by summations over the total number of boundary nodes (NNOD) in the problem as before (equations 2-18 and 2-23). Assuming further that the plastic strains are constant within each internal element, the volume integrals in these equations can be replaced by summations over the total number of internal elements (NELM) as follows

$$\int_R \Sigma_{ijk}(x,z)\dot{\varepsilon}^p_{jk}dV = \sum_{IP=1}^{NELM} \dot{\varepsilon}^p_{jk}(IP) \int_{V_{IP}} \Sigma_{ijk}(x,z)dV_{IP} \tag{3-8}$$

$$\frac{\partial}{\partial \xi_1} \int_R \Sigma_{ijk}(x,\xi)\dot{\varepsilon}^p_{jk}dV = \sum_{IP=1}^{NELM} \dot{\varepsilon}^p_{jk}(IP) \frac{\partial}{\partial \xi_1} \int_{V_{IP}} \Sigma_{ijk}(x,\xi)dV_{IP} \tag{3-9}$$

The volume integrals in equations (3-8) and (3-9) have been evaluated in closed form for a general multi-lateral element in Appendix D.

Introducing the following shorthand notation

$$\Delta\Sigma_{ijk}(M,JP) = \int_{V_{JP}} \Sigma_{ijk}(z_M, x_{JP})dV_{JP}, \tag{3-10}$$

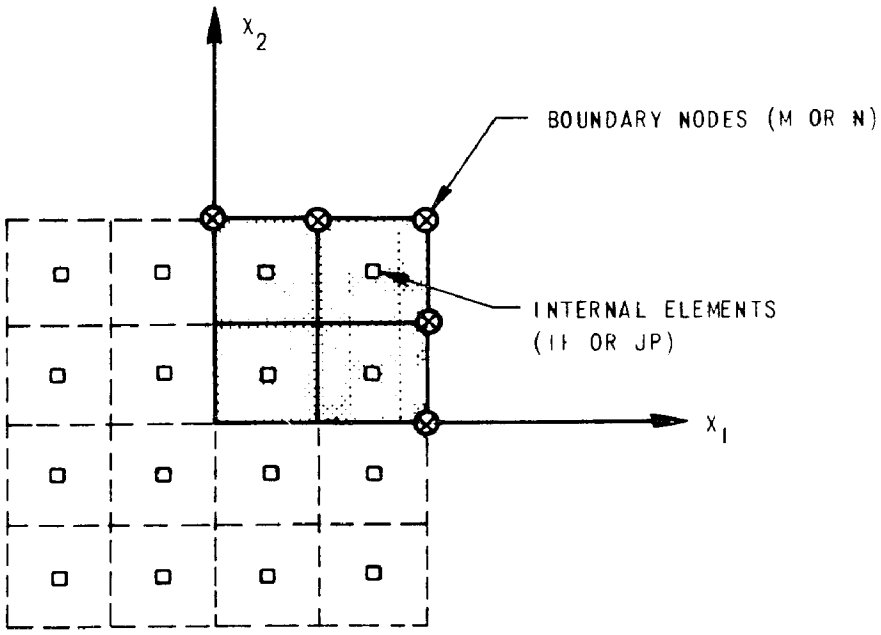

Figure 3-1 Descretization Technique for Elasto-Plastic Problems

the elasto-plastic boundary constraint equation (3-6) can be written in the following discrete form

$$A_{ij}(M,N)\dot{u}_i(N) = B_{ij}(M,N)\dot{t}_i(M) + \Delta\Sigma_{jmn}(M,JP)\dot{\varepsilon}^p_{mn}(JP) \qquad (3\text{-}11)$$

where M and N refer to boundary nodes and JP refers to internal elements (Figure 3-1). The matrices $A_{ij}(M,N)$ and $B_{ij}(M,N)$ are defined exactly as in the elastic case (equation 2-21).

Similarly, introducing the shorthand notation

$$\Delta E_{lijk}(IP,JP) = \frac{\partial}{\partial \xi_l}\int_{V_{JP}} \Sigma_{ijk}(\xi_{IP},x_{JP})dV_{JP}, \qquad (3\text{-}12)$$

the differentiated elasto-plastic Somigliana identity can be written in the following discrete form for total strain rates

$$\dot{\varepsilon}_{li}(IP) = \Delta E_{lijk}(IP,JP)\dot{\varepsilon}^p_{jk}(JP) + \Delta S_{lin}(IP,M)\dot{t}_n(M) - \Delta D_{lin}(IP,M)\dot{u}_n(M), \qquad (3\text{-}13)$$

where IP and JP refer to internal elements and M refers to boundary nodes (Figure 3-1). The matrices ΔS_{lin} and ΔD_{lin} are defined exactly as in the elastic case (equation 2-25).

Equations (3-11) and (3-13) are tensorial matrix equations, and care must be taken to maintain consistency in subscripts and terms of the matrices. For illustrative purposes it is convenient to expand the two sets of equations tensorially as follows

$$\begin{bmatrix} A_{11}(M,N) & A_{12}(M,N) \\ A_{21}(M,N) & A_{22}(,NN) \end{bmatrix} \begin{Bmatrix} \dot{u}_1(N) \\ \dot{u}_2(N) \end{Bmatrix} = \begin{bmatrix} B_{11}(M,N) & B_{12}(M,N) \\ B_{21}(M,N) & B_{22}(M,N) \end{bmatrix} \begin{Bmatrix} \dot{t}_1(N) \\ \dot{t}_2(N) \end{Bmatrix}$$

$$+ \begin{bmatrix} \Delta\Sigma_{111}(M,IP) & \Delta\Sigma_{112}(M,IP) & \Delta\Sigma_{122}(M,IP) \\ \Delta\Sigma_{211}(M,IP) & \Delta\Sigma_{212}(M,IP) & \Delta\Sigma_{222}(M,IP) \end{bmatrix} \begin{Bmatrix} \dot{\varepsilon}^P_{11}(IP) \\ \dot{\varepsilon}^P_{12}(IP) \\ \dot{\varepsilon}^P_{22}(IP) \end{Bmatrix} \qquad (3\text{-}14)$$

$$\begin{Bmatrix} \dot{\varepsilon}_{11}(IP) \\ \dot{\varepsilon}_{12}(IP) \\ \dot{\varepsilon}_{22}(IP) \end{Bmatrix} = \begin{bmatrix} \Delta E_{1111}(IP,JP) & \Delta E_{1112}(IP,JP) & \Delta E_{1122}(IP,JP) \\ \Delta E_{1211}(IP,JP) & \Delta E_{1212}(IP,JP) & \Delta E_{1222}(IP,JP) \\ \Delta E_{2211}(IP,JP) & \Delta E_{2212}(IP,JP) & \Delta E_{2222}(IP,JP) \end{bmatrix} \begin{Bmatrix} \dot{\varepsilon}^P_{11}(JP) \\ \dot{\varepsilon}^P_{12}(JP) \\ \dot{\varepsilon}^P_{22}(JP) \end{Bmatrix}$$

$$+ \begin{bmatrix} \Delta S_{111}(IP,M) & \Delta S_{112}(IP,M) \\ \Delta S_{121}(IP,M) & \Delta S_{122}(IP,M) \\ \Delta S_{221}(IP,M) & \Delta S_{222}(IP,M) \end{bmatrix} \begin{Bmatrix} \dot{t}_1(M) \\ \dot{t}_2(M) \end{Bmatrix} \qquad (3\text{-}15)$$

$$- \begin{bmatrix} \Delta D_{111}(IP,M) & \Delta D_{112}(IP,M) \\ \Delta D_{121}(IP,M) & \Delta D_{122}(IP,M) \\ \Delta D_{221}(IP,M) & \Delta D_{222}(IP,M) \end{bmatrix} \begin{Bmatrix} \dot{u}_1(M) \\ \dot{u}_2(M) \end{Bmatrix}$$

The constitutive relations for elasto-plastic flow are discussed at length in references [3, 33, and 34]. The form of the flow rule to be used presently is developed in Appendix E. Using the flow rule, the plastic strain rates $\dot{\varepsilon}^{p}_{ij}$ can be expressed in terms of the total strain rates $\dot{\varepsilon}_{ij}$ at each internal element as follows

$$\dot{\varepsilon}^{p}_{ij} = \frac{3}{2} \frac{S_{ij}S_{kl}\dot{\varepsilon}_{kl}}{\sigma_{eq}^{2}(1+P/3\mu)} = \Gamma_{ijkl}\dot{\varepsilon}_{kl} \qquad (3\text{-}16)$$

where σ_{eq} is the current von Mises equivalent stress, S_{ij} and S_{kl} are the current deviatoric stress tensors, P is the current plastic modulus ($\dot{\sigma}_{eq}/\dot{\varepsilon}^{p}_{eq}$) and μ is the elastic shear modulus of the material.

At any point in time during the loading or unloading of the structure, equation (3-16) can be incorporated into (3-15) to eliminate explicit reference to total strain rates ($\dot{\varepsilon}_{ij}$) in that equation. Thus equation (3-15), when combined with the flow rule, represents a total of 3xNELM equations whose unknowns are internal plastic strain rates (3xNELM) and either boundary traction or boundary displacement rates (2xNNOD). Equation (3-14) represents another 2xNNOD equations in the same unknowns, and thus the total number of equations is consistent with the total number of unknowns at a discrete time point during loading. All that remains is to devise a solution procedure.

Two solution procedures were considered and discarded before deciding upon the actual strategy used to solve the equations. The first and most straightforward would be to combine equations (3-14)

and (3-15) into one large set of simultaneous equations, to be solved at each load increment during the loading and unloading of the structure. However, this method would be very costly in terms of computer storage requirements, and thus would greatly limit the allowable problem size. For example, assuming that 60,000 octal words of core are available for matrix manipulations, the maximum problem size that could be solved would be equivalent to 22 boundary nodes and 22 internal elements. Most of the interesting problems solved with the elastic program (Chapter II-D) required more than 30 boundary nodes to obtain satisfactory solutions, so it was decided that this limitation would be overly restrictive.

The second solution procedure to be considered and discarded was an iterative approach. Equation (3-14) could be solved using a trial set of plastic strain rates. The boundary traction and displacement rates could then be substituted into equation (3-15) to come up with a new set of plastic strain rates, and this process could be repeated until the solution converged. However, since the procedure is already incremental with respect to loading or unloading, it was decided that the computer time required to iterate at each load increment would be prohibitive.

In order to avoid the undesirable aspects of the previously discussed solution procedures, a set of auxiliary relationships were developed from the flow rule, and equation (3-14) was then

expanded into a square matrix equation by means of these relationships.* Equation (3-14) could then be inverted to yield an explicit relation for plastic strains which was used in conjunction with equation (3-15) to yield a set of equations which contain only the boundary displacement and traction rates, and which contain the effect of the volume integral of plastic strain rates implicitly rather than explicitly. The total size of the matrix equation is (3xNNOD) by (3xNNOD), and thus 60,000 octal words of core for matrix manipulation would allow a maximum problem size of 36 boundary nodes and 36 internal elements. Furthermore, this solution procedure requires no iteration. Internal stress and strain data for an increment are obtained by straightforward quadrature after the boundary solution has been obtained. The development of this third solution technique is summarized below.

The elastic strain rates must satisfy Hooke's law

$$\dot{\sigma}_{ij} = 2\mu\dot{\varepsilon}^{e}_{ij} + \left(\frac{2\mu\nu}{1-2\nu}\right)\dot{\varepsilon}^{e}_{kk}, \tag{3-17}$$

$$\text{but} \quad \dot{\varepsilon}^{e}_{ij} = \dot{\varepsilon}_{ij} - \dot{\varepsilon}^{p}_{ij}$$

$$\dot{\varepsilon}^{p}_{kk} = 0 .$$

Therefore equation (3-17) can be written in terms of total strain rates

---

*Inherent in this procedure is the requirement that the number of boundary nodes (NNOD) be equal to the number of internal elements (NELM). This requirement was not considered to be overly restrictive.

$$\dot{\sigma}_{ij} = 2\mu(\dot{\varepsilon}_{ij} - \dot{\varepsilon}^{p}_{ij}) + \left(\frac{2\mu\nu}{1-2\nu}\right) \dot{\varepsilon}_{kk}. \tag{3-18}$$

Expanding equation (3-18) in the x_3 (out of plane) direction yields

$$\frac{\dot{\sigma}_{33}}{2\mu} = \dot{\varepsilon}_{33} - \dot{\varepsilon}^{p}_{33} + \left(\frac{\nu}{1-2\nu}\right) (\dot{\varepsilon}_{11}+\dot{\varepsilon}_{22}+\dot{\varepsilon}_{33}), \tag{3-19}$$

and utilizing the last of equations (3-17)

$$\frac{\dot{\sigma}_{33}}{2\mu} = \dot{\varepsilon}_{33} + (\dot{\varepsilon}^{p}_{11}+\dot{\varepsilon}^{p}_{22}) + \left(\frac{\nu}{1-2\nu}\right) (\dot{\varepsilon}_{11}+\dot{\varepsilon}_{22}+\dot{\varepsilon}_{33}). \tag{3-20}$$

It is convenient now to introduce the notation of traction and displacement rates for each internal element in the x_3 direction

$$\begin{aligned} \dot{t}_3(IP) &= \dot{\sigma}_{33} \\ \dot{u}_3(IP) &= \dot{\varepsilon}_{33}. \end{aligned} \tag{3-21}$$

From equation (3-15), the sum of the total strain rates can be expressed as the following quadrature

$$\begin{aligned} \dot{\varepsilon}_{11}(JP) + \dot{\varepsilon}_{22}(JP) = {} & [\Delta E_{11ik}(IP,JP) + \Delta E_{22ik}(IP,JP)]\dot{\varepsilon}^{p}_{ik}(JP)] \\ & + [\Delta S_{11i}(IP,N) + \Delta S_{22i}(IP,N)]\dot{t}_i(N) - [\Delta D_{11i}(IP,N) \\ & + \Delta D_{22i}(IP,N)]\dot{u}_i(N) \end{aligned} \tag{3-22}$$

Finally, substituting equations (3-21) and (3-22) back into (3-20) and rearranging yields the auxiliary relationship for the x_3 direction

$$\left[\Delta D_{11i}(IP,N) + \Delta D_{22i}(IP,N)\right] \left\{\dot{u}_i(N)\right\} + \left(\frac{\nu-1}{\nu}\right) \dot{u}_3(IP) =$$

$$\left[\Delta S_{11i}(IP,N) + \Delta S_{22i}(IP,N)\right] \left\{\dot{t}_i(N)\right\} + \left(\frac{2\nu-1}{\mu\nu}\right) \dot{t}_3(IP)$$

$$+ \left[-\Delta E_{11ik}(IP,JP) - \Delta E_{22ik}(IP,JP)\right] \left\{\dot{\varepsilon}^p_{ik}(JP)\right\} \qquad (3\text{-}23)$$

$$+ \left(\frac{1-2\nu}{\nu}\right) \left[\dot{\varepsilon}^p_{11}(IP) + \dot{\varepsilon}^p_{22}(IP)\right]$$

The auxiliary relationship (3-23) can now be added to the elasto-plastic boundary constraint equation (3-14), converting that equation into a square matrix equation (provided the number of boundary nodes is equal to the number of internal elements)

$$\begin{bmatrix} A_{11}(M,N) & A_{12}(M,N) & 0 \\ A_{21}(M,N) & A_{22}(M,N) & 0 \\ \Delta D_{111}(JP,N) + \Delta D_{221}(JP,N) & \Delta D_{112}(JP,N) + \Delta D_{222}(JP,N) & \begin{matrix} \frac{\nu-1}{\nu} & & 0 \\ & \ddots & \\ 0 & & \end{matrix} \end{bmatrix} \begin{Bmatrix} \dot{u}_1(N) \\ \dot{u}_2(N) \\ \dot{u}_3(N) \end{Bmatrix} =$$

$$
\begin{bmatrix}
B_{11}(M,N) & B_{12}(M,N) & 0 \\
B_{21}(M,N) & B_{22}(M,N) & 0 \\
\Delta S_{111}(JP,N) + \Delta S_{221}(JP,N) & \Delta S_{112}(JP,N) + \Delta S_{222}(JP,N) & \frac{2\nu-1}{\mu\nu} \quad 0
\end{bmatrix}
\begin{Bmatrix}
\dot{t}_1(N) \\ \dot{t}_2(N) \\ \dot{t}_3(N)
\end{Bmatrix}
$$

(3-24)

$$
+
\begin{bmatrix}
\Delta\Sigma_{111}(M,IP) & \Delta\Sigma_{112}(M,IP) & \Delta\Sigma_{122}(M,IP) \\
\Delta\Sigma_{211}(M,IP) & \Delta\Sigma_{212}(M,IP) & \Delta\Sigma_{222}(M,IP) \\
\left(\frac{1-2\nu}{\nu}\right) I(M,IP) & & \left(\frac{1-2\nu}{\nu}\right) I(M,IP) \\
-\Delta E_{1111}(JP,IP) & -\Delta E_{1112}(JP,IP) & -\Delta E_{1122}(JP,IP) \\
-\Delta E_{2211}(JP,IP) & -\Delta E_{2212}(JP,IP) & -\Delta E_{2222}(JP,IP)
\end{bmatrix}
\begin{Bmatrix}
\dot{\varepsilon}^p_{11}(IP) \\ \dot{\varepsilon}^p_{12}(IP) \\ \dot{\varepsilon}^p_{22}(IP)
\end{Bmatrix}
$$

We are now dealing with square matrices of size (3xNNOD) by (3xNNOD), and can proceed to solution using standard matrix operations as follows.

Solving equation (3-24) for plastic strain rates yields

$$\left\{ \dot{\varepsilon}^{p}_{ij}(IP) \right\} = \left[\Delta\Sigma^{-1}_{ijk}(IP,M) \right]\left[A_{kl}(M,N) \right] \left\{ \dot{u}_{l}(N) \right\} - \left[\Delta\Sigma^{-1}_{ijk}(IP,M) \right]\left[B_{kl}(M,N) \right] \left\{ \dot{t}_{l}(N) \right\} \tag{3-25}$$

where $\Delta\Sigma^{-1}_{ijk}(IP,M)$ is the matrix inverse of $\Delta\Sigma_{ijk}(IP,M)$. A further limitation of the implementation occurs here. Since the $\Delta\Sigma_{ijk}(IP,M)$ matrix has been inverted, it must not contain redundant rows. However, the zero-length segment convenience which was introduced in Chapter II-C and Appendix B would result in two identical rows in that matrix. This problem was circumvented by using very short (but not zero-length) segments to characterize a step change in boundary tractions. While the presence of very short boundary segments adjacent to larger segments is detrimental to the conditioning of the resulting matrix equations, it was not found to be debilitating in the sample problems which were solved (Chapter III-D)

Substituting equation (3-25) back into (3-15), and applying the flow rule (3-16) yields a second expression for plastic strain rates

$$\left\{\dot{\varepsilon}^{p}_{ij}(IP)\right\} = \left\{\Gamma_{ijmn}(IP)\right\}\left[\ \alpha_{mnq}(IP,N)\ \right]\left\{\dot{u}_q(N)\right\} - \left\{\Gamma_{ijmn}(IP)\right\}\left[\ \beta_{mnq}(IP,N)\ \right]\left\{\dot{t}_q(N)\right\} \tag{3-26a}$$

where:

$$\left[\alpha_{mnq}(IP,N)\right] = \left[\Delta E_{mnkl}(IP,JP)\right]\left[\Delta\Sigma^{-1}_{klp}(JP,N)\right]\left[A_{pq}(M,N)\right] - \left[\Delta D_{mnq}(IP,N)\right] \tag{3-26b}$$

$$\left[\beta_{mnq}(IP,N)\right] = \left[\Delta E_{mnkl}(IP,JP)\right]\left[\Delta\Sigma^{-1}_{klp}(JP,N)\right]\left[B_{pq}(M,N)\right] - \left[\Delta S_{mnq}(IP,N)\right]$$

Finally, setting the two expressions for plastic strain rates (3-25 and 3-26) equal to each other yields a single matrix equation for boundary traction and displacement rates, which contains the volume integral over the plastic strain rates implicitly

$$\left[\left[\Delta\Sigma^{-1}_{ijp}(IP,N)\right]\left[\ A_{pq}(M,N)\ \right] - \left\{\Gamma_{ijmn}(IP)\right\}\left[\alpha_{mnq}(IP,N)\right]\right]\left\{\dot{u}_q(N)\right\} = \left[\left[\Delta\Sigma^{-1}_{ijp}(IP,N)\right]\left[\ B_{pq}(M,N)\ \right] - \left\{\Gamma_{ijmn}(IP)\right\}\left[\beta_{mnq}(IP,N)\right]\right]\left\{\dot{t}_q(N)\right\} . \tag{3-27}$$

Equation (3-27) is particularly well suited to an incremental approach to the elasto-plastic flow problem [35], because the only quantity which changes during the course of loading or unloading is the $\Gamma_{ijmn}(IP)$ matrix. The other matrices need be computed only once at the beginning of the problem, and can be stored in peripheral storage for use thereafter. Note that in the case of elasticity, the $\Gamma_{ijmn}(IP)$ term goes to zero, and equation (3-27) reduces to the familiar elastic boundary constraint equation (2-20), with a constant multiplier on both sides of the equation ($\Delta\Sigma^{-1}_{ijp}$).

In order to apply equation (3-27) to an elasto-plastic flow problem, the loading or unloading of the structure is considered to occur as a series of discrete load increments, which are input as either displacement rates or traction rates (or a mixture, providing the problem is well-posed). The first increment should be of a magnitude to just cause incipient yielding of the highest stressed element in the model. Thus for the first step, the $\Gamma_{ijmn}(IP)$ terms will be zero. The resulting solution will yield values for the unknown traction or displacement rates which can then be substituted into equation (3-25) or (3-26) to obtain plastic strains, from which the remaining stress and strain internal data can be computed using the flow rule. From the internal stress and strain data, new values of the $\Gamma_{ijmn}(IP)$ terms can be computed for use in the next load step. This process can be continued to as high a level of applied

loading as desired. Equation (3-27) must be solved once for each load step, and the remaining data for the load step are generated by simple quadrature from that solution.

A computer program (BITEP) has been written to implement this solution procedure. A flow chart and a set of input instructions for this program are given in Appendix F. The program requires approximately 150,000 octal words of core to execute, of which only 60,000 are available for matrix manipulations. Thus the program admits a maximum of thirty-six boundary segments and internal elements. An additional 200,000 octal words of peripheral storage are used to store the various matrices in equation (3-27) which are computed once and then reused at each load step. The program is currently operating on a CDC-7600 computer, on which extended core storage area is used for peripheral storage, however, it could be modified rather easily to make use of disc or drum area for peripheral storage in order to run on machines which do not have extended core storage capability. The range, accuracy, and limitations of the computer program BITEP are demonstrated through a series of example problems in the following Section.

D. NUMERICAL RESULTS

This Section presents a series of example problems in two-dimensional elasto-plasticity (plane strain) solved using the boundary-integral technique developed in Section C of this Chapter. The complexity of the problems solved ranged from very simple problems with homogeneous stress and strain fields, which were used to check out the basic functioning and limitations of the computer program, to relatively complex problems involving large stress and strain concentrations. Comparisons are made with exact solutions where such solutions are available, and in some cases comparison runs were made using an elasto-plastic finite element computer program [36]. A variety of stress-strain curves were used for these problems, ranging from a relatively smooth curve with large amounts of strain hardening to a relatively flat curve with a sharp yield point. (See Figure 3-2).

1. Unit Square Problems - As in Chapter II, the basic unit square problem, loaded both in uniaxial tension and pure shear, was used as a qualification check for the computer program. The models used are shown in Figure 3-3. This figure shows both the boundary node and the internal element configurations which were used. Curve A from Figure 3-2 was used as a stress-strain for these problems.

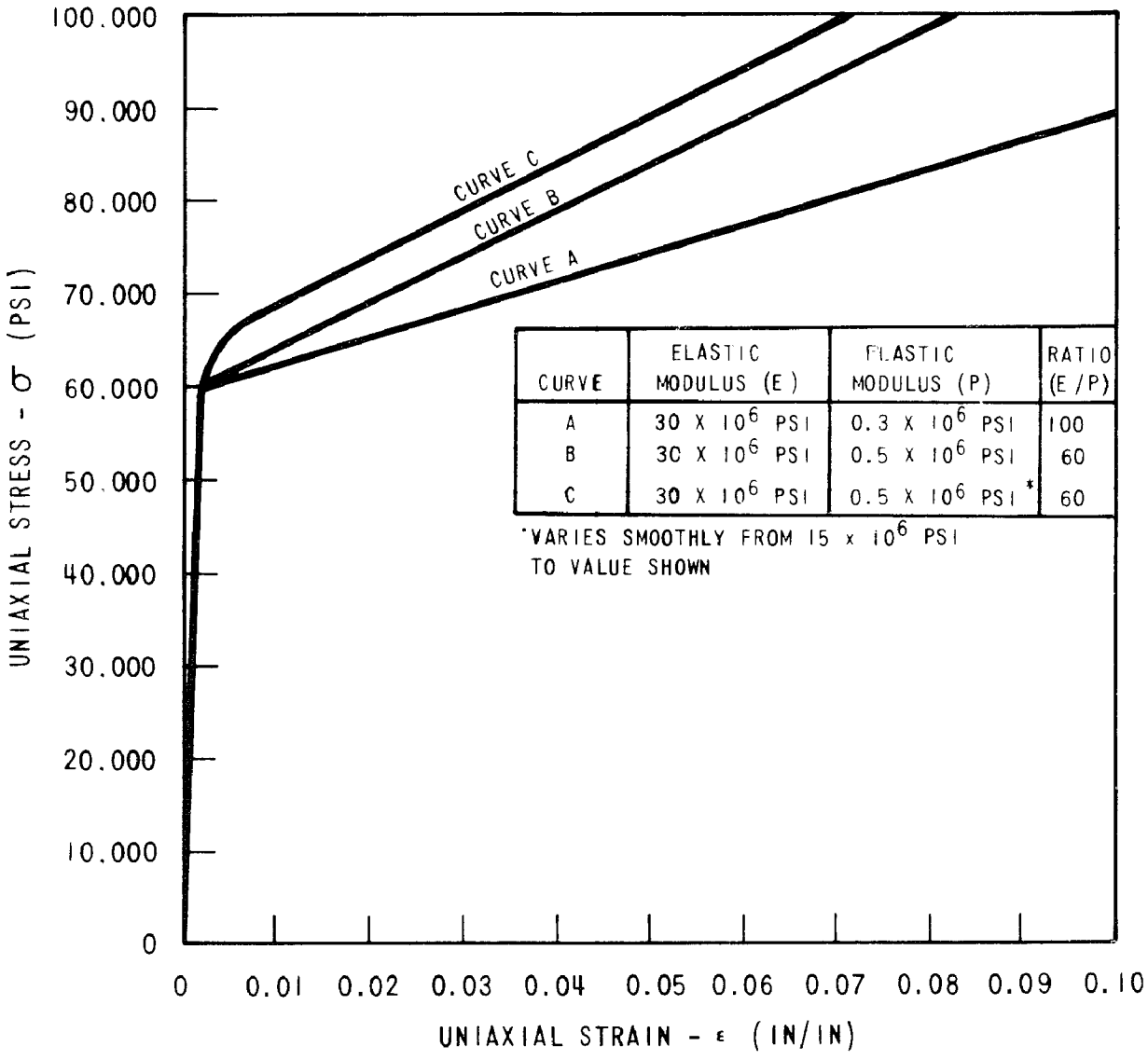

Figure 3-2 Stress-Strain Data Used for Elasto-Plastic Example Problems

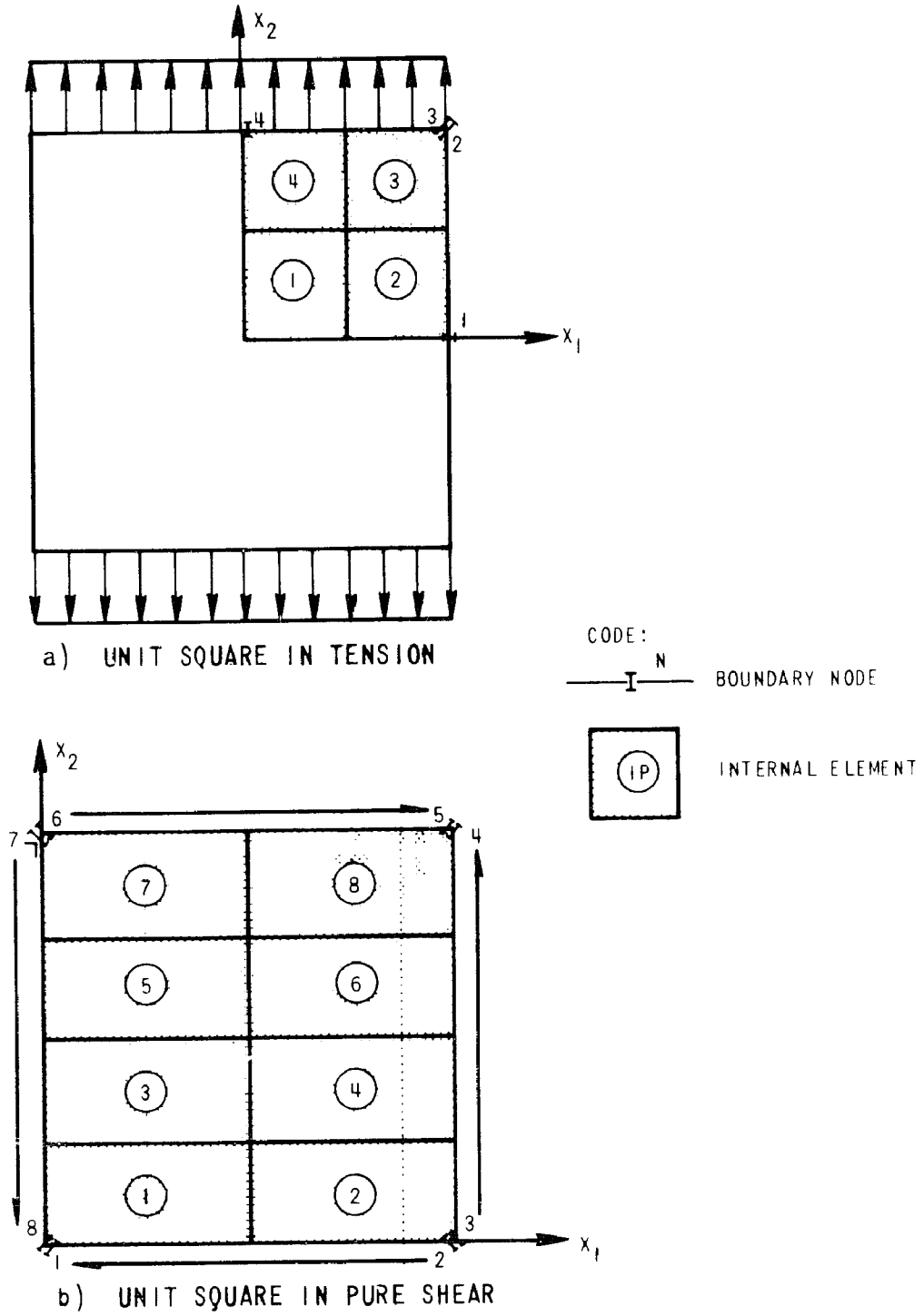

Figure 3-3. Elasto-Plastic Boundary-Integral Models for Unit Square Problems

An initial load increment of 67,622 PSI was applied to the unit square in tension, and subsequent load increments of 1,000 PSI were used, up to a total load of 82,622 PSI. The initial loading was chosen so that incipient yielding occurs on the first load step. Figure 3-4 shows the computed results for load step 12, which is far enough past the knee of the strain stress curve for the plasticity to have stabilized. This figure gives the boundary traction and displacement data, both incremental and total, and the internal stress and strain data. Note that there is more variation in the stresses from element to element than there was in the elastic case (Figure 2-6). Also, small but non-zero reaction forces appear on nodes 1 and 4, where there were none in the elastic case. These numerical perturbations are probably due to the very short (but not "zero length") boundary segment which must be inserted in the elasto-plastic case. Figure 3-5 shows a comparison of the numerical results with the exact load-deflection curve for the problem. Two sets of numerical data are given: The load versus displacement at the boundary, and the average stress versus strain in the x_2-direction in the four internal elements. The agreement between the numerical and exact solutions is excellent, and serves as an initial indication that the boundary-integral technique can be applied to elasto-plastic problems.

INCREMENTAL BOUNDARY SOLUTION (STEP 12)

NODE	X1-COORDINATE DIRECTION KNOWN	DELTA-U1	DELTA-T1	X2-COORDINATE DIRECTION KNOWN	DELTA-U2	DELTA-T2	X3-COORDINATE DIRECTION KNOWN	DELTA-U3	DELTA-T3
1	TRAC	-0.001250541	-0.000	DISP	-0.000000000	2.294	DISP	-0.000000000	498.686
2	TRAC	-0.001249714	0.000	TRAC	0.001259485	0.000	DISP	0.000000000	498.945
3	TRAC	-0.001247216	-0.000	TRAC	0.001259496	1000.000	DISP	-0.000000000	503.412
4	DISP	-0.000000000	14.615	TRAC	0.001260774	1000.000	DISP	-0.000000000	499.185

TOTAL BOUNDARY VALUES (STEP 12)

NODE	TOTAL DISPLACEMENTS U1	U2	U3	TOTAL TRACTIONS T1	T2	T3
1	-0.010295990	0.000000000	0.000000000	0.000	145.720	38692.585
2	-0.010278947	0.011047737	0.000000000	0.000	0.000	38685.864
3	-0.010258400	0.011048545	0.000000000	0.000	78000.000	38821.222
4	0.000000000	0.011080255	0.000000000	276.717	78000.000	38688.329

INTERNAL STRESSES (STEP 12, ITER 1)

IP	KEY	SIGMA-11	SIGMA-12	SIGMA-22	SIGMA-33	GEN STRESS	YIELD STRESS
1	3	-120.4	1.9	77809.7	38692.6	67489.7	67489.7
2	3	-76.4	9.7	77753.2	38685.9	67402.5	67402.5
3	3	32.9	-17.5	77915.8	38821.2	67448.7	67448.7
4	3	-62.8	-8.1	77744.4	38688.3	67383.2	67383.2

INTERNAL STRAINS (STEP 12, ITER 1)

IP	KEY	EPS-11	EPS-12	EPS-22	EPS-33	GEN PL STRAIN	RSOS
1	3	-0.020604299	0.000000905	0.022156057	0.000000000	0.024468499	0.326491E-09
2	3	-0.020580548	0.000004375	0.022132050	0.000000000	0.024335586	0.327317E-09
3	3	-0.020589006	-0.000018808	0.022145938	0.000000000	0.024395262	0.326880E-09
4	3	-0.020552389	-0.000014914	0.022103989	0.000000000	0.024286275	0.327503E-09

Figure 3-4 Computer Results for Unit Square in Tension (Elasto-Plastic)

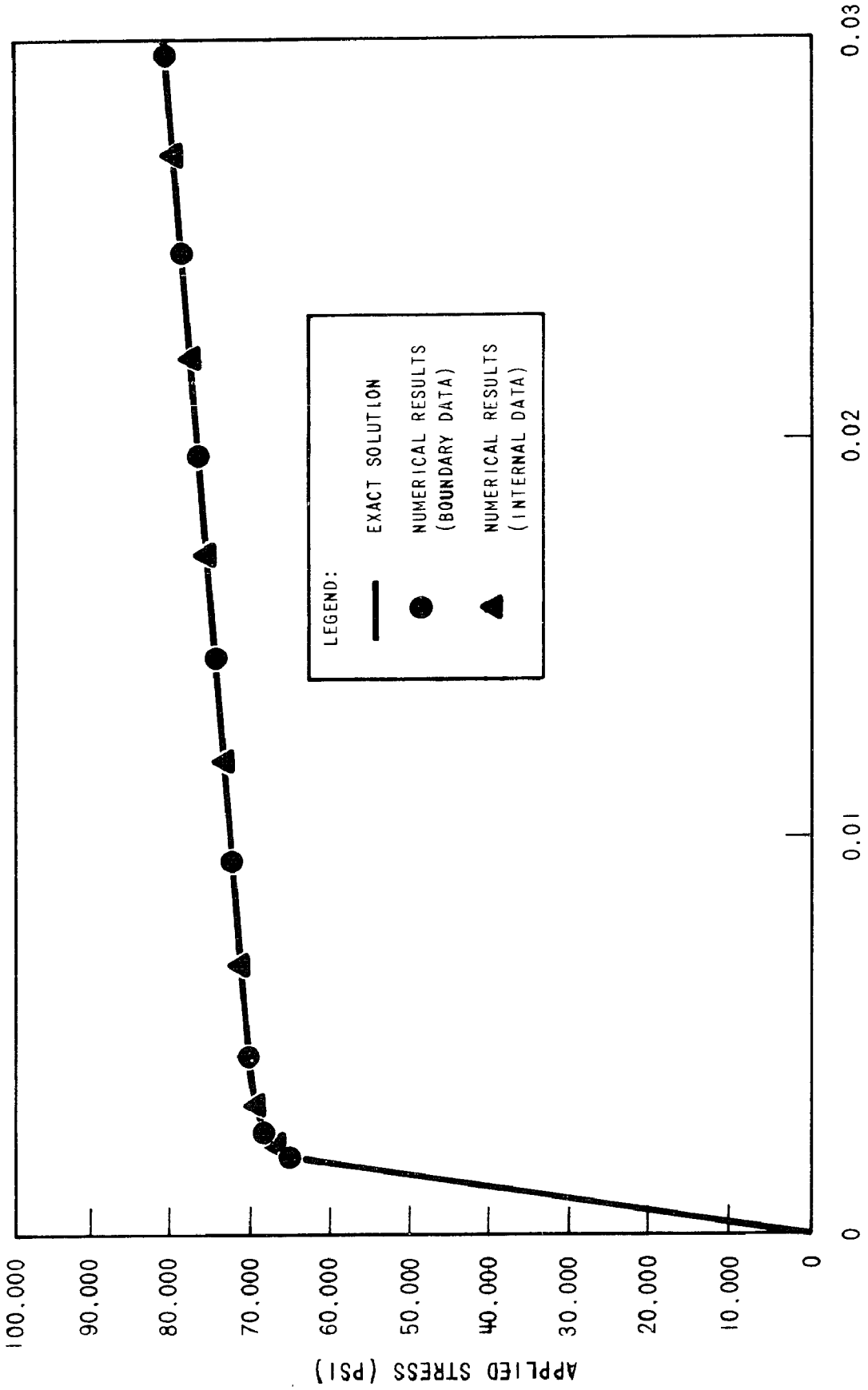

Figure 3-5 Comparison of Analytical and Numerical Data for Elasto-Plastic Unit Square in Tension Problem

An initial pure shear loading of 34,600 psi was chosen for the unit square in pure shear problem, in order to obtain incipient yielding on the first load step. Subsequent load increments of 500 PSI were then applied, up to a total load of 39,600 PSI. A shear load versus shear strain plot for this problem is given in Figure 3-6. Numerical results from both the boundary data and the internal data are compared to the exact solution to the problem in this figure. The agreement between the numerical and exact solutions is again excellent.

While these two problems are trivial in nature, they do serve as verification that the boundary integral technique, as formulated in [32] and implemented here, does in fact work for problems of elasto-plasticity. Such verification was necessary before proceeding to more complex problems.

2. *Circular Cutout Problems* - The problem of an infinite plate with a circular cutout under uniform tension (both biaxial and uniaxial) at the infinite boundary was the next to be considered (See Figure 3-7). This problem is considerably more challenging than the previous example problems in that it contains significant stress and strain gradients.

The superposition technique illustrated in Figure 2-10 could not be applied here due to non-linearity. The boundary-integral model used for these problems is shown in Figure 3-8. Only the

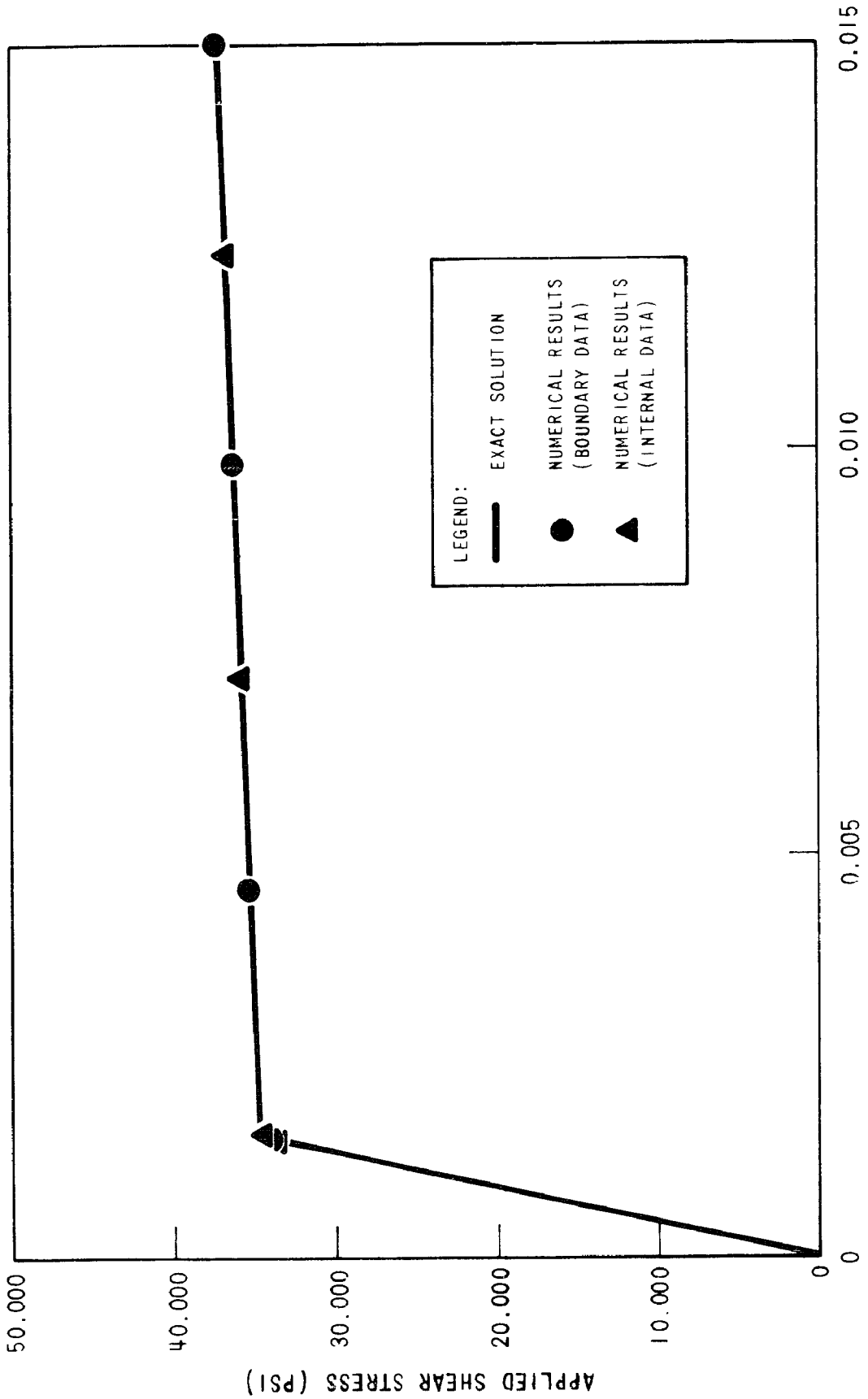

Figure 3.6 Comparison of Analytical and Numerical Data for Unit Square in Pure Shear

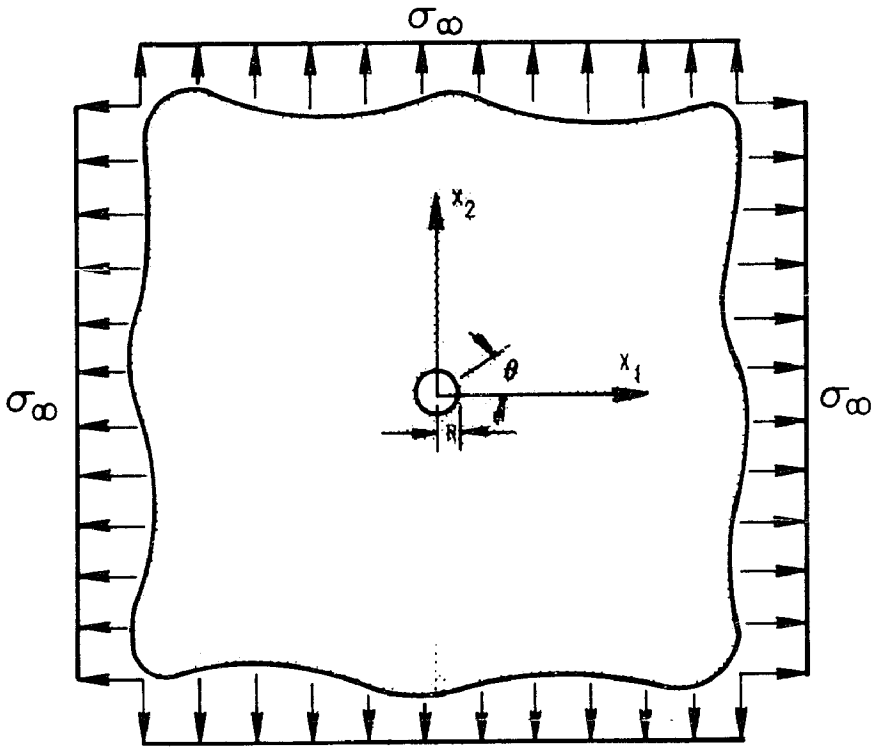

a) BIAXIAL TENSION CASE

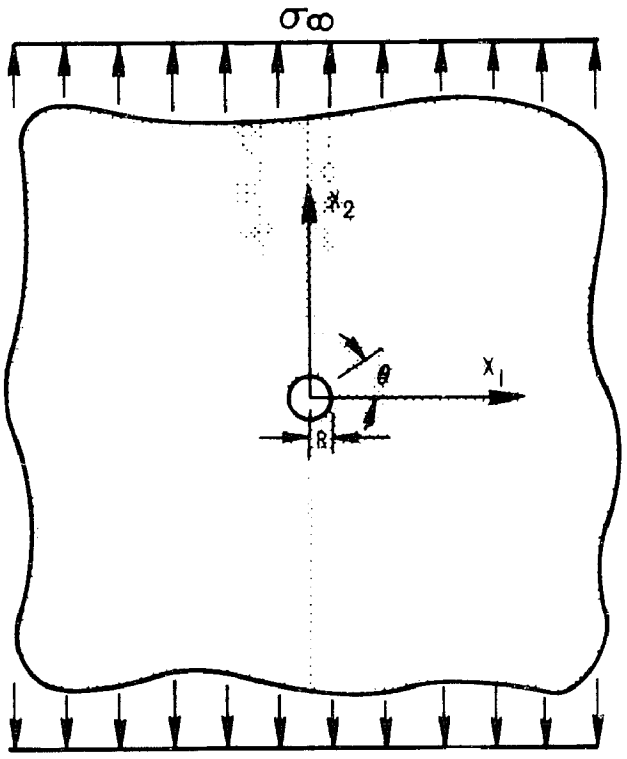

b) UNIAXIAL TENSION CASE

Figure 3-7 **Elasto-Plastic Infinite Plate** with Circular **Cutout Problems**

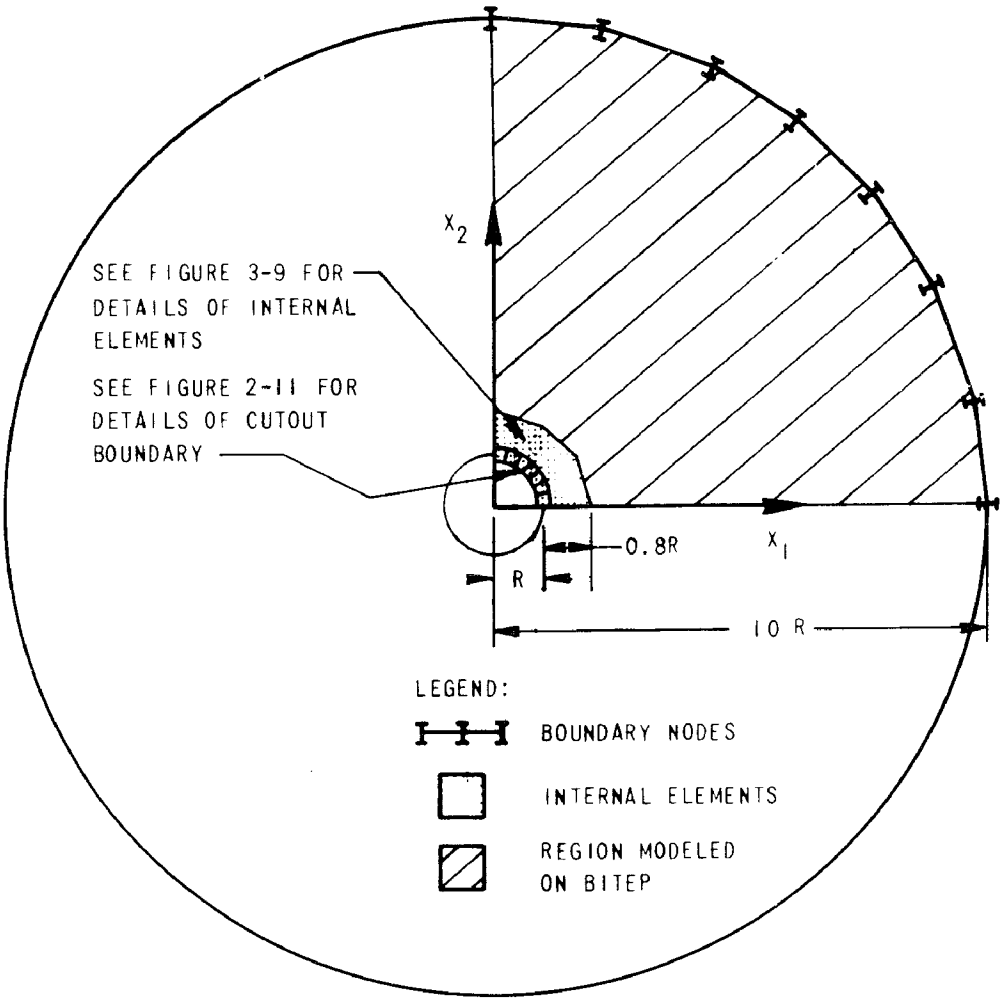

Figure 3-8 **Boundary Integral Model Used for Elasto-Plastic Circular Cutout Problems**

first quadrant was modelled due to symmetry. Twenty-five boundary segments were used to model the circular cutout boundary (see Figure 2-11), and an additional seven segments were used to model the outer circular boundary, which was placed at a radius equal to ten times that of the cutout. A total of thirty-four boundary nodes are required for this model, and thus thirty-four internal elements were used for the volume integration procedure (see Figure 3-9). In order to provide adequate detail very close to the cutout, only the region within 0.8R of the cutout was included in the internal element array, and thus the analysis is expected to break down when the plastic zone exceeds this region. Stress-strain curve A from Figure 3-2 was again used for these problems.

For the biaxial loading case, a uniform radial traction was applied to the outer circular boundary as follows

$$\sigma_{11} = \sigma_\infty \cos\theta$$
$$\sigma_{22} = \sigma_\infty \sin\theta \qquad (3\text{-}52)$$

Where θ is the angle from the x_1 axis (See Figure 3-7). For the uniaxial case, σ_{11} was set equal to zero in equations (3-52). The initial load increment in both cases was chosen so as to cause incipient yielding of the most highly stressed element. This level of loading corresponded to

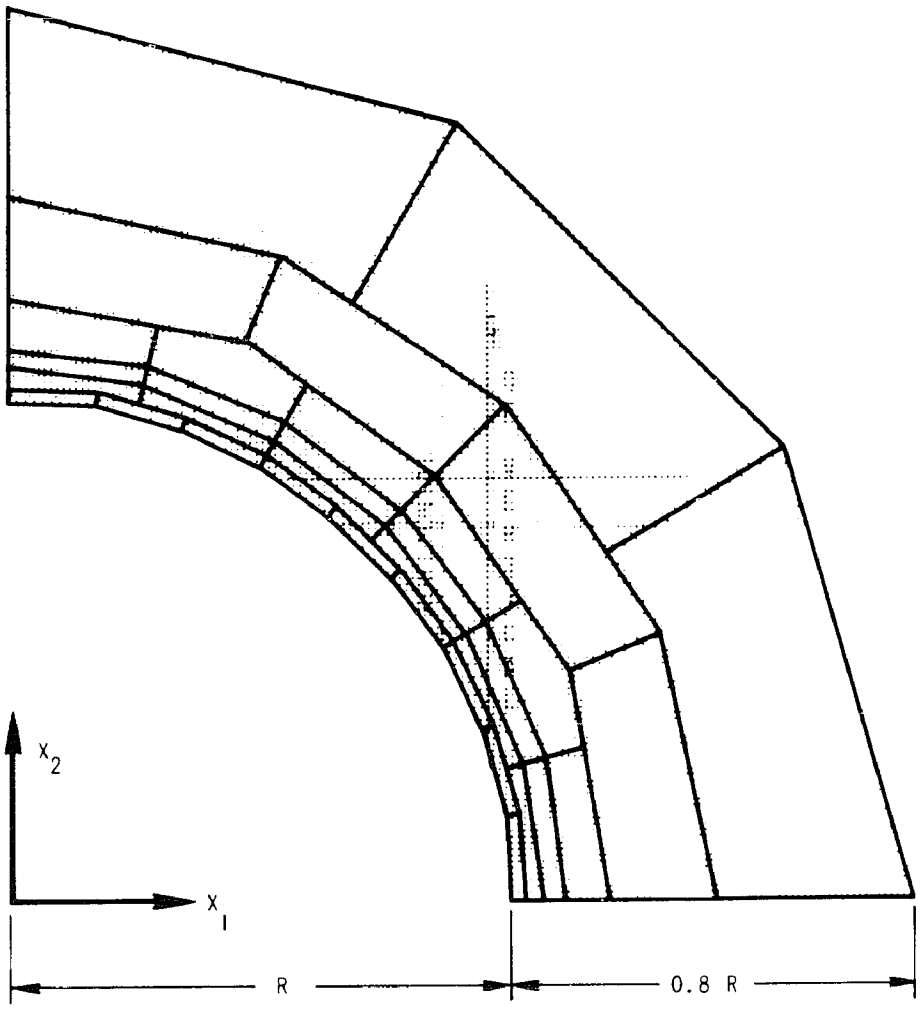

Figure 3-9 **Internal Element Configuration** for Bited Model of **Elasto-Plastic Circular** Cutout Problems

$$\lambda = 0.562 \quad \text{(Biaxial)}$$
$$\lambda = 0.381 \quad \text{(Uniaxial)} \tag{3-53}$$

where λ is defined as the ratio of the applied stress (σ_∞) to the material yield strength. Note that that biaxial case requires a significantly higher load to cause yielding than the uniaxial case. The loading was then successively incremented by 2.5 percent per load step, up to a load ratio (λ) equal to unity. This required twenty-four load steps for the biaxial case and forty load steps for the uniaxial case. The amount of computation time required for each of these problems on a CDC-7600 computer is summarized in Table III.

TABLE III - BOUNDARY INTEGRAL COMPUTER TIME FOR CIRCULAR CUTOUT PROBLEMS

Loading	Number of Load Steps	CDC-7600 CPU Time
Biaxial	24	1.50 Min
Uniaxial	40	2.24 min

The same set of problems was also solved with an elasto-plastic finite element computer program [36], using the model shown in Figure 3-10. This model required significantly more input data to

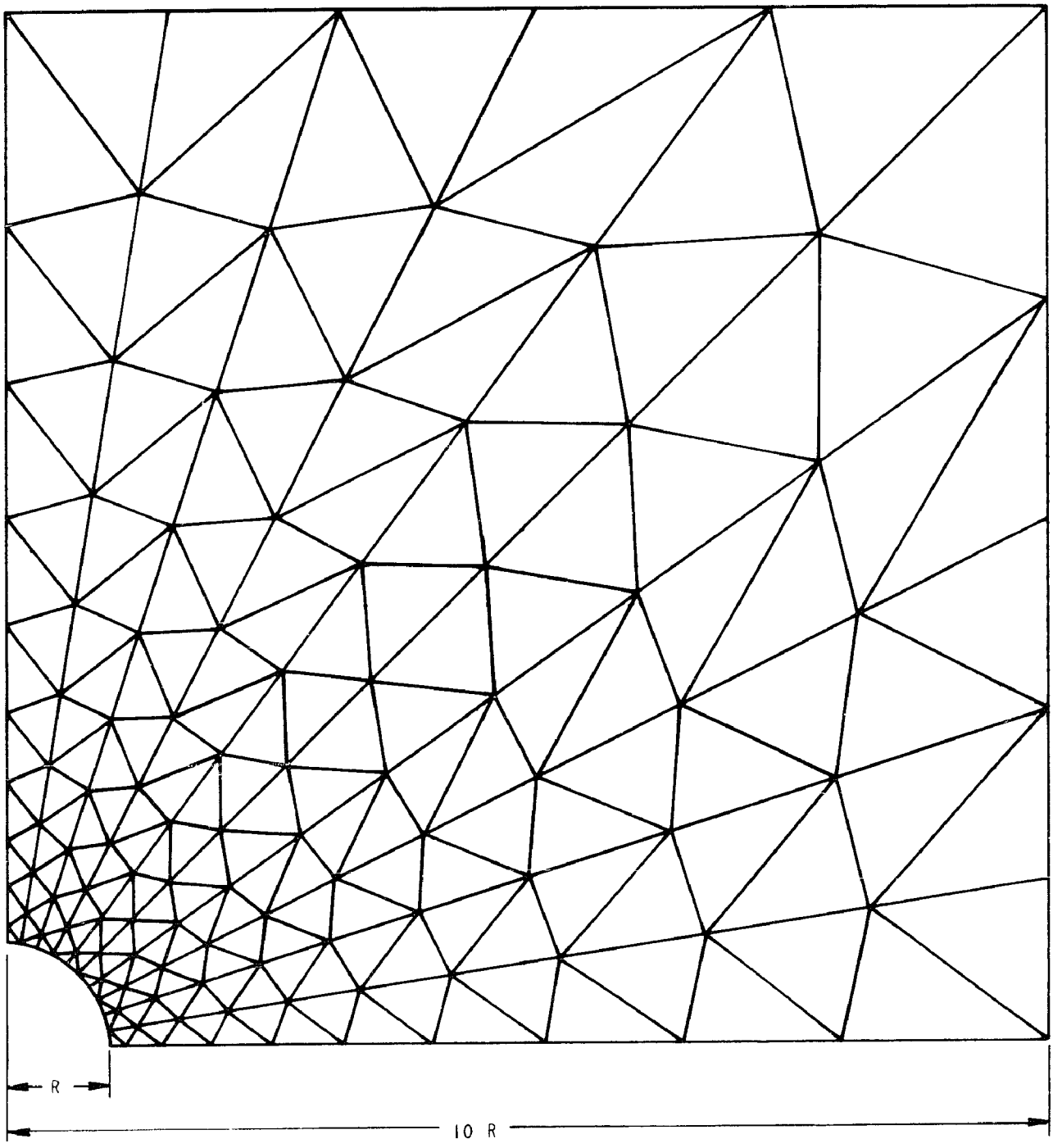

Figure 3-10 Finite Element Model Used for Elasto-Plastic Circular Cutout Problems

construct, yet will be seen to give less detail in the vicinity of the cutout than the boundary integral model of Figures 3-8 and 3-9. The same stress-strain data and loading procedure were used, only in the finite element analyses, incipient yielding occurred at the following load ratios

$$\lambda = 0.583 \quad \text{(Biaxial)}$$
$$\lambda = 0.4027 \quad \text{(Uniaxial)} \tag{3-54}$$

The fact that these load ratios are slightly higher than those of equations (3-53) is consistent since the innermost element in the boundary integral model is closer to the cutout boundary than the corresponding element in the finite element mesh. Required computation times for the finite element analyses are given in Table IV; however, direct comparisons to Table III are not meaningful since the finite element work was performed on a UNIVAC-1108 computer. Generally speaking the CDC-7600 is significantly faster than the UNIVAC-1108 which would indicate that the boundary-integral program is running slower than the finite element program. However, it will be seen from the results of these analyses that the boundary-integral model which was used provides significantly more detail in the vicinity of the cutout. A much smaller boundary-integral model would be employed if the same resolution as the finite element model were desired, and the smaller model would result in shorter running

times. A more meaningful running time comparison will be provided on a later sample problem for which the degree of resolution of the two models is comparable.

TABLE IV - FINITE ELEMENT COMPUTER TIME FOR CIRCULAR CUTOUT PROBLEMS

Loading	Number of Load Steps	UNIVAC-1108 CPU Time
Biaxial	23	2.08 min
Uniaxial	38	3.30 min

The results of the two methods of analysis for the circular cutout problem are summarized in Figure 3-11 for the biaxial load case and in Figure 3-12 for the uniaxial load case. Values of effective stress concentration factor ($\sigma_{22}/\sigma_{\infty}$) are given as a function of normalized distance along the horizontal axis ($X = \frac{x_1 - R}{R}$) for several values of load ratio (λ) between initial yielding and unity. The agreement between the two methods is excellent. The boundary-integral model provides data much closer to the cutout boundary ($X = 0.013$ versus $X = 0.055$ for the finite element model), and is therefore expected to be more accurate there. However, no boundary-integral data are available for X greater than 0.6. In the uniaxial case, the plastic zone exceeded the boundary-integral

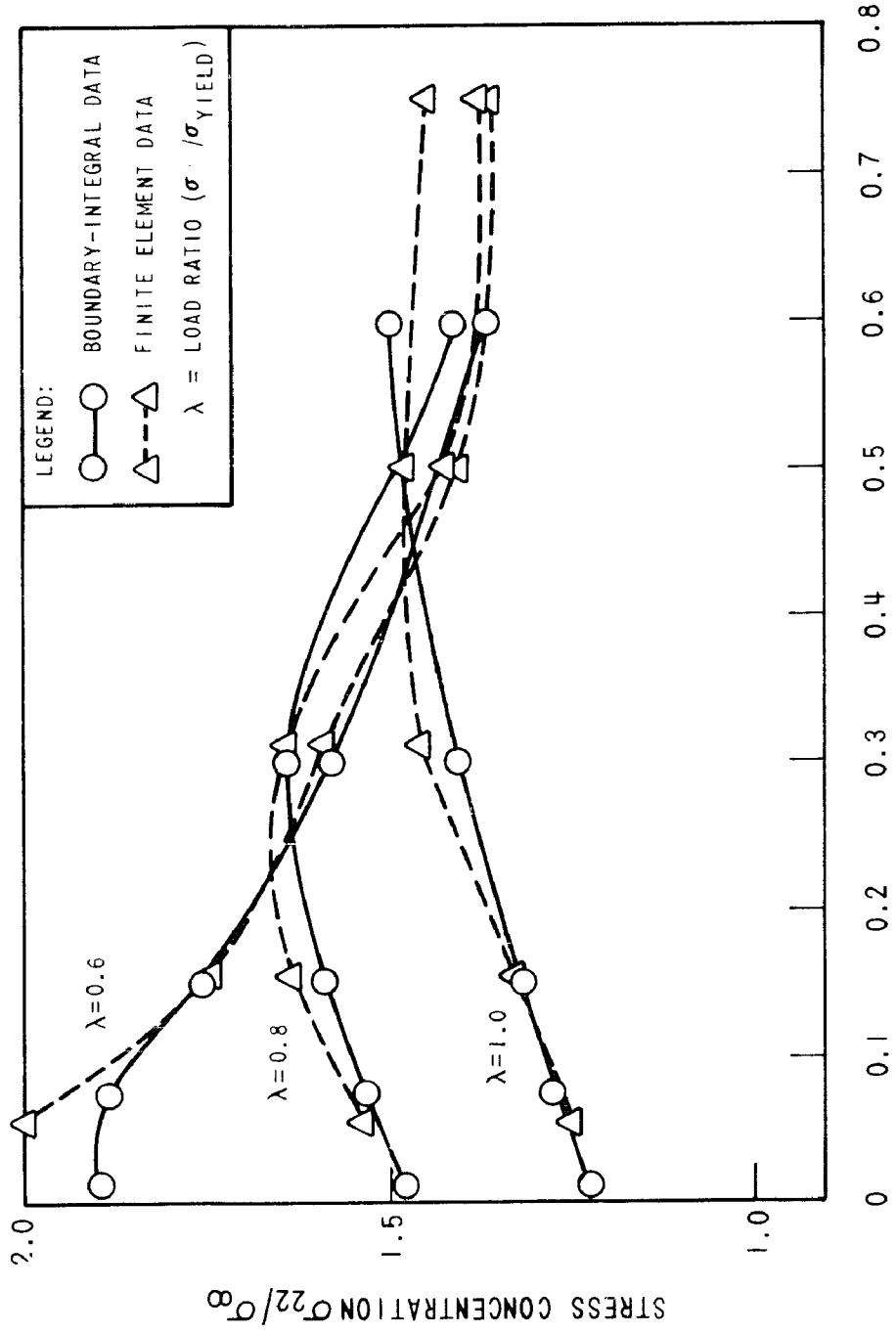

Figure 3-11 Elasto-Plastic Load Redistribution for Infinite Plate with Circular Cutout under Biaxial Tension

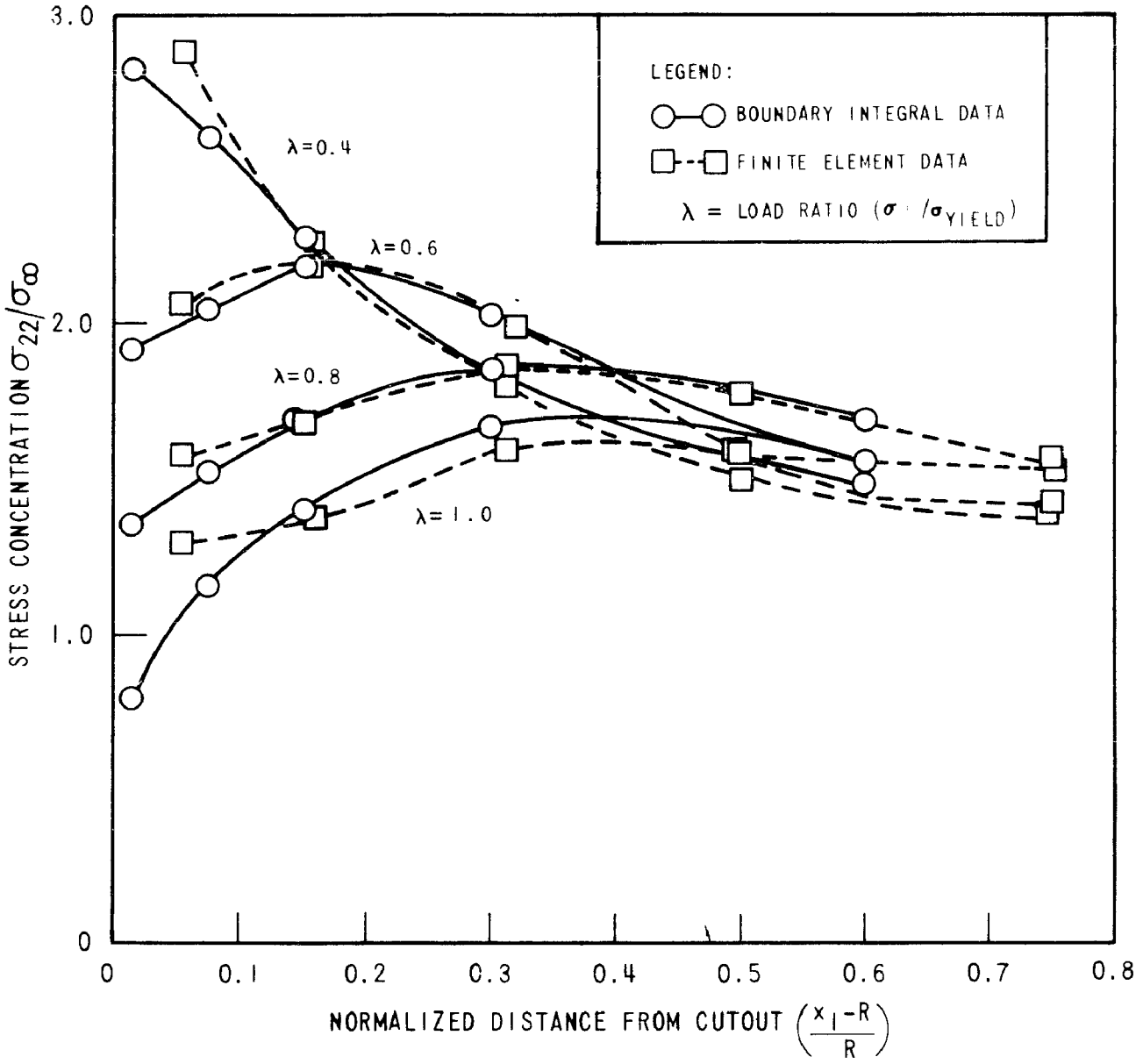

Figure 3-12 Elasto-Plastic Load Redistribution for Infinite Plate with Circular Cutout Under Uniaxial Tension

internal element array at a load ratio of approximately 0.9, which probably explains the greater than usual disagreement between the two models at $\lambda = 1.0$.

The analysis of these circular cutout problems demonstrates that the boundary-integral technique for elasto-plastic problems, as implemented by the computer program BITEP, can be used to solve elasto-plastic flow problems with stress and strain gradients. One can imagine a wide range of problems of real engineering interest which are not too dissimilar to the two basic cutout problems solved here, and which could be solved with relative ease using this approach. Elasto-plastic stress and strain concentrations for cutouts of shapes other than circular, and for cutouts and fillets in finite plates are not generally available in the literature. Thus the sample problems presented here demonstrate the usefulness of the elasto-plastic boundary integral implementation for a wide range of interesting problems.

3. *Solid Disk Problems: Parametric Study* - While the results of the foregoing sample problems are encouraging, it is important to note that the two circular cutout problems, albeit exhibiting significant elasto-plastic load redistribution, did not involve large amounts of plastic straining. The maximum plastic strain in both problems was approximately 1.5 percent. In attempting to apply the present implementation to problems with very large strain gradients, such as

crack problems, some numerical limitations were encountered. It is informative at this point to present a parametric study which was performed on a relatively simple geometry to evaluate these limitations.

The problem chosen for this parametric study is a solid circular disk of unit radius under uniaxial tensile loading. The boundary integral model used to model this disk is shown in Figure 3-13. Only the first quadrant was modelled due to symmetry, and a total of ten boundary nodes and internal elements was used. Two parameters which were found to strongly influence the numerical conditioning of the matrix equations developed in Section III-C are the ratio of elastic to plastic modulus of the stress strain curve, and the load increment size. The first of these parameters was studied by analyzing disks with material behavior characterized by stress-strain curves A, B and C in Figure 3-2. Load steps of 1.0 percent, 2.5 percent and 5.0 percent were applied with each stress-strain curve to study the effect of the second parameter.

Figures 3-14,-15 and -16 summarize the results of this parametric study. Values of applied traction versus internal strain are compared to the exact solution for each stress-strain curve. Computed values of the ratio of transverse (x_3-direction) stress to applied (x_2-direction) stress at the end of each load increment are also plotted as a function of strain. It is evident from these results that the

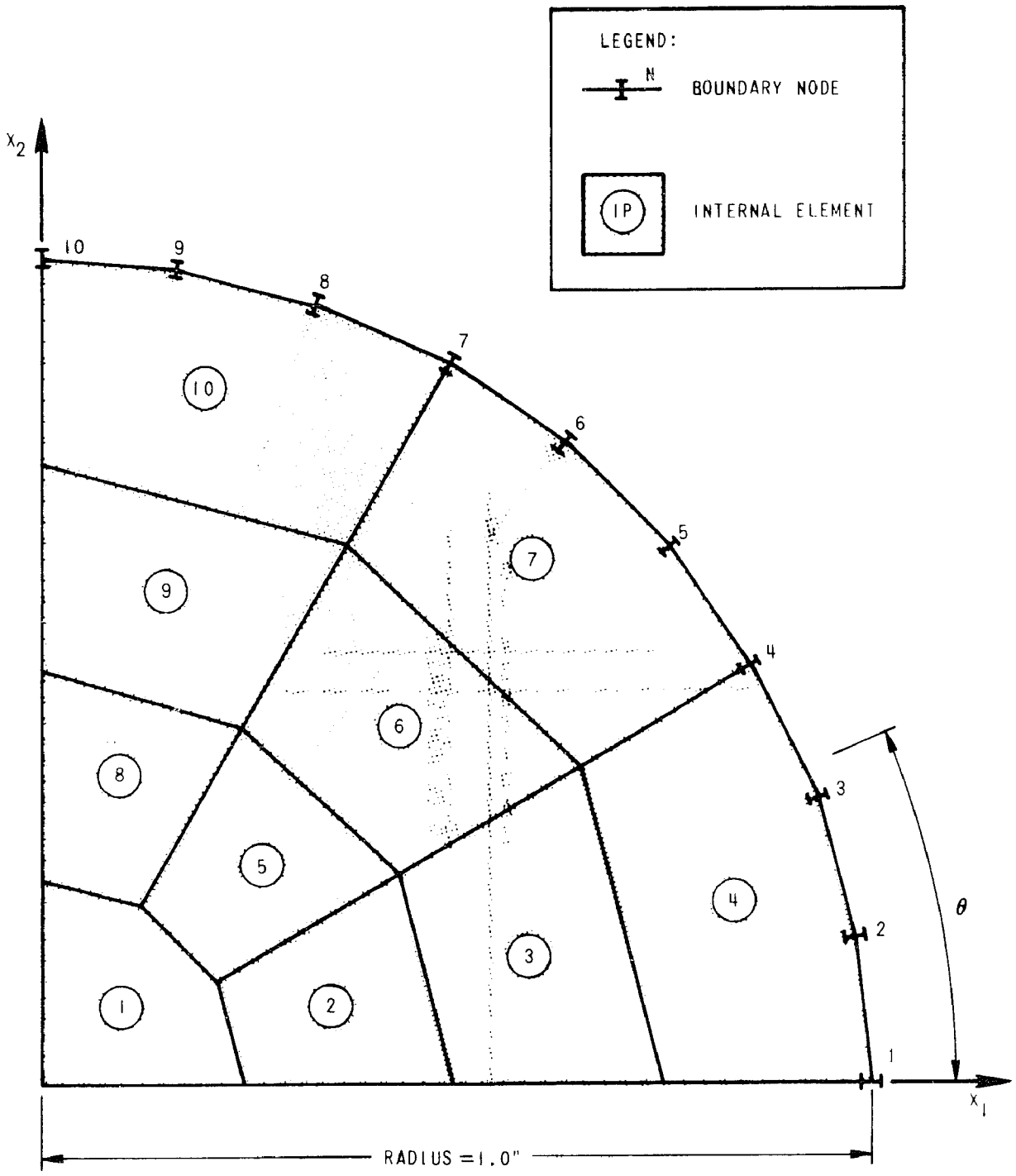

Figure 3-13 Boundary-Integral Model of Solid Disk Problem Used for Elasto Plastic Parametric Study

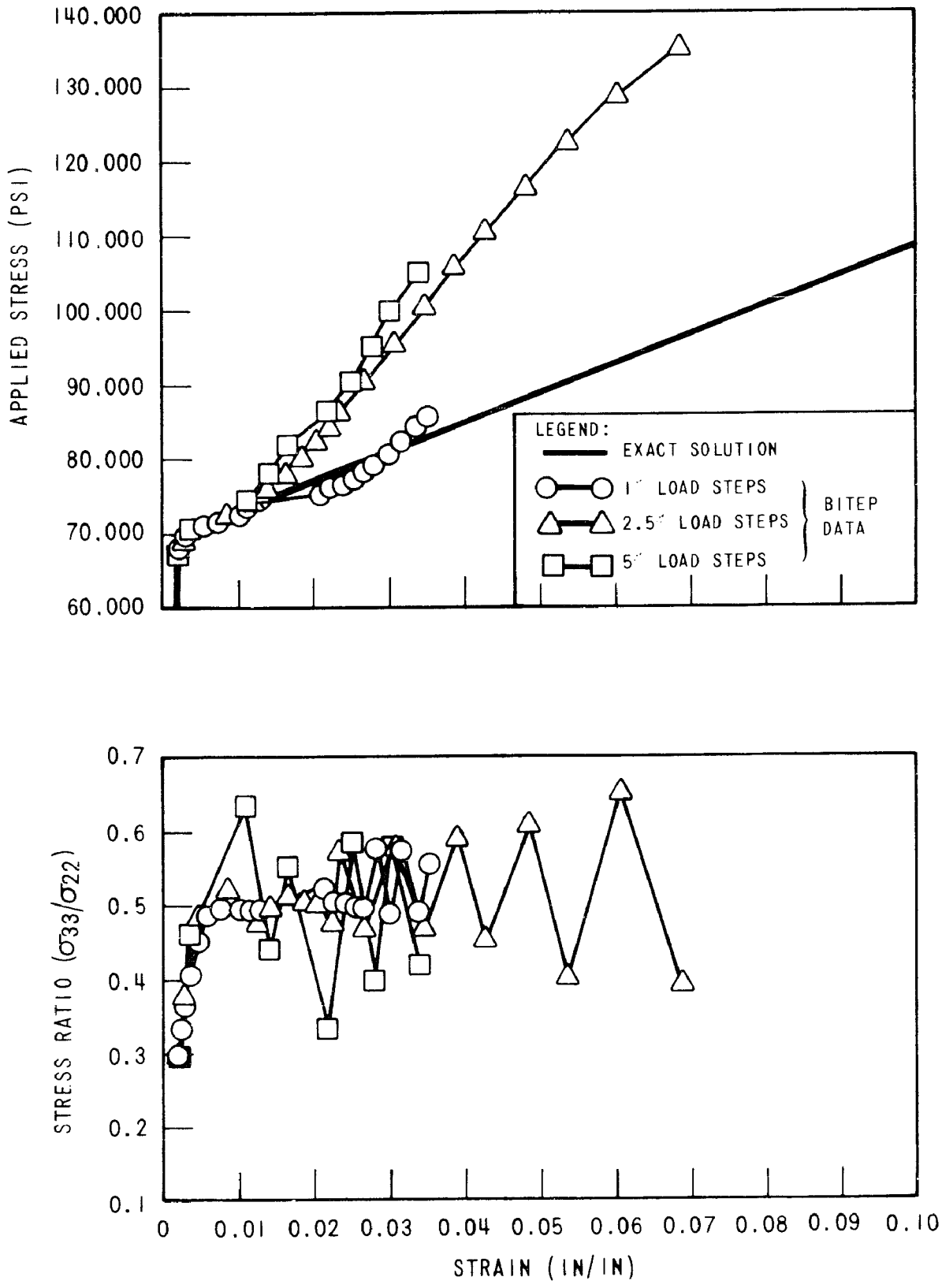

Figure 3-14 Parametric Study for Stress-Strain Curve A

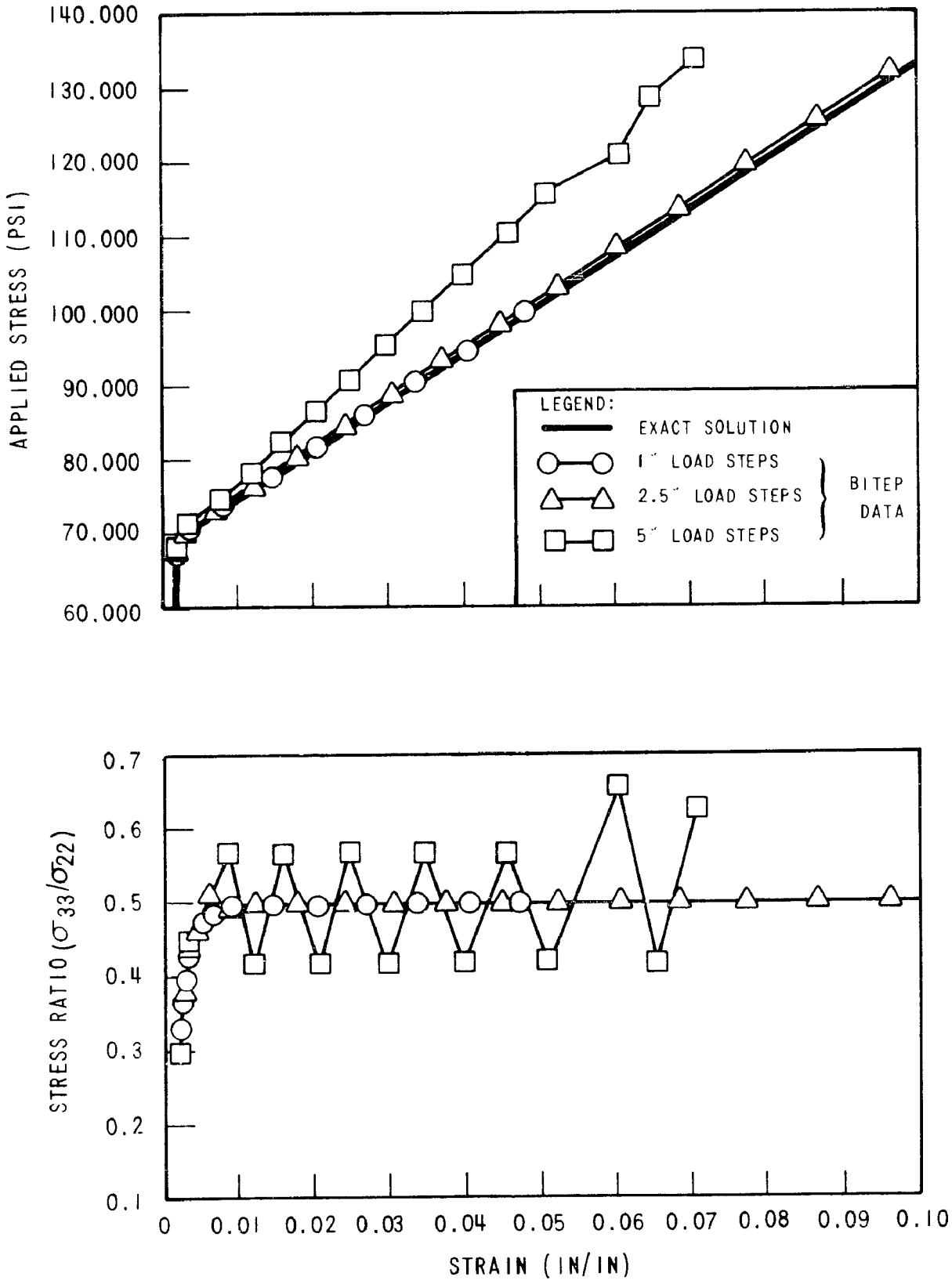

Figure 3-15 Parametric Study for Stress-Strain Curve

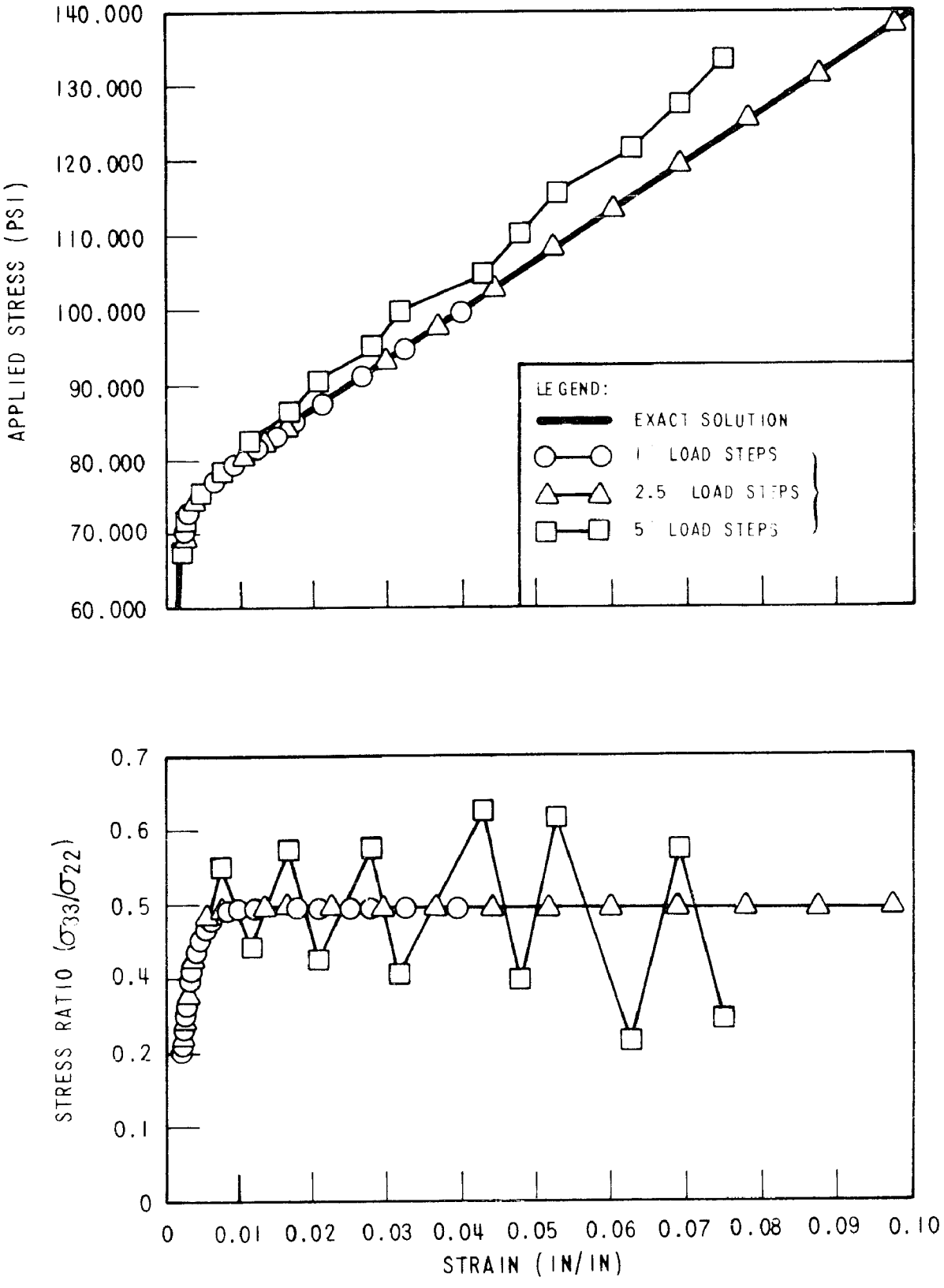

Figure 3-16 Parametric Study for Stress-Strain Curve C

solution technique is significantly better for smaller load increments and steeper stress-strain curves. None of the load increment sizes used is small enough to give a satisfactory solution for this problem using stress-strain Curve A. However, the 1.0 percent load step runs give excellent results for stress strain Curves B and C. The 2.5 percent load step runs, while not as good as the 1.0 percent data, are still reasonably accurate for Curves B and C. The 5.0 percent load case runs do not give satisfactory results for either Curve B or C, however, they are significantly better for Curve C than for Curve B.

Further insight into these numerical limitations can be gained through investigation of the stress ratio plots in Figures 3-14, -15 and -16. Note that for all of the runs which gave satisfactory solutions, the stress ratio varied very smoothly from 0.3 for elasticity to 0.5 for large amounts of plasticity. However, in the unsatisfactory runs, the stress ratio overshot 0.5 as it approached it, and from there on oscillated wildly. It can also be seen that the unsatisfactory runs do give reasonable results up to the point at which the stress ratios begin to oscillate. This explains why accurate results were obtained in the previous sample problems even though stress strain Curve A was used in conjunction with 2.5 percent load steps. The level of loading in those problems was not high enough to cause oscillation of the out-of-plane stress ratio.

It can be demonstrated from the elasto-plastic flow rule (equation 3-16) that the occurrence of an out-of-plane stress ratio exactly equal to 0.5 coincides with a condition of incompressibility of total strain rates. While this condition is never achieved in a strain hardening material, it is approached as the stress-strain curve becomes more flat ($P \to 0$). Further examination of the development of the auxiliary relation (equations 3-17 through 3-23) shows why the approach of this incompressibility condition causes numerical difficulties in the solution procedure. The right hand side of equation (3-20) approaches zero as the total strain rates become incompressible. However, in the development of the auxiliary relation (equation 3-23), these terms were approximated by summations over the boundary tractions and displacements. Thus, the auxiliary relation involves the summation of a large number of terms which, in the nearly incompressible case, add up to a very small number. Relatively small numerical errors in the summation procedure can thus become significant with regard to the solution for the out-of-plane unknowns ($\dot{t}_3(IP)$ or $\dot{u}_3(IP)$), and since the auxiliary relation is incorporated directly into the boundary constraint equation, these errors are fed back into the in-plane solution. Larger load steps merely amplify this effect since the individual terms in the summations are proprotional to load step size.

The above discussion strongly suggests that the numerical difficulties observed in this problem set are characteristics of the particular implementation rather than of the elasto-plastic boundary-integral technique in general. This implementation is unique among two-dimensional solution methods in that it incorporates the out-of-plane direction (plane stress or plane strain) directly into the equations for the primary direction (x_1 and x_2). On the basis of this problem set, it is apparent that direct inclusion of the out-of-plane direction is undesirable from the standpoint of numerical stability, and that another approach should be used in future elasto-plastic boundary-integral work. (Perhaps one of the two approaches which were considered and discarded for other reasons in Section C would be preferable for this reason). The results of this problem set also serve to help select parameters for the final sample problem, which follows, in order to minimize the potential for numerical difficulties.

4. *Elasto-Plastic Center Cracked Plate Problem* - In this final sample problem, the backlog of experience in modelling elastic crack problems which was developed in Chapter II is combined with the elasto-plastic modelling experience obtained in the foregoing sample problems of this section in an attempt to perform an elasto-plastic boundary-integral analysis of a relatively difficult center cracked plate problem. As in the circular cutout problems, a com-

parison to the same problem solved using a finite element program is presented. The problem to be solved is shown in Figure 3-17. In order to minimize numerical difficulties due to out-of-plane terms, stress strain curve C of Figure 3-2 was used.

The boundary integral model used for this analysis is shown in Figure 3-18, and an enlargement of the details of the cracktip region is given in Figure 3-19. The standard twenty-six segment model of a 19.5 aspect ratio ellipse was used to model the crack surface (Figure 2-22) and six additional segments were used to model the external boundary, including a very short segment at the corner to approximate the step change in traction boundary condition at that point. A total of thirty-four boundary nodes and internal elements was used in the model, and care was taken to distribute the internal elements so as to provide adequate detail in the vicinity of the cracktip (Figure 3-19). A finite element model was also set up for the same problem, and is shown in detail in Figure 3-20. Cracktip details in both models were chosen so as to provide a high degree of resolution in the elastic singularity region (Figure 2-21).

Preliminary elastic analyses were performed with both models in order to compare the relative level of resolution of the two methods. Cracktip stress intensity factors were computed from the numerical results according to the methods described in Chapter II (Figure 2-24), and the results are listed in Table V.

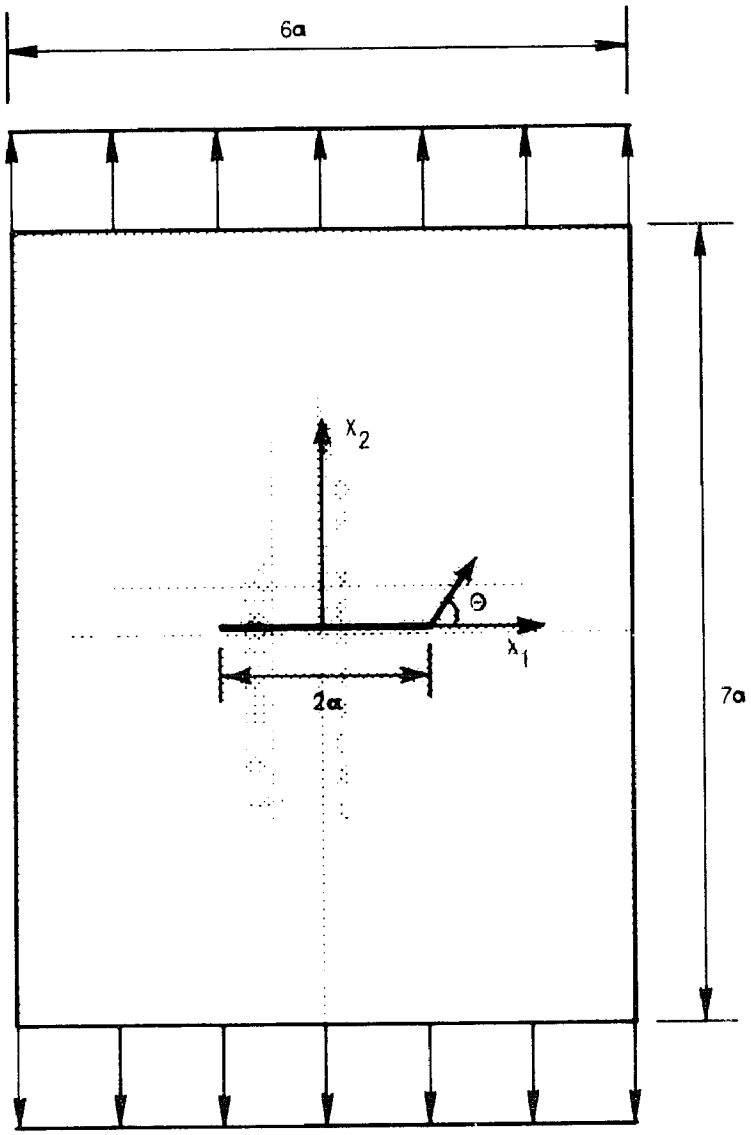

a = 0.5"

Figure 3-17 Elasto-Plastic Center Cracked Plate Problem

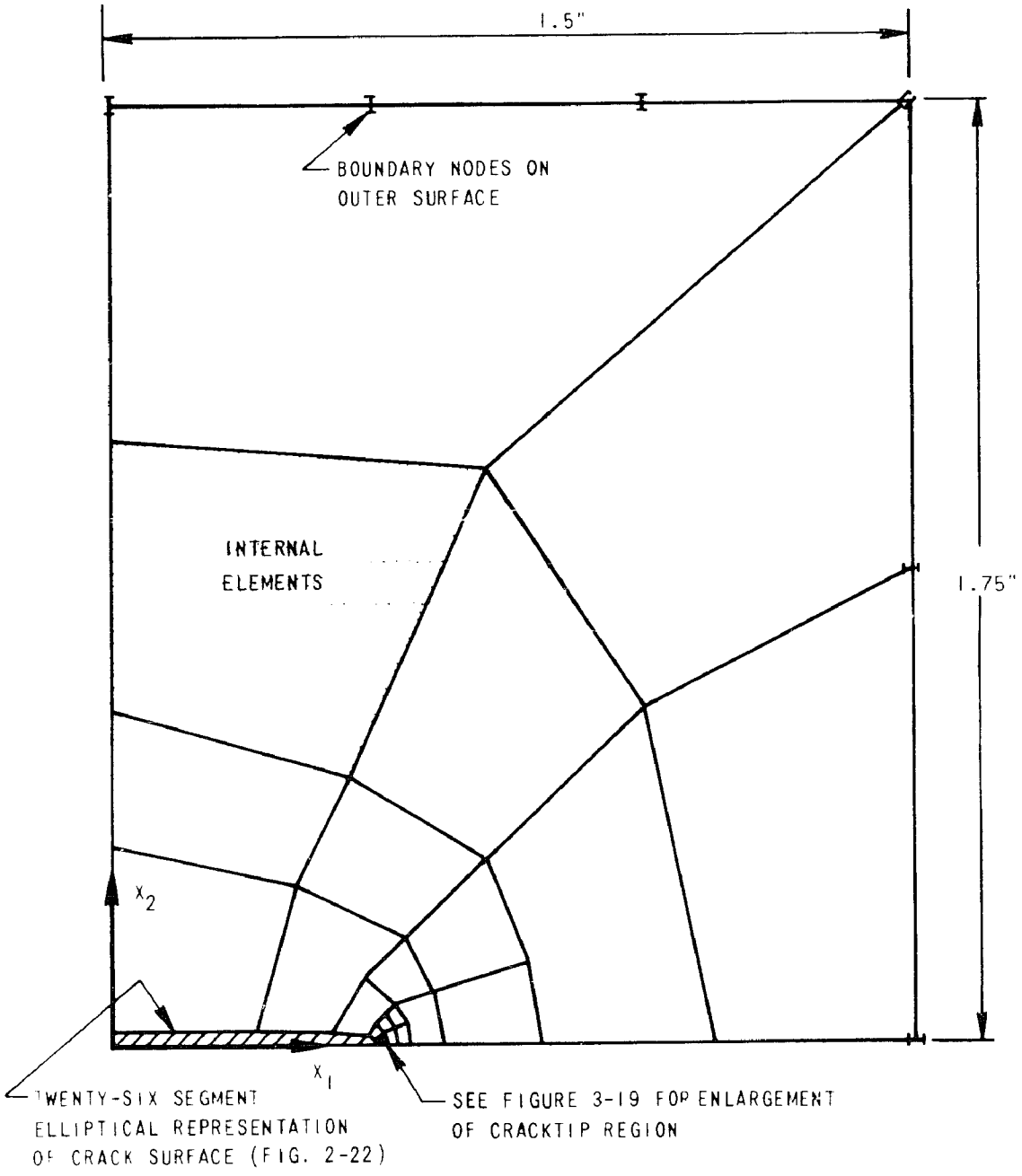

Figure 3-18 **Boundary-Integral Model Used for Elasto-Plastic Center Cracked Plate Problem**

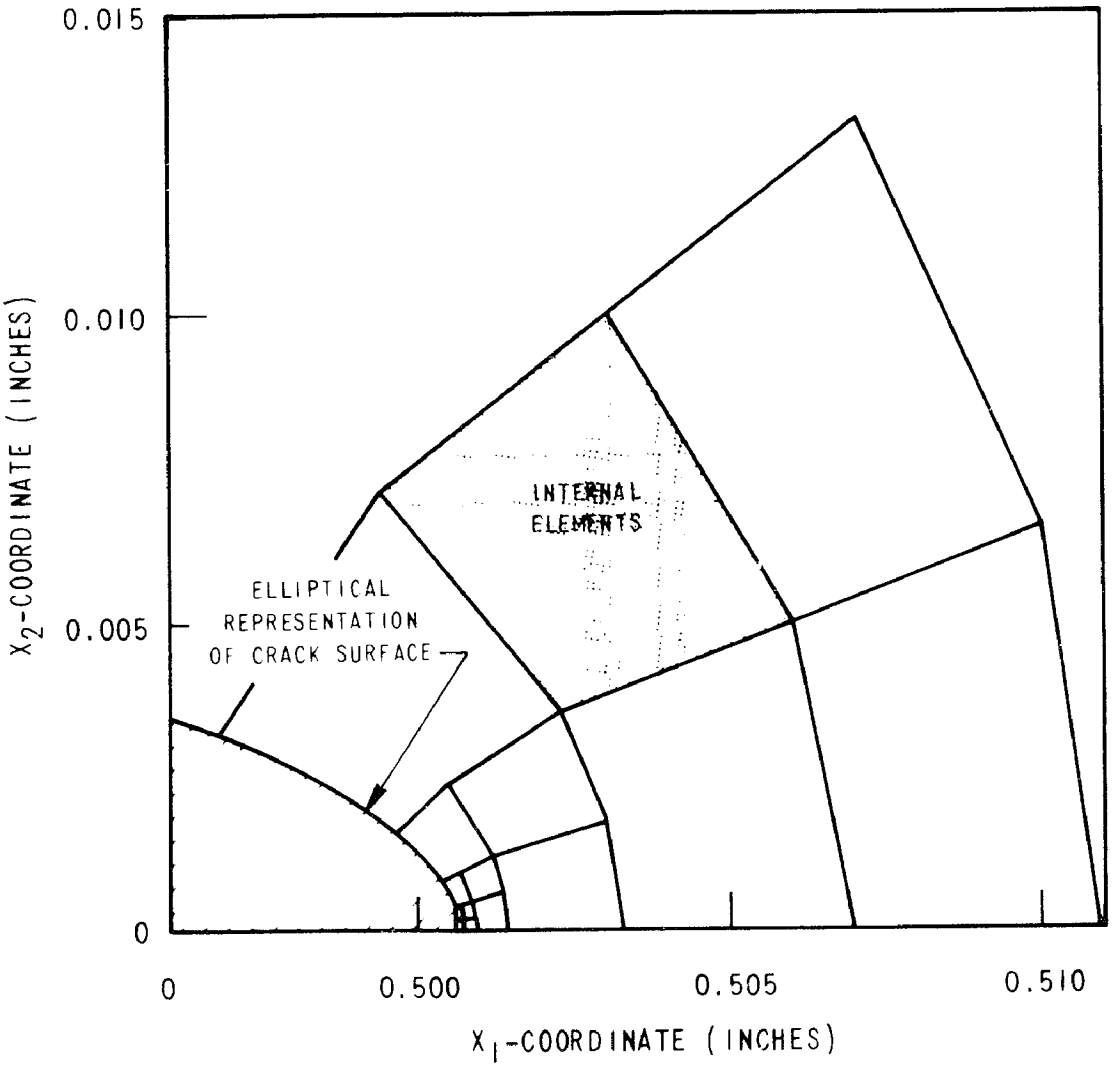

Figure 3-19 Crack Tip Details of Boundary-Integral Model Used for Elasto-Plastic Center Cracked Plate Problem

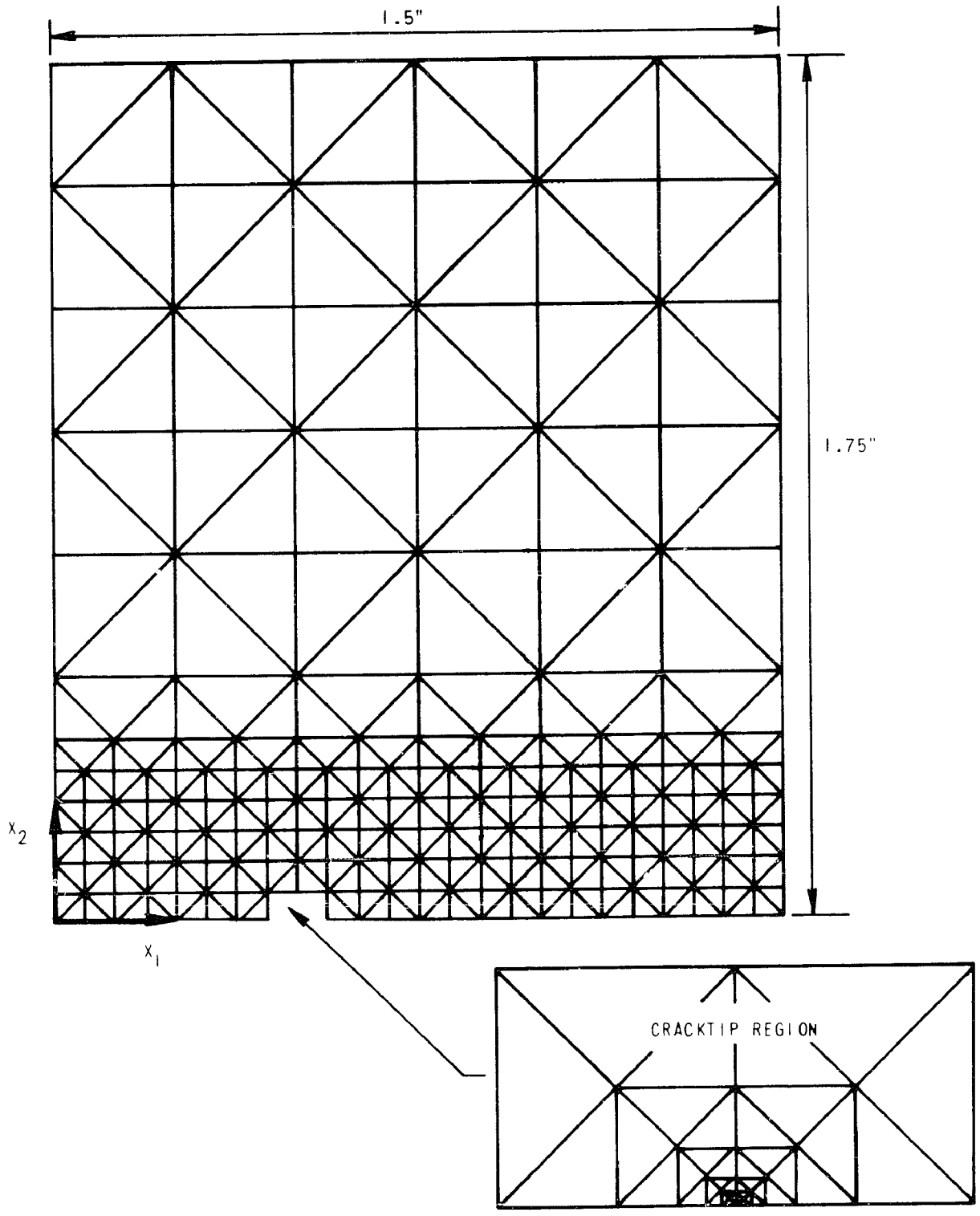

Figure 3-20 Finite Element Model Used for Elasto-Plastic Center Cracked Plate Problem

TABLE V - ELASTIC STRESS INTENSITY FACTORS FOR CENTER CRACKED PLATE PROBLEM

	K_{IA} (Numerical)	K_{IB} (Reference 31)	RATIO (K_{IA}/K_{IB})
Boundary-Integral Results	1.38	1.35	1.02
Finite Element Results	1.40	1.35	1.04

Both numerical solutions are in excellent agreement with the accepted solution to the problem from the literature [31]. Figure 3-21 summarizes the data used in arriving at these stress intensity values. It is evident from this figure that the resolution of the two models is comparable. Both models contain a few points in the cracktip process zone ($r \leq 0.01$ a) in which the approximations of the numerical techniques break down. Both models also contain several points in the elastic singularity region (0.01 a $\leq r \leq 0.1$ a), which is the region of key importance in crack problems, and both give accurate representations of the stress field in this region which lead to the excellent stress intensity predictions in Table V.

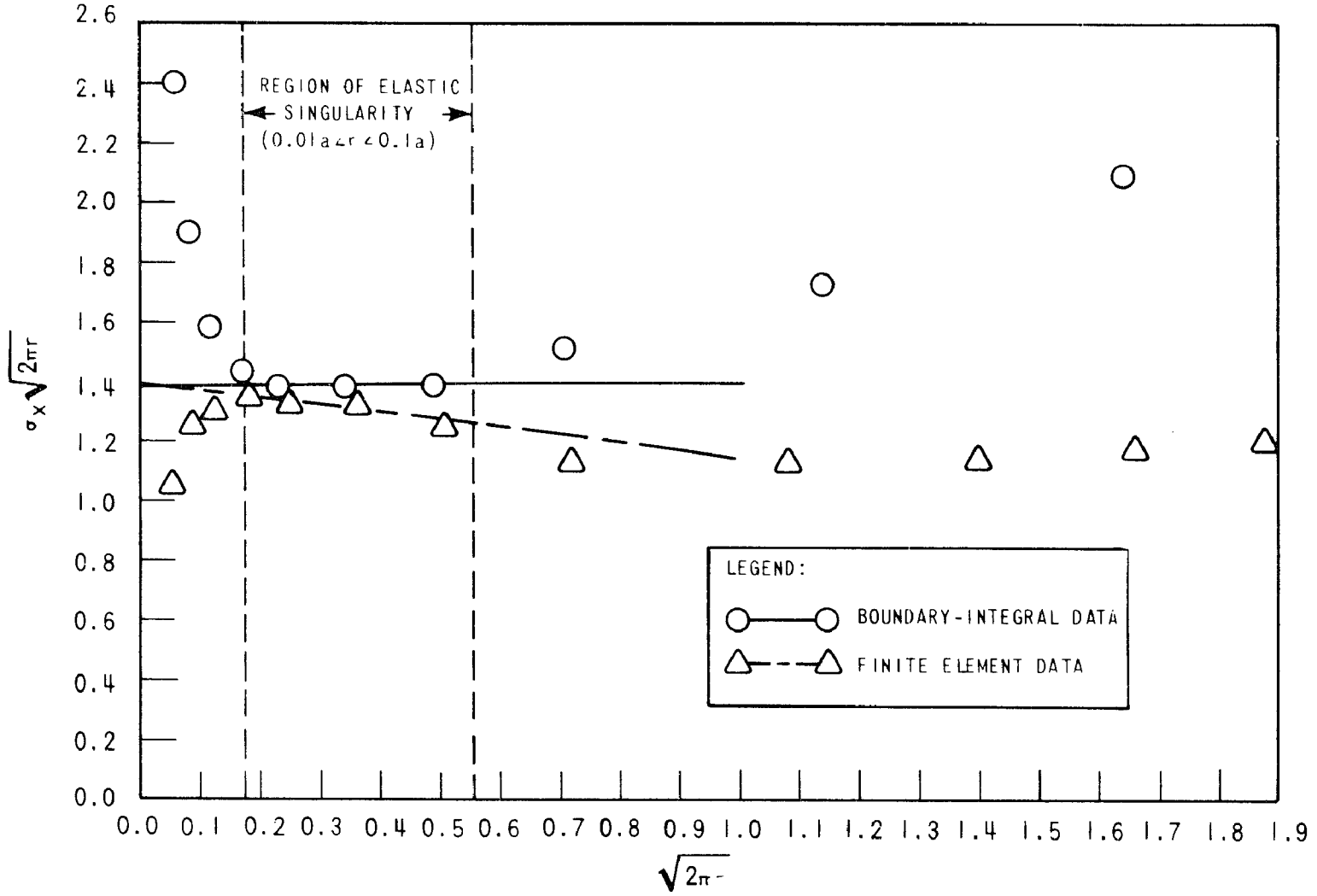

Figure 3-21. Elastic Stress Intensity Factor Determination from Boundary-Integral and Finite Element Models of Elasto-Plastic Center Cracked Plate Problem

One distinction between the two models should be pointed out. It will be recalled from Chapter II (Figure 2-21) that the Inglis solution for x_2-direction stresses in a 19.5 aspect ratio ellipse overestimates the elastic singularity for a crack problem by about 7 percent, but that this error is compensated by the fact that the boundary-integral model underestimates the exact solution by nearly the same amount. The high degree of accuracy of the boundary-integral stress intensity prediction (Table V) is to some extent a result of these compensating errors in x_2-direction stresses. However, the x_1-direction stresses from the Inglis solution do not significantly overestimate the elastic singularity, and for these stresses, the boundary-integral underestimate is not compensated. For this reason, x_2-direction rather than x_1-direction stresses were used for computing the boundary-integral stress intensity prediction in Figure 3-21. With the finite element method, on the other hand, the x_2-direction stresses overestimate the correct values by approximately 10 percent and the x_1-direction stresses underestimate the correct values by approximately 10 percent. For this reason mean stress values $\left(\frac{\sigma_{11}+\sigma_{22}}{2}\right)$ were used for computing the finite element stress intensity prediction in Figure 3-21. Thus, while both methods take advantage of compensating errors to compute accurate stress intensity values, the type of compensation is fundamentally different. This distinction explains the apparent divergence of the far field data ($r > 0.1a$) in Figure 3-21. In order to preserve a

meaningful basis for comparison of the two methods, this distinction must be accounted for when interpreting the elasto-plastic data.

Proceeding with the elasto-plastic analyses, initial load increments were chosen with both methods so as to just cause incipient yielding of the most highly stressed element. This condition corresponds to the following values of load ratio ($\lambda = \sigma_\infty/\sigma_{yield}$):

$$\lambda_{BITEP} = 0.0323$$

$$\lambda_{\substack{finite \\ element}} = 0.0435 \qquad (3\text{-}55)$$

The load ratio for incipient yielding in the boundary-integral model is lower for two reasons. First, the innermost element in the boundary integral model gives a higher stress concentration than that of the finite element model; and second, the elliptical nature of the boundary-integral model causes the transverse (x_1-direction) stress to approach zero at the cracktip, thus yielding less triaxiality there than the finite element model. Both of these effects tend to cause yielding at a lower level of applied load in the boundary integral analysis, but both are restricted to the cracktip process zone, and are not significant in the elastic singularity region which is of most interest.

Figure 3-22 shows values of stress concentration in selected elements along the crackline as a function of load ratio for both analyses. The elements chosen are those in the elastic singularity

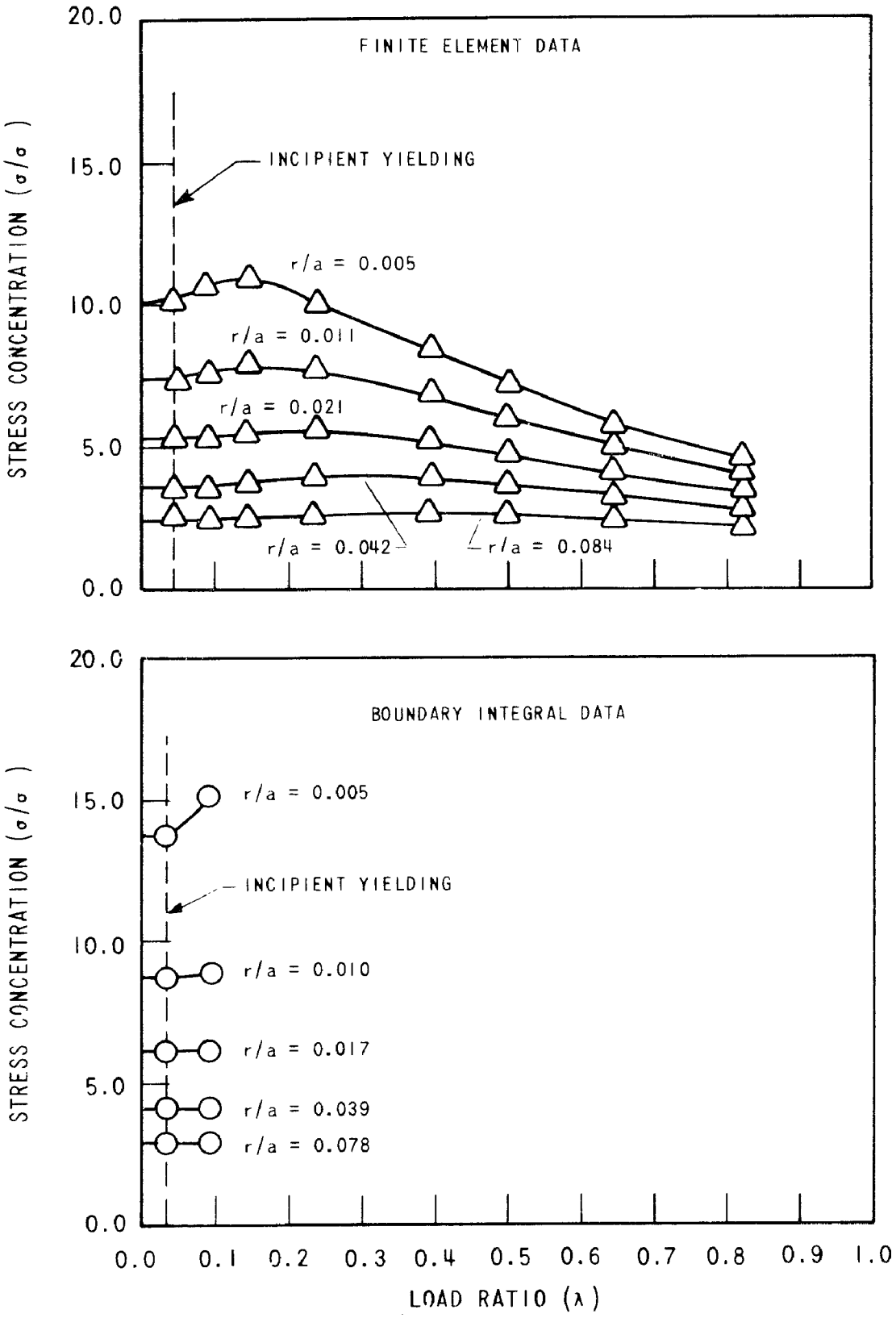

Figure 3-22. Loading Paths in Crackline Elements for Elasto-Plastic Center Cracked Plate Problem

region ($0.01 < r/a < 0.1$). For the finite element data the mean stress $\frac{\sigma_{11}+\sigma_{22}}{2}$ was used in calculating stress concentration and for the boundary-integral data the x_2-direction stress was used in order to provide a basis for comparison which at least gives reasonable agreement in the elastic case. The finite element results show a slight increase in stress concentration in each element followed by a decrease. The boundary integral data show a similar slight increase in stress concentration; however, the numerical difficulties due to out-of-plane stress terms set in before the loading progressed to a high enough load level to show any decrease in stress concentration. The innermost element in the boundary-integral model reaches a relatively high level of plastic strain at a low load ratio ($\lambda = 0.1$), and as a result, the ratio of transverse (x_3-direction) stress to applied (x_2-direction) stress in this element approaches the imcompressibility value (0.5) at this load level. At this point the previously described numerical difficulties which are associated with the approach of incompressibility caused the equations to become ill-conditioned. Thus the elasto-plastic boundary integral approach, as implemented here, was not capable of providing significant elasto-plastic data in the elastic singularity region for this center cracked plate problem. This point is further demonstrated by the data of Figure 3-23. In this figure the same stress concentration data are shown as a function of normalized distance from the cracktip (r/a) for several values of load ratio λ. The

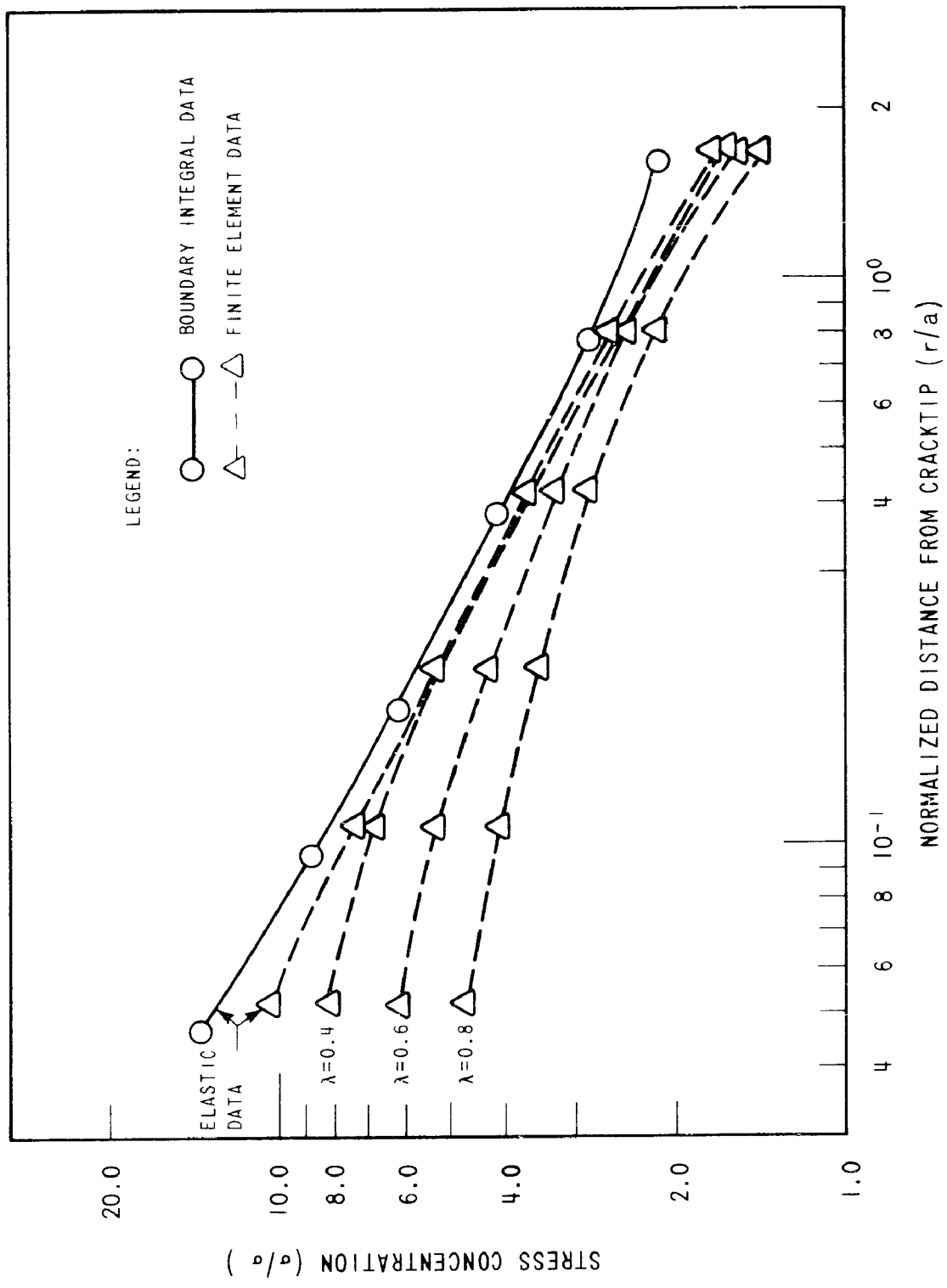

Figure 3-23. Elasto-Plastic Load Redistribution for Center Cracked Plate Problem

finite element data show that significant deviation from the elastic line does not occur in the elastic singularity region until a load ratio of 0.4 is reached. Since the boundary-integral program could only reach a load ratio of 0.1 for this problem, no significant deviation from elastic behavior was achieved.

Despite the limited amount of data which was obtained, the analysis of this elasto-plastic center cracked plate problem does serve two useful purposes. First, it demonstrates the importance of the limitations of this elasto-plastic implementation of the boundary-integral technique which were brought out in the previous problem set. Secondly, since the two models are comparable in resolution, a meaningful computer time comparison can be presented. Table VI gives a running time comparison for solution of this problem using both techniques on a CDC-7600 computer. The running times are broken down into initial setup time and time per load step. Except for a nominal amount of initial setup time required for the boundary-integral technique, the running times for the two numerical approaches are comparable. While the results of this sample problem are not as encouraging as the previous ones, it should be re-emphasized that the problems encountered are most probably characteristic of this initial elasto-plastic implementation, and generalizations should not be inferred from them concerning the application of the boundary-integral technique to elasto-plastic problems in general.

TABLE VI - COMPARISON OF RUNNING TIMES FOR ELASTO-PLASTIC CENTER CRACKED PLATE PROBLEM

	Initial Setup Time	Time Per Load Step
Boundary-Integral Technique	30 sec.	2.3 sec.
Finite Element Technique	Negligible	2.2 sec.

E. SUMMARY

An implementation of the boundary-integral technique for problems of two-dimensional elasto-plasticity is developed in this chapter. The basic boundary-integral equations of Chapter II are recast in terms of boundary displacement and traction rates, and are appended to include a volume integration over the plastic strain rates which is required by the elasto-plastic theory. The procedure is automated by means of a FORTRAN computer program, and several sample problems are presented which demonstrate the range and limitations of the implementation.

The initial sample problems of this chapter serve to demonstrate basic feasibility of the approach. They consist of very simple, homogeneous stress and strain problems, for which exact solutions are trivial. Through these problems it is demonstrated that the boundary-integral technique does, in fact, work for elasto-plastic problems. A second set of sample problems of substantially more interest is then presented and it is demonstrated that the elasto-plastic boundary-integral approach, as implemented here, offers a simple and straightforward solution procedure to a wide range of elasto-plastic stress concentration problems, the solutions of which are not generally available in the literature. The high degree of resolution of the procedure in these problems is demonstrated through comparisons with solutions to the same problems obtained using a conventional finite element computer program.

Finally, in attempting to solve an elasto-plastic crack problem with the present technique, a numerical difficulty was experienced as the strains at the cracktip became large. A parametric study was performed on a conceptually simpler problem to investigate the nature of the difficulty, and the results strongly suggest that the problem is a symptom of this particular implementation rather than of the technique in general. Alternate approaches which may alleviate this difficulty are discussed in the text, and it is recommended that any further elasto-plastic boundary integral work be done along these or other lines in order to avoid the numerical problems experienced here.

CHAPTER IV - CONCLUSIONS

The boundary-integral technique offers potential advantages over conventional numerical solution methods for solid mechanics problems (such as the finite element technique) in the following three areas:

1. Savings in computer running times and storage requirements.
2. Greater resolution in problems with high stress and strain gradients.
3. Ease of modelling to the analyst.

Implementations of the boundary-integral technique are developed in this dissertation for planar problems of elasticity and elasto-plasticity. These implementations are evaluated with regard to their degree of realization of the potential advantages of the technique through application to real engineering problems. Conclusions based upon these evaluations are best discussed separately for the elastic and elasto-plastic implementations.

The elastic boundary-integral solution technique developed herein represents a second generation implementation of an approach which has been available in the literature for several years. Therefore, as should be expected, this implementation is highly efficient and possesses to a large extent all three of the potential advantages of the boundary-integral technique mentioned above. Computer running

times and storage requirements for problems of any complexity are significantly lower than those experienced with finite element programs. The resolution of the stress and strain field is shown to be highly accurate, not only in comparison to the finite element technique, but also in comparison to first generation boundary-integral implementations. The ease of modelling of the technique is evident in all of the problems solved, and the favorable comparison to finite elements is readily apparent to anyone with finite element modelling experience.

On the other hand, the elasto-plastic boundary-integral solution technique developed here represents the very first attempt at implementation of this approach for elasto-plastic problems. While the results are not as convincing as those of the second generation elastic implementation, they are encouraging. First and foremost, it is demonstrated that the boundary-integral technique does, in fact, work for elasto-plastic problems. While a general development of the necessary equations was available in the literature, there were no *a priori* guarantees that these relations could be implemented into a viable elasto-plastic solution procedure. The present implementation was demonstrated to have the ability to solve many problems of real interest in the field of elasto-plasticity, and the advantages of greater resolution and easier modelling are evident in several sample problems which are presented. However, computer running times and storage requirements appear to be comparable to those

experienced with finite element programs. The large advantages in computer time and storage which were present in the elastic boundary-integral technique do not appear to carry over into the elasto-plastic case. This reduction in computational efficiency can be explained by the fact that the technique becomes no longer strictly a boundary technique since an internal integral over the plastic region is required. While more efficient means for carrying out this internal integration may be devised, it must be recognized that the full extent of the time and storage advantage which the boundary-integral technique exhibits in elasticity might never be achieved in elasto-plasticity. Nevertheless, the resolution and modelling advantages of the method make it well worth pursuing further, especially with regard to three dimensional elasto-plastic applications.

The boundary-integral technique offers the potential to be a very powerful tool for the solution of linear and non-linear problems in the area of solid mechanics. The amount of emphasis which has been given to the development of this tool in the past, in comparison to that given to the finite element technique, is disproportionate to the relative potential of the two approaches. It is therefore strongly recommended that development effort on non-linear applications of the boundary-integral technique be continued. The obvious next step is the development of second generation elasto-plastic capability, including extension of the approach to three dimensions. Further two

dimensional work should avoid direct inclusion of the out-of-plane direction because of the numerical difficulties which it apparently created in this implementation. Looking further into the future, the procedure is potentially applicable to axially-symmetric problems, finite deformation, and plate and shell theory. As greater computational capability becomes available, the advantages of the boundary-integral technique should become more consequential since it inherently tends to increase the portion of problem solving effort performed by the computer and to decrease the effort required of the analyst.

REFERENCES

1. J. H. Argyris, "Energy Theorems and Structural Analysis," *Aircraft Engineering*, Vol. 26, pp. 347-356, 383-387, 394 (1954).

2. M. J. Turner, R. W. Clough, H. C. Martin, and L. J. Topp, "Stiffness and Deflection Analysis of Complex Structures," *J. Aero. Sci.*, Vol. 23, pp. 805-823 (1956).

3. J. L. Swedlow, M. L. Williams, and W. H. Yang, "Elasto-Plastic Stresses and Strains in Cracked Plates," *Proc. 1st Int. Conf. Fracture*, Sendai, Vol. 1, pp. 259-282 (1966).

4. O. C. Zienkiewicz, S. Valliappan, and I. P. King, "Elasto-Plastic Solutions of Engineering Problems: Initial Stress, Finite Element Approach," *Int. J. Num. Meth. in Eng.*, Vol. 1, pp. 75-100 (1969).

5. P. V. Marcal and I. P. King, "Elastic-Plastic Analysis of Two-Dimensional Stress Systems by the Finite Element Method," *Int. J. Mech. Sci.*, Vol. 9, pp. 143-155 (1967).

6. A. Mendelson, *Plasticity: Theory and Application*, The Macmillan Company (1968).

7. P. V. Marcal, "Finite Element Analysis of Combined Problems of Material and Geometric Behavior," *Proc. A.S.M.E. Conf. on Computational Approaches in Applied Mechanics*, p. 133 (1969).

8. H. C. Martin, "Finite Elements and the Analysis of Geometrically Non-Linear Problems," *U.S. - Japan Seminar on Matrix Methods in Structural Analysis and Design*, Tokyo (1970).

9. C. Visser, S. E. Gabrielse, and W. VanBuren, *A Two-Dimensional Elastic-Plastic Analysis of Fracture Test Specimens*, Heavy Section Steel Technology Program Technical Report No. 4 (October 1969).

10. J. R. Osias, *Finite Deformation of Elasto-Plastic Solids: The Example of Necking in Flat Tensile Bars*, Carnegie-Mellon University, PhD. Dissertation (August 1972).

11. *The NASTRAN User's Manual*, National Aeronautics and Space Administration, Report No. NASA-SP-222 (1970).

12. *MARC-CDC, Non-Linear Finite Element Analysis Program*, Control Data Corporation, Report No. 17309500 (1971).

13. *ASKA Users Reference Manual*, Institut Statik und Dynamik, Report No. 73, Stuttgart (1971).

14. *ANSYS Engineering Analysis System*, Swanson Analysis Systems, Inc. (1971).

15. O. D. Kellogg, *Foundations of Potential Theory*, Dover (1953).

16. F. J. Rizzo, "An Integral Equation Approach to Boundary Value Problems of Classical Elastostatics," *Q. of Appl. Math*, Vol. 25, pp. 83-95 (1967).

17. T. A. Cruse and F. J. Rizzo, "A Direct Formulation and Numerical Solution of the General Transient Elasto-Dynamic Problem - I and II," *J. Math. Analysis Applic.*, Vol. 22, pp. 244-259 and 341-355 (1968).

18. W. VanBuren, *The Indirect Potential Method for Three Dimensional Value Problems of Classical Elastostatics*, Westinghouse Research Laboratories, Research Report 68 ID7-MEKMA-R2 (1968).

19. G. Miranda, *Application of Singular Integral Equation Methods to the Static Displacement Problem of Non-Smooth Elastic Bodies*, Courant Institute, New York Univ., New York.

20. V. D. Kupradze, *Potential Methods in the Theory of Elasticity*, Davey (1965).

21. T. A. Cruse and W. VanBuren, "Three-Dimensional Elastic Stress Analysis of a Fracture Specimen with an Edge Crack," *International Journal of Fracture Mechanics*, Vol. 7, pp. 1-16 (1971).

22. O. C. Zienkiewicz, *The Finite Element Method in Engineering Science*, McGraw-Hill (1971).

23. T. A. Cruse, "Numerical Solutions in Three Dimensional Elastostatics," *Int. J. Solids Struct.*, Vol. 5, pp. 1259-1274 (1969).

24. T. A. Cruse, "Lateral Constraint in a Cracked, Three Dimensional Elastic Body," *Int. J. Fract. Mech.*, Vol. 6, pp. 326-328 (1970).

25. W. Bamford, *Numerical Solution Accuracy for the Infinite Plate with a Cutout - Progress Report*, Report SM-50, and *Final Report*, Report SM-66, Department of Mechanical Engineering, Carnegie-Mellon University (1971).

26. C. E. Pearson, *Theoretical Elasticity*, Harvard (1959).

27. S. P. Timoshenko and J. N. Goodier, *Theory of Elasticity*, McGraw-Hill Book Co., 2nd Edition (1951).

28. C. E. Inglis, *Trans. Inst. Naval Arch.*, Vol. 95, p. 415, London (1913).

29. N. I. Muskhelishvili, *Some Basic Problems of the Mathematical Plane Theory of Elasticity*, English Translation, P. Noordhoof and Co. (1962).

30. F. A. McClintock and G. R. Irwin, "Plasticity Aspects of Fracture Mechanics," *Fracture Toughness Testing and Its Applications*, ASTM Special Technical Publication No. 381, pp. 84-113 (1965).

31. W. F. Brown and J. E. Srawley, *Plane Strain Crack Toughness Testing of High Strength Metallic Materials*, ASTM Special Technical Publication No. 410 (1966).

32. J. L. Swedlow and T. A. Cruse, "Formulation of Boundary Integral Equations for Three-Dimensional Elasto-Plastic Flow," *Int. J. of Solids Structures*, Vol. 7, pp. 1673-1683 (1971).

33. J. L. Swedlow, "Character of the Equations of Elasto-Plastic Flow in Three Independent Varaibles," *Int. J. Non-Linear Mech.*, Vol. 3, pp. 325-336 (1968); Vol. 4, p. 77 (1969).

34. J. L. Swedlow, "Elasto-Plastic Cracked Plates in Plane Strain," *Int. J. of Fract. Mech.*, Vol. 5, pp. 33-44 (1969).

35. J. L. Swedlow, *A Procedure for Solving Problems of Elasto-Plastic Flow*, Carnegie-Mellon Univ., Report SM-73 (September 1971).

36. J. L. Swedlow, *Information for Users of Finite Element Programs ANISEL, ASYMEL, PLANEL, ELAXI5, ELSIG5*, Carnegie-Mellon Univ., Report SM-33A,(February 1971).

37. D. C. Drucker, "A More Fundamental Approach to Plastic Stress-Strain Relations," *1st U.S. Congress of Applied Mechanics*, A.S.M.E., pp. 487-491 (1952).

APPENDIX A - EVALUATION OF INTEGRALS FOR LINEAR BOUNDARY VARIATION

1. Boundary Constraint Equation - The kernels of the integrals in the boundary constraint equation for two dimensions (plane strain) are given by

$$U_{ij} = C_1(C_2\delta_{ij} \log r - r_{,i}r_{,j})$$

$$T_{ij} = C_3(1/r)\left[\frac{\partial r}{\partial n}(C_4\delta_{ij}+2r_{,i}r_{,j}) - C_4(r_{,i}n_j - r_{,j}n_i)\right] \tag{A1}$$

where C_1 through C_4 are the following material property constants

$$C_1 = -1/[8\pi\mu(1-\nu)]$$

$$C_2 = (3-4\nu)$$

$$C_3 = 1/[4\pi(1-\nu)] \tag{A2}$$

$$C_4 = (1-2\nu)$$

r is the vector distance from node N to any point on the segment to be integrated over (MF or MB) and n is the unit normal to that segment. The case of plane stress is handled by use of an effective Poisson's ratio given by $[\nu/(1+\nu)]$.

Basically, four types of integrals must be evaluated

$$\Delta U_{ij} = \int_{\Delta S} U_{ij} dS$$

$$\Delta \bar{U}_{ij} = \frac{1}{\Delta S} \int_{\Delta S} U_{ij} S dS$$

$$\Delta T_{ij} = \int_{\Delta S} T_{ij} dS \qquad \text{(A3)}$$

$$\Delta \bar{T}_{ij} = \frac{1}{\Delta S} \int_{\Delta S} T_{ij} S dS$$

Notice that the references to Node N and segment MF or MB are assumed here and that no superscript (F or B) notation is required to distinguish between integrals over MF or MB since the integral evaluation procedure is the same for both.

Using the notation introduced in Figure A-1, these integrals can be cast in terms of the perpendicular distance (D) from the Node N to the segment, and the angle (θ) between D and the vector r. Introducing the (ζ_1,ζ_2) coordinate system, with unit vectors (e_1,e_2) which is rotated from the (x_1,x_2) system such that ζ_1 is the outward normal direction to the line segment and ζ_2 is the positive tangential direction, we can write

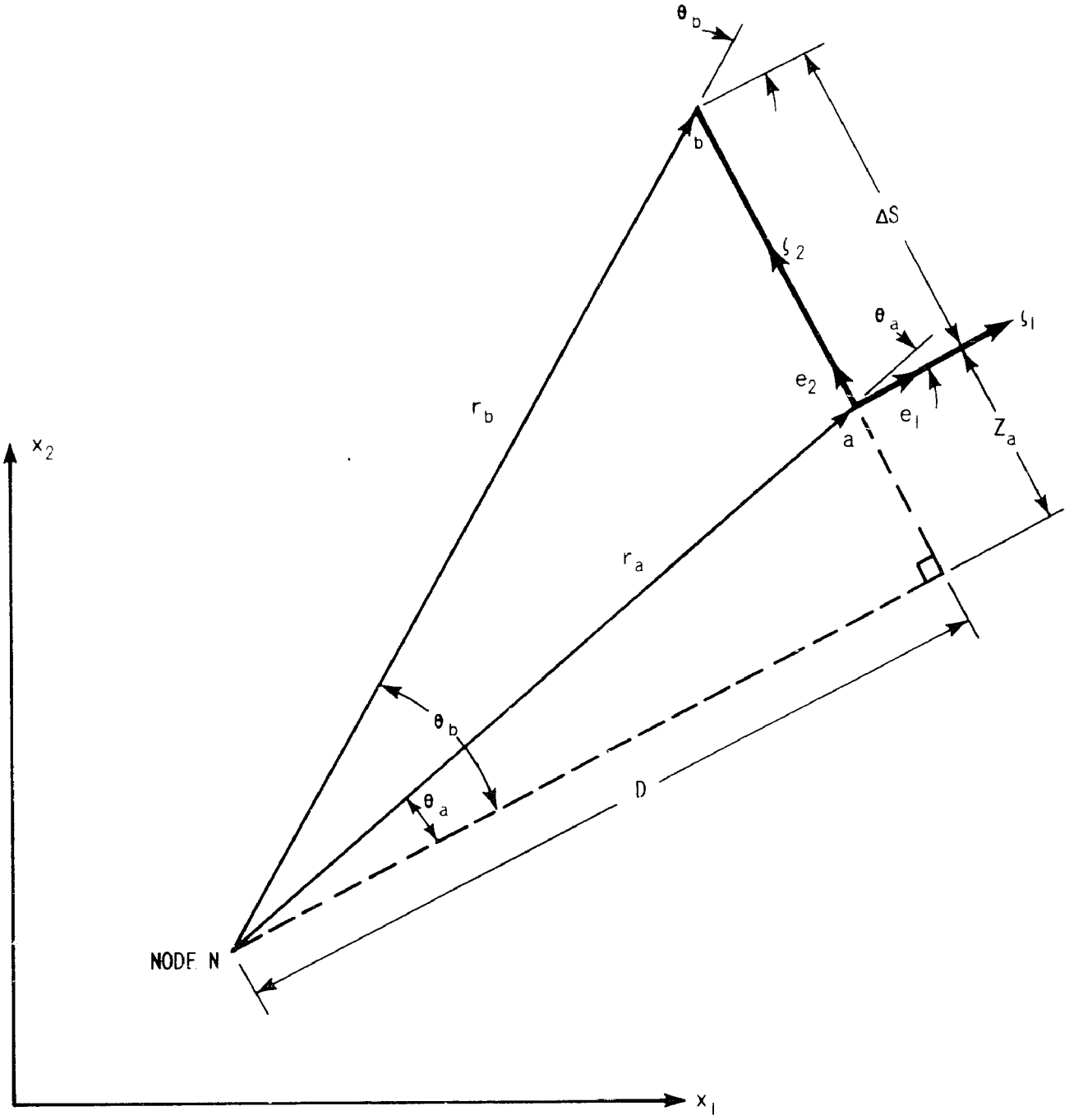

Figure A-1. Notation Used in Evaluation of Integrals

$$n = e_1 \text{ (or using indicial notation: } n_i = e_{1i})$$

$$\frac{\partial r}{\partial n} = \frac{\partial r}{\partial \zeta_1} = \cos\theta$$

$$\frac{\partial r}{\partial S} = \frac{\partial r}{\partial \zeta_2} = \sin\theta$$

$$r_{,i} = \frac{\partial r}{\partial \zeta_1}\left(\frac{\partial \zeta_1}{\partial x_i}\right) + \frac{\partial r}{\partial \zeta_2}\left(\frac{\partial \zeta_2}{\partial x_i}\right) \tag{A4}$$

$$= (\cos\theta)(e_{1i}) + (\sin\theta)(e_{2i}),$$

and thus the kernels become

$$U_{ij} = C_1[C_2\delta_{ij}\log r - e_{1i}e_{1j}\cos^2\theta - (e_{1i}e_{2j} + e_{2i}e_{ij})\sin\theta\cos\theta$$

$$- e_{2i}e_{2j}\sin^2\theta] \tag{A5}$$

$$T_{ij} = C_3\left(\frac{1}{r}\right)\Big\{\cos\theta[C_4\delta_{ij} + 2e_{1i}e_{1j}\cos^2\theta + 2(e_{1i}e_{2j} + e_{2i}e_{ij})$$

$$\cos\theta\sin\theta + 2e_{2i}e_{2j}\sin^2\theta] - C_4(e_{2i}e_{ij} - e_{1i}e_{2j})\sin\theta\Big\}.$$

Also from Figure A-1 we note that

$$r = D/\cos\theta$$

$$\Delta S = D\tan\theta - z \tag{A6}$$

$$dS = (D/\cos^2\theta)\,d\theta$$

Substituting equations (A5) and (A6) into (A3) yields the following forms of the four integrals to be evaluated

$$\Delta U_{ij} = \int_{\theta_a}^{\theta_b} C_1[C_2\delta_{ij} \log\left(\frac{D}{\cos\theta}\right) - e_{1i}e_{1j}\cos^2\theta$$

$$- (e_{1i}e_{2j}+e_{2i}e_{1j})\cos\theta \sin\theta - e_{2i}e_{2j}\sin^2\theta]$$

$$(D/\cos^2\theta)d\theta$$

$$\Delta u_{ij} = \frac{1}{\Delta S}\int_{\theta_a}^{\theta_b} C_1[C_2\delta_{ij} \log\left(\frac{D}{\cos\theta}\right) - e_{1i}e_{1j}\cos^2\theta$$

$$- (e_{1i}e_{2j}+e_{2i}e_{ij})\cos\theta \sin\theta - e_{2i}e_{2j}\sin^2\theta]$$

$$(D\tan\theta)(D/\cos^2\theta) - C_1[C_2\delta_{ij}\log\left(\frac{D}{\cos\theta}\right)$$

$$- (e_{1i}e_{1j}\cos^2\theta - (e_{1i}e_{2j}+e_{2i}e_{1j})\cos\theta \sin\theta$$

$$- e_{2i}e_{2j}\sin^2\theta] Z_a(D/\cos^2\theta)d\theta$$

$$\Delta T_{ij} = \int_{\theta_a}^{\theta_b} C_3 \frac{\cos\theta}{D} \Big\{ \cos\theta[C_4\delta_{ij} + 2e_{1i}e_{1j}\cos^2\theta +$$

$$+ 2(e_{1i}e_{2j}+e_{2i}e_{1j})\cos\theta \sin\theta + 2e_{2i}e_{2j}\sin^2\theta]$$

$$- C_4(e_{2i}e_{1j}-e_{1i}e_{2j})\sin\theta \Big\} (D/\cos^2\theta)d\theta \qquad (A7)$$

$$\Delta T_{ij} = \frac{1}{\Delta S} \int_{\theta_a}^{\theta_b} C_3 \frac{\cos\theta}{D} \Big\{ \cos\theta[C_4\delta_{ij} + 2e_{1i}e_{1j}\cos^2\theta$$

$$+ 2(e_{1i}e_{2j}+e_{2i}e_{1j})\cos\theta \sin\theta + 2e_{2i}e_{2j}\sin^2\theta]$$

$$- C_4(e_{2i}e_{1j}-e_{1i}e_{2j})\sin\theta \Big\} (D\tan\theta)\ (D/\cos^2\theta)$$

$$- C_3 \frac{\cos\theta}{D} \Big\{ \cos\theta[C_4\delta_{ij} + 2e_{1i}e_{1j}\cos^2\theta$$

$$+ 2(e_{1i}e_{2j}+e_{2i}e_{1j})\cos\theta \sin\theta + 2e_{2i}e_{2j}\sin^2\theta]$$

$$- C_4(e_{2i}e_{1j}-e_{1i}e_{2j})\sin\theta \Big\} Z_a(D/\cos^2\theta)\, d\theta\ .$$

Rearranging and carrying out the integrations with respect to θ

$$\Delta U_{ij} = C_1C_2\delta_{ij}I_{U1} - C_1e_{1i}e_{1j}I_{U2} - C_1(e_{1i}e_{2j}+e_{ei}e_{1j})I_{U3}$$

$$- C_1e_{2i}e_{2j}I_{U4}\,, \qquad (A8)$$

where $I_{U1} = D[\tan\theta_b(\log r_b - 1) - \tan\theta_a(\log r_a - 1) + (\theta_b - \theta_a)]$

$I_{U2} = D(\theta_b - \theta_a)$

$I_{U3} = D \log(ra/rb)$

$I_{U4} = D[\tan\theta_b - \tan\theta_a - (\theta_b - \theta_a)]$;

$$\Delta u_{ij} = \frac{C_1 C_2 \delta_{ij}}{\Delta S}(I_{U5} - I_{U4}) - \frac{C_1 e_{1i} e_{1j}}{\Delta S}(I_{U6} - I_{U10}) - \frac{C_1(e_{1i}{}^2{}_{2j} + e_{2i} e_{1j})}{\Delta S}(I_{U7} - I_{U11}) - \frac{C_1 e_{2i} e_{2j}}{\Delta S}(I_{U8} - I_{U12}), \tag{A9}$$

where $I_{U5} = (r_b^2/4)(2\log r_b - 1) - r_a^2/4(2\log r_a - 1)$

$I_{U6} = D^2 \log(r_b/r_a)$

$I_{U7} = D^2[\tan\theta_b - \tan\theta_a - (\theta_b - \theta_a)]$

$I_{U8} = D^2[1/2(\tan^2{}_b - \tan^2{}_a) - \log(r_b/r_a)]$

$I_{U9} = Z_a I_{U1}$

$I_{U10} = Z_a I_{U2}$

$I_{U11} = Z_a I_{U3}$

$I_{U12} = Z_a I_{U4}$;

$$\Delta T_{ij} = C_3C_4\delta_{ij}I_{T1} + C_3e_{1i}e_{1j}I_{T2} + C_3(e_{1i}e_{2j}+e_{2i}e_{1j})I_{T3}$$

$$+ C_3e_{ei}e_{2j}I_{T4} - C_3C_4(e_{2i}e_{1j}-e_{1i}e_{2j})I_{T5}\,, \tag{A10}$$

where $I_{T1} = (\theta_b-\theta_a)$

$I_{T2} = (\theta_b-\theta_a) + \sin\theta_b \cos\theta_b - \sin\theta_a \cos\theta_a$

$I_{T3} = \sin^2\theta_b - \sin^2\theta_a$

$I_{T4} = (\theta_b-\theta_a) - \sin\theta_b \cos\theta_b + \sin\theta_a \cos\theta_a$

$I_{T5} = \log (r_b/r_a)$;

and $$\Delta T_{ij} = \frac{C_3C_4\delta_{ij}}{\Delta S}\ (I_{T6}-I_{T11}) + \frac{C_3e_{1i}e_{1j}}{\Delta S}\ (I_{17}-I_{T12})$$

$$+ \frac{C_3(e_{1i}e_{2j} + e_{2i}e_{1j})}{\Delta S}\ (I_{T8}-I_{T13}) \tag{A11}$$

$$+ \frac{C_3e_{2i}e_{2j}}{\Delta S}\ (I_{T4}-I_{T14}) - C_3C_4(e_{2i}e_{1j}-e_{1i}e_{2j})$$

$$(I_{T10}-I_{T15})\,,$$

where $I_{T6} = D \log (r_b/r_a)$

$I_{T7} = D(\sin^2\theta_b - \sin^2\theta_a)$

$I_{T8} = D[(\theta_b-\theta_a) - \sin\theta_b \cos\theta_b + \sin\theta_a \cos\theta_b]$

$I_{T9} = D[\cos^2\theta_b - \cos^2\theta_a + 2 \log (r_b/r_a)]$

$$I_{T10} = D[\tan\theta_b - \tan\theta_a - (\theta_b - \theta_a)]$$

$$I_{T11} = Z_a I_{T1}$$

$$I_{T12} = Z_a I_{T2}$$

$$I_{T13} = Z_a I_{T3}$$

$$I_{T14} = Z_a I_{T4}$$

$$I_{T15} = Z_a I_{T5} .$$

For the special case of D = 0, θ becomes either plus or minus $\pi/2$ depending upon whether the node N is behind or in front of the segment being integrated over, and the forms of integrands in terms of θ given in equations (A7) become indeterminate. Introducing the parameter

$$SGN = \begin{cases} +1 \text{ for node N behind the segment } (\theta=+\pi/2) \\ -1 \text{ for node N in front of the segment } (\theta=-\pi/2) \end{cases},$$

and noting that for D = 0

$$\begin{aligned} SIN\ \theta &= SGN \\ COS\ \theta &= 0 , \end{aligned} \tag{A12}$$

the kernels in equations (A5) become

$$\begin{aligned} U_{ij} &= C_1(C_2\delta_{ij} \log r - e_{2i}e_{2j}) \\ T_{ij} &= - C_3C_4 \left(\frac{1}{r}\right) (e_{2i}e_{1j}-e_{1i}e_{2j})(SGN). \end{aligned} \tag{A13}$$

Also noting that for D = 0

$$\Delta S = (SGN)\ (r) - Z_a \tag{A14}$$

$$dS = (SGN)\ dr,$$

the integrals for the special case of D = 0 become

$$\Delta U_{ij} = \int_{r_a}^{r_b} C_1(C_2\delta_{ij} \log r - e_{2i}e_{2j})(SGN)\ dr$$

$$\Delta U_{ij} = \frac{1}{\Delta S} \int_{r_a}^{r_b} [C_1(C_2\delta_{ij} \log r - e_{2i}e_{2j})\ r \tag{A15}$$

$$- C_1(C_2\delta_{ij} \log r - e_{2i}e_{2j})Z_a(SGN)]\ dr$$

$$\Delta T_{ij} = \int_{r_a}^{r_b} C_3C_4\ \frac{1}{r}\ (e_{2i}e_{1j}-e_{1i}e_{2j})\ dr$$

$$\Delta T_{ij} = -\frac{1}{\Delta S} \int_{r_a}^{r_b} [C_3C_4\ \frac{1}{r}\ (e_{2i}e_{1j} - e_{1i}e_{2j})\ (SGN)\ r$$

$$- C_3C_4\ \frac{1}{r}\ (e_{2i}e_{1j}-e_{1i}e_{2j})Z_a]\ dr.$$

Rearranging and carrying out the integrations with respect to r

$$\Delta U_{ij} = C_1C_{2\ ij}I_{U13} - C_1e_{2i}e_{2j}I_{U14}\ , \tag{A16}$$

where $I_{U13} = (SGN)\ [r_b(\log r_b - 1) - r_a(\log r_a - 1)\ ]$

$I_{U14} = (SGN)\ (r_b - r_a)$;

$$\Delta u_{ij} = \frac{C_1 C_2 \delta_{ij}}{\Delta S}\ (I_{U15} - I_{U17}) - \frac{C_1 e_{2i} e_{2j}}{\Delta S}\ (I_{U16} - I_{U18}), \tag{A17}$$

where $I_{U15} = [(r_b^2/4)(2 \log r_b - 1) - (r_a^2/4)(2 \log r_a - 1)]$

$I_{U16} = (r_b^2 - r_a^2)/2$

$I_{U17} = Z_a I_{U13}$

$I_{U18} = Z_a I_{U14}$;

$$\Delta T_{ij} = - C_3 C_4 (e_{2i} e_{1j} - e_{1i} e_{2j}) I_{T16}, \tag{A18}$$

where $I_{T16} = \log(r_b/r_a)$;

and $$\Delta T_{ij} = - \frac{C_3 C_4 (e_{2i} e_{1j} - e_{1i} e_{2j}}{\Delta S}\ (I_{T17} - I_{T18})\ , \tag{A19}$$

where $I_{T17} = (SGN)(r_b - r_a)$

$I_{T18} = Z_a I_{T16}$.

2. *Differentiated Somigliana Identity* - The kernels of the differentiated Somigliana identity for two dimensions are given by

$$U_{ij,k} = C_1 \left(\frac{1}{r}\right) [C_2\delta_{ij}r_{,k} - \delta_{ik}r_{,j} - \delta_{jk}r_{,i} + 2r_{,i}r_{,j}r_{,k}]$$

$$T_{ij,k} = C_3 \left(\frac{1}{r^2}\right) \left\{ \frac{\partial r}{\partial n} [-2C_4\delta_{ij}r_{,k} + 2\delta_{ik}r_{,j} + 2\delta_{jk}r_{,i} - 8r_{,i}r_{,j}r_{,k}] \right. \tag{A20}$$

$$+ C_4[n_k\delta_{ij} + n_i\delta_{jk} - n_j\delta_{ik} - 2n_ir_{,j}r_{,k} + 2n_jr_{,i}r_{,k}]$$

$$\left. + 2n_kr_{,i}r_{,j} \right\},$$

where C_1 through C_4 are defined in equation (A2), and the geometric quantities are defined, as before, in Figure A-1.

Four types of integrals are required for the internal displacement gradient quadrature

$$\begin{aligned} \Delta D_{ijk} &= \int_{\Delta S} U_{ij,k}\, dS \\ \Delta \mathcal{D}_{ijk} &= \frac{1}{\Delta S} \int_{\Delta S} U_{ij,k}\, S\, dS \\ \Delta S_{ijk} &= \int_{\Delta S} T_{ij,k}\, dS \\ \Delta \mathcal{S}_{ijk} &= \frac{1}{\Delta S} \int_{\Delta S} T_{ij,k}\, S\, dS. \end{aligned} \tag{A21}$$

Again using the notation introduced in Figure A-1 and equations (A4), the kernels (A20) can be rewritten in the following form

$$U_{ik,k} = C_1\left(\frac{1}{r}\right)\Big\{C_2\delta_{ij}(e_{1k}\cos\theta + e_{2k}\sin\theta) - \delta_{ik}(e_{1j}\cos\theta + e_{2j}\sin\theta)$$

$$- \delta_{jk}(e_{1i}\cos\theta + e_{2i}\sin\theta) + 2e_{1i}e_{1j}e_{1k}\cos^3\theta$$

$$+ 2(e_{2i}e_{1j}e_{1k}+e_{1i}e_{2j}e_{1k}+e_{1i}e_{1k}e_{2k})\cos^2\theta\sin\theta \qquad \text{(A22a)}$$

$$+ 2(e_{1i}e_{2j}e_{2k}+e_{2i}e_{1j}e_{2k}+e_{2i}e_{2j}e_{1k})\sin^2\theta\cos\theta$$

$$+ 2e_{2i}e_{2j}e_{2k}\sin^3\theta\Big\}$$

$$T_{ij,k} = C_3\left(\frac{1}{r}\right)^2 \Big\{ (-2C_4\delta_{ij}e_{1k}+2\delta_{ik}e_{1j}+2\delta_{jk}e_{1i})\cos^2\theta$$

$$+ (-2C_4\delta_{ij}e_{2k}+2\delta_{ik}e_{1i})\sin\theta\cos\theta - 8\cos\theta[e_{1i}e_{1j}e_{1k}\cos^3\theta$$

$$+ (e_{2i}e_{1j}e_{1k}+e_{1i}e_{2j}e_{1k}+e_{1i}e_{1j}e_{2k})\sin\theta\cos^2\theta$$
$$+ (e_{1i}e_{2j}e_{2k}+e_{2i}e_{1j}e_{2k}+e_{2i}e_{2j}e_{2k})\sin^2\theta\cos\theta + e_{2i}e_{2j}e_{2k}\sin^3\theta]\Big\}$$
$$+ C_3C_4\left(\frac{1}{r}\right)^2\Big\{ e_{1k}\delta_{ij} + e_{1i}\delta_{jk} - e_{1j}\delta_{ik} - 2e_{1i}[e_{1j}e_{1k}\cos^2\theta \qquad \text{(A22b)}$$

$$+ (e_{1j}e_{2k}+e_{2j}e_{1k})\sin\theta\cos\theta + e_{2j}e_{2k}\sin^2\theta] + 2e_{1j}[e_{1i}e_{1k}\cos^2\theta$$

$$+ (e_{1i}e_{2k}+e_{2i}e_{1k})\sin\theta\cos\theta + e_{2i}e_{2k}\sin^2\theta]\Big\} + 2C_3\left(\frac{1}{r}\right)^2 e_{1k}$$

$$[e_{1i}e_{1j}\cos^2\theta + (e_{1i}e_{2j}+e_{ei}e_{1j})\sin\theta\cos\theta + e_{2i}e_{2j}\sin^2\theta].$$

Finally, substituting equations (A22) into (A21), and integrating with respect to θ yields

$$\Delta D_{ijk} = C_1(C_2\delta_{ij}e_{1k}-\delta_{ik}e_{1j}-\delta_{jk}e_{1i})I_{D1} + C_1(C_2\delta_{ij}e_{2k}-\delta_{ik}e_{2j}-\delta_{jk}e_{2i})I_{D2}$$

$$+ C_1(e_{1i}e_{1j}e_{1k})I_{D3} + C_1(e_{2i}e_{1j}e_{1k}+e_{1i}e_{2j}e_{1k}+e_{1i}e_{1j}e_{2k})I_{D4} \qquad \text{(A23)}$$

$$+ C_1(e_{1i}e_{2j}e_{1k}+e_{2i}e_{1j}e_{2k}+e_{2i}e_{2j}e_{1k})I_{D5} + C_1(e_{2i}e_{2j}e_{2k})I_{D6},$$

where $I_{D1} = (\theta_b - \theta_a)$

$I_{D2} = \log (r_b/r_a)$

$I_{D3} = (\theta_b - \theta_a) + \sin \theta_b \cos \theta_b - \sin \theta_a \cos \theta_a$

$I_{D4} = \sin^2 \theta_b - \sin^2 \theta_a$

$I_{D5} = (\theta_b - \theta_a) - \sin \theta_b \cos \theta_b + \sin \theta_a \cos \theta_a$

$I_{D6} = \cos^2 \theta_b - \cos^2 \theta_a + 2 \log (r_b/r_a)$;

$$\Delta \mathcal{D}_{ijk} = \frac{C_1(C_2\delta_{ij}e_{1k} - \delta_{ik}e_{1j} - \delta_{jk}e_{1i})}{\Delta S} (I_{D7} - I_{D13})$$

$$+ \frac{C_1(e_{1i}e_{1j}e_{1k})}{\Delta S} \quad (I_{D9} - I_{D15})$$

$$+ \frac{C_1(e_{2i}e_{1j}e_{1k} + e_{1i}e_{2j}e_{1k} + e_{1i}e_{1j}e_{2k})}{\Delta S} \quad (I_{D10} - I_{D16}) \qquad \text{(A24)}$$

$$+ \frac{C_1(e_{1i}e_{2j}e_{2k} + e_{2i}e_{1j}e_{2k} + e_{2i}e_{2j}e_{1k})}{\Delta S} \quad (I_{D11} - I_{D17})$$

$$+ \frac{C_1(e_{2i}e_{2j}e_{2k})}{\Delta S} \quad (I_{D12} - I_{D18}),$$

where $I_{D7} = D \log (r_b/r_a)$

$I_{D8} = D[\tan \theta_b - \tan \theta_a - (\theta_b - \theta_a)]$

$I_{D9} = D[\sin^2 \theta_b - \sin^2 \theta_a]$

$$I_{D10} = D[(\theta_b-\theta_a) - \sin\theta_b \cos\theta_b + \sin\theta_a \cos\theta_a]$$

$$I_{D11} = D[\cos^2\theta_b - \cos^2\theta_a + 2 \log (r_b/r_a)]$$

$$I_{D12} = D[2(\tan\theta_b - \tan\theta_a) - 3(\theta_b-\theta_a) + \sin\theta_b \cos\theta_b - \sin\theta_a \cos\theta_a]$$

$$I_{D13} = Z_a I_{D1}$$

$$I_{D14} = Z_a I_{D2}$$

$$I_{D15} = Z_a I_{D3}$$

$$I_{D16} = Z_a I_{D4}$$

$$I_{D17} = Z_a I_{D5}$$

$$I_{D18} = Z_a I_{D6} ;$$

$$\begin{aligned}
\Delta S_{ijk} = {} & C_3(-C_4\delta_{ij}e_{1k} + \delta_{jk}e_{1i} + e_{1i}e_{1j}e_{1k})I_{S1} \\
& + C_3[-C_4\delta_{ij}e_{2k} + \delta_{ik}e_{2j} + \delta_{jk}e_{2i} + e_{1i}e_{2j}e_{1k}(1-C_4) \\
& + e_{2i}e_{1j}e_{1k}(1+C_4)]I_{S2} - C_3(e_{1i}e_{1j}e_{1k})I_{S3} \\
& - C_3(e_{2i}e_{1j}e_{1k} + e_{1i}e_{2j}e_{1k} + e_{1i}e_{1j}e_{2k})I_{S4} \\
& - C_3(e_{1i}e_{2j}e_{2k} + e_{2i}e_{1j}e_{2k} + e_{2i}e_{2j}e_{1k})I_{S5} \\
& - C_3(e_{2i}e_{2j}e_{2k})I_{S6} + C_3C_4(e_{1k}\delta_{ij} + e_{1i}\delta_{jk} - e_{1j}\delta_{ik})I_{S7} \\
& - C_3[C_4(-e_{1i}e_{2j}e_{2k} + e_{21}e_{1j}e_{2k}) + (e_{2i}e_{2j}e_{1k})]I_{S8},
\end{aligned} \tag{A25}$$

where $I_{S1} = [(\theta_b-\theta_a) + \sin\theta_a \cos\theta_b - \sin\theta_a \cos\theta_a]/D$

$I_{S2} = (\sin^2\theta_b-\sin^2\theta_a)/D$

$I_{S3} = [3(\theta_b-\theta_a) + 5(\sin\theta_b \cos\theta_b - \sin\theta_a \cos\theta_a)$

$- 2(\sin^3\theta_b \cos\theta_b - \sin^3\theta_a \cos\theta_a)]/D$

$I_{S4} = -2(\cos^4\theta_b - \cos^4\theta_a)/D$

$I_{S5} = [(\theta_b-\theta_a) - (\sin\theta_b \cos\theta_b - \sin\theta_a \cos\theta_a)$

$+ (\sin^3\theta_b \cos\theta_b - \sin^3\theta_a \cos\theta_b)]/D$

$I_{S6} = 2(\sin^4\theta_b - \sin^4\theta_a)/D$

$I_{S7} = (\theta_b-\theta_a)/D$

$I_{S8} = [(\theta_b-\theta_a) - \sin\theta_b \cos\theta_a + \sin\theta_a \cos\theta_a]/D$;

$$\begin{aligned}\text{and } \Delta S_{ijk} = {} & \frac{C_3}{\Delta S}(-C_4\delta_{ij}e_{1k}+\delta_{ik}e_{1j}+\delta_{jk}e_{1i}+e_{1i}e_{1j}e_{1k})(I_{S9}-I_{S17}) \\ & + \frac{C_3}{\Delta S}[-C_4\delta_{ij}e_{2k} + \delta_{ik}e_{2j} + \delta_{jk}e_{2i} + e_{1i}e_{2j}e_{1k}(1-C_4) \\ & + e_{2i}e_{1j}e_{1k}(1+C_4)](I_{S10}-I_{S18}) - \frac{C_3}{S}(e_{1i}e_{1j}e_{1k})(I_{S11}-I_{S19}) \\ & - \frac{C_3}{\Delta S}(e_{2i}e_{1j}e_{1k}+e_{1i}e_{2j}e_{1k}+e_{1i}e_{1j}e_{2k})(I_{S12}-I_{S20}) \\ & - \frac{C_3}{\Delta S}(e_{1i}e_{2j}e_{2k}+e_{2i}e_{1j}e_{2k}+e_{2i}e_{2j}e_{1k})(I_{S13}-I_{S21})\end{aligned} \tag{A26}$$

$$- \frac{C_3}{\Delta S} (e_{2i}e_{2j}e_{2k})(I_{S14}-I_{S22})$$

$$+ \frac{C_3C_4}{\Delta S} (e_{1k}\delta_{ij}+e_{1i}\delta_{jk}-e_{1j}\delta_{ik})(I_{S15}-I_{S23})$$

$$+ \frac{C_3}{\Delta S} [C_4(-e_{1i}e_{2j}e_{2k}+e_{2i}e_{1j}e_{2k}) + (e_{2i}e_{2j}e_{1k})](I_{S16}-I_{S24}),$$

where $I_{S9} = (\sin^2 \theta_b - \sin^2 \theta_a)$

$I_{S10} = [(\theta_b-\theta_a) - \sin \theta_b \cos \theta_b + \sin \theta_a \cos \theta_a]$

$I_{S11} = -2(\cos^4 \theta_b-\cos^4 \theta_a)$

$I_{S12} = [(\theta_b-\theta_a) - (\sin \theta_b \cos \theta_b - \sin \theta_a \cos \theta_a)$
$+ 2(\sin^3 \theta_b \cos \theta_b - \sin^3 \theta_a \cos \theta_a)]$

$I_{S13} = 2(\sin^4 \theta_b - \sin^4 \theta_a)$

$I_{S14} = [3(\theta_b-\theta_a) - 3(\sin \theta_b \cos \theta_b - \sin \theta_a \cos \theta_a)$
$- 2(\sin^3 \theta_b \cos \theta_b - \sin^3 \theta_a \cos \theta_a)]$

$I_{S15} = \log (r_b/r_a)$

$I_{S16} = \cos^2 \theta_b - \cos^2 \theta_a + 2 \log (r_b/r_a)$

$I_{S17} = Z_a I_{S1}$

$I_{S18} = Z_a I_{S2}$

$I_{S19} = Z_a I_{S3}$

$I_{S20} = Z_a I_{S4}$

$$I_{S21} = Z_a I_{S5}$$

$$I_{S22} = Z_a I_{S6}$$

$$I_{S23} = Z_a I_{S7}$$

$$I_{S24} = Z_a I_{S8}.$$

Again the case when D = 0 must be given special consideration.

Using the same notation as before (A12)

$$\Delta D_{ijk} = C_1(C_2\delta_{ij}e_{2k}-\delta_{ik}e_{2j}-\delta_{jk}e_{2i}+2e_{2i}e_{2j}e_{2k})I_{D19}, \tag{A27}$$

$$\text{where} \quad I_{D19} = \ln(r_b/r_a);$$

$$\Delta D_{ijk} = \frac{C_1}{\Delta S}(C_2\delta ije_{2k}-\delta_{ik}e_{2j}-\delta_{jk}e_{2i}+2e_{2i}e_{2j}e_{2k})(I_{D20}-I_{D21}), \tag{A28}$$

$$\text{where} \quad I_{D20} = SGN(r_b-r_a)$$

$$I_{D21} = Z_a I_{D19};$$

$$\Delta S_{ijk} = C_3[C_4(e_{1k}\delta_{ij}+e_{1i}\delta_{jk}-e_{1j}\delta_{ik}-2e_{1i}e_{2j}e_{2k}+2e_{2i}e_{1j}e_{2k}) + 2e_{2i}e_{2j}e_{1k}]I_{S25}, \tag{A29}$$

$$\text{where} \quad I_{S25} = -SGN(1/r_b-1/r_a);$$

$$\text{and } \Delta S_{ijk} = \frac{C_3}{\Delta S}\,[C_4(e_{1k}\delta_{ij}+e_{1i}\delta_{jk}-e_{1j}\delta_{ik}-2e_{1i}e_{2j}e_{2k}+2e_{2i}e_{1j}e_{2k}) + 2e_{2i}e_{2j}e_{1k}](I_{S26}-I_{S27}), \tag{A30}$$

$$\text{where} \quad I_{S26} = \ln(r_b/r_a)$$

$$I_{S27} = Z_a I_{S25}$$

APPENDIX B - VALUE OF INTEGRALS FOR A ZERO-LENGTH SEGMENT

In order to determine the contribution to the matrices A(M,N) and B(M,N) from a zero-length segment, the results of the integrations performed in Appendix A must be transformed into terms of the segment length (ΔS), and their limits taken as ΔS approaches zero. The results of Appendix A are given in terms of the parameters of end a of the segment (r_a and θ_a) and the parameters of end of the segment (r_b and θ_b), with the segment constants D, Z_a, and ΔS also appearing. (See Figure B1 for definition of terms.) Using the following geometric relations

$$r_b^2 = r_a^2 + (\Delta S)^2 + 2(\Delta S)(Z_a)$$

$$\tan \theta_b = \frac{Z_a + \Delta S}{D} \qquad \text{(B1)}$$

$$(\theta_b - \theta_a) \simeq \frac{(\Delta S)(D)}{D^2 + Z_a^2 + (\Delta S)(Z_a)} \qquad [\text{for small } (\theta_b - \theta_a)],$$

reference to the b end parameters (r_b and θ_b) can be eliminated and thus all dependence of the integrals upon segment length (ΔS) will appear explicitly. The limit of the integrals as ΔS approaches zero can then be evaluated straightforwardly. To simplify the expressions the segment length ΔS will be denoted by ℓ in the remainder of this Appendix.

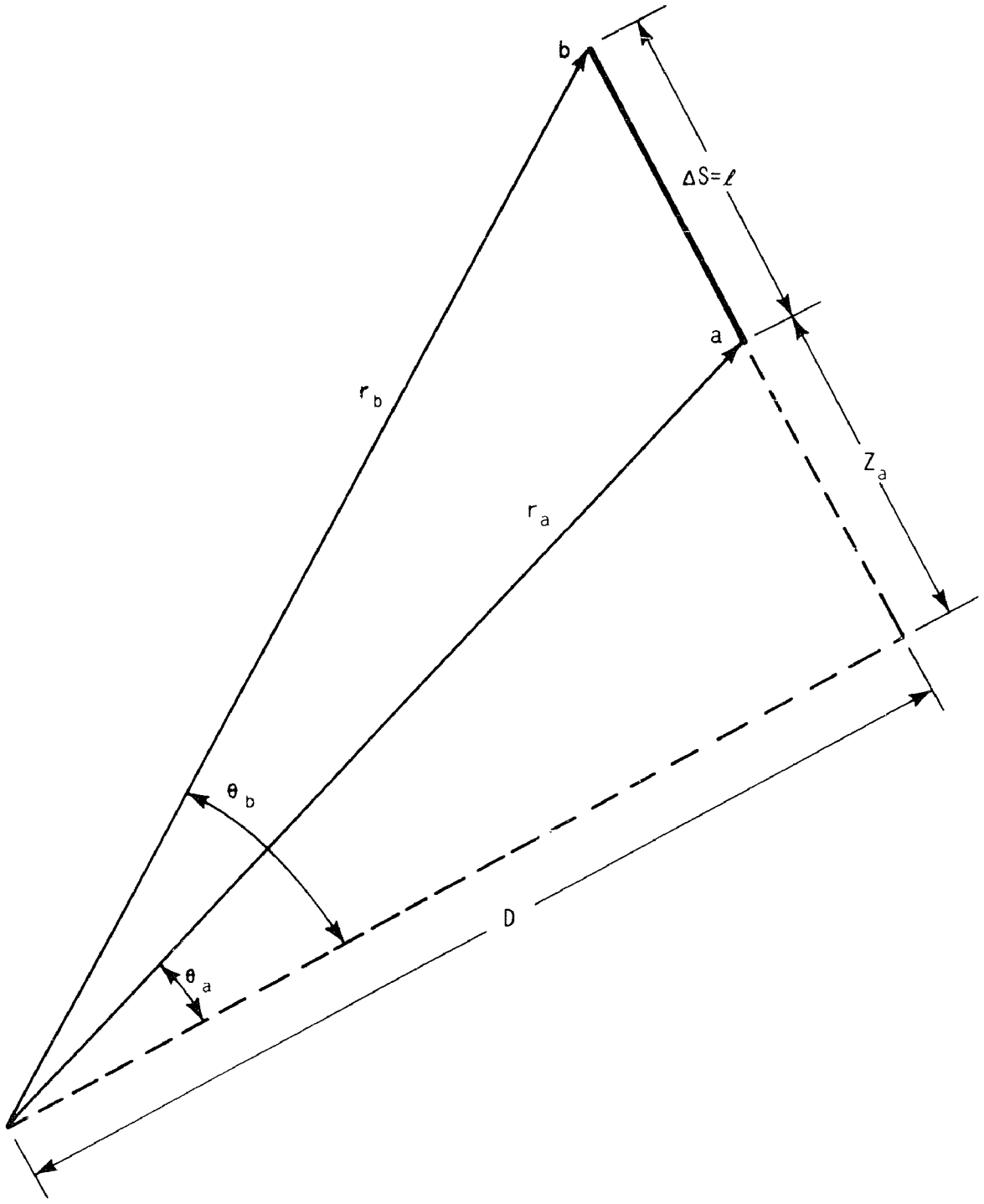

Figure B-1. Notation Used in Integral Limiting Procedure

Recalling expression (A8)

$$U_{ij} = C_1C_2\,\delta_{ij}I_{U1} - C_1e_{1i}e_{1j}I_{U2} - C_1(e_{1i}e_{2j}+e_{2i}e_{1j})I_{U3} - C_1e_{2i}e_{2j}I_{U4}. \tag{A8}$$

But $$\lim_{\ell\to 0} I_{U1} = \lim_{\ell\to 0}\left\{ \ell\left[\frac{\log(r_a^2+\ell^2+2\,Z_a)}{2} - 1\right] + D\left(\frac{\tan\theta_a}{2}\right)\log(1+\ell^2/r_a^2\ell+2\,Z_a/r_a^2) + \frac{\ell D^2}{D^2+Z_a^2+\ell Z_a}\right\}$$

$$= 0$$

$$\lim_{\ell\to 0} I_{U2} = \lim_{\ell\to 0}\left\{\frac{\ell D^2}{D^2+Z_a^2+\ell Z_a}\right\}$$

$$= 0$$

$$\lim_{\ell\to 0} I_{U3} = \lim_{\ell\to 0}\left\{\frac{D}{2}\log(1+\ell^2/r_a^2+2\,Z_a^2/r_a)\right\}$$

$$= 0$$

$$\lim_{\ell\to 0} I_{U4} = \lim_{\ell\to 0}\left\{D\left(\frac{\ell}{D} - \frac{\ell D}{D^2+Z_a^2+\ell Z_a}\right)\right\}$$

$$= 0.$$

Substituting these limits into equation (A8)

$$\lim_{\ell\to 0} \Delta U_{ij} = 0 \tag{B2}$$

Recalling expression (A9)

$$\Delta u_{ij} = C_1 C_2 \delta_{ij} \frac{(I_{U5}-I_{U9})}{\ell} - C_1 e_{1i} e_{1j} \frac{(I_{U6}-I_{U10})}{\ell}$$
$$- C_1 (e_{1i} e_{2j} + e_{2i} e_{1j}) \frac{(I_{U7}-I_{U11})}{\ell} - C_1 e_{21} e_{2j} \frac{(I_{U8}-I_{U12})}{\ell} . \qquad \text{(A9)}$$

But $$\lim_{\ell \to 0} \left(\frac{I_{U5}}{\ell}\right) = \lim_{\ell \to 0} \left\{ \frac{r_a^2}{4\ell} \log \left(1 + \frac{\ell^2}{r_a^2} + \frac{2\ell Z_a}{r_a^2}\right) + \left(\frac{\ell + 2Z_a}{4}\right) \right.$$
$$\left. [\log (r_a^2 + \ell + 2\ell Z_a) - 1] \right\}$$
$$= Z_a \log r_a$$

$$\lim_{\ell \to 0} \left(\frac{I_{U6}}{\ell}\right) = \lim_{\ell \to 0} \left\{ \frac{D^2}{2\ell} \log (1 + \ell^2/r_a^2 + 2\ell Z_a/r_a^2) \right\}$$
$$= Z_a (D^2/r_a^2)$$

$$\lim_{\ell \to 0} \left(\frac{I_{U7}}{\ell}\right) = \lim_{\ell \to 0} \left\{ D \left(1 - \frac{D}{D^2 + Z_a^2 + \ell Z_a}\right) \right\}$$
$$= D(1 - D^2/r_a)$$

$$\lim_{\ell\to 0}\left(\frac{I_{U8}}{\ell}\right) = \lim_{\ell\to 0}\left\{\frac{D^2}{2}\left[\frac{2Z_a+\ell}{D^2} - \log\frac{(1+\ell^2/r_a^2+2\ell Z_a/r_a^2)}{\ell}\right]\right\}$$

$$= Z_a(1-D^2/r_a^2)$$

$$\lim_{\ell\to 0}\left(\frac{I_{U9}}{\ell}\right) = \lim_{\ell\to 0}\left\{\left[Z_a \log\frac{(r_a^2+\ell^2+2\ell Z_a)}{2} - 1\right] + \frac{DZ_a}{\ell}\left(\frac{\tan\theta_a}{2}\right)\right.$$

$$\left.\log(1+\ell^2/r_a+2\ell Z_a/r_a^2) + \frac{Z_a D^2}{D^2+Z_a^2+\ell Z_a}\right\}$$

$$= Z_a \log r_a$$

$$\lim_{\ell\to 0}\left(\frac{I_{U10}}{\ell}\right) = \lim_{\ell\to 0}\left\{\frac{Z_a D^2}{D^2+Z_a^2+\ell Z_a}\right\}$$

$$= Z_a D^2/r_a^2$$

$$\lim_{\ell\to 0}\left(\frac{I_{U11}}{\ell}\right) = \lim_{\ell\to 0}\left\{\frac{Z_a D}{2\ell}\log\left(1+\frac{\ell^2}{r_a^2}+\frac{2\ell Z_a}{r_a^2}\right)\right\}$$

$$= D(Z_a^2/r_a^2)$$

$$\lim_{\ell\to 0}\left(\frac{I_{U12}}{\ell}\right) = \lim_{\ell\to 0}\left\{ Z_a\left[1 - \frac{D^2}{D^2+Z_a^2+\ell Z_a}\right]\right\}$$

$$= Z_a(1-D^2/r_a^2)\,.$$

Substituting these limits into equation (A9) and noting $D^2+Z_a^2 = r_a^2$ yields

$$\lim_{\ell\to 0}\ \Delta u_{ij} = 0\,. \tag{B3}$$

Recalling expression (A10)

$$\Delta T_{ij} = C_3C_4\delta_{ij}I_{T1} + C_3e_{1i}e_{1j}I_{T2} = C_3(e_{1i}e_{2j}+e_{2i}e_{1j})I_{T3}$$
$$+ C_3e_{2i}e_{2j}I_{T4} - C_3C_4(e_{2i}e_{1j}-e_{1i}e_{2j})I_{T5}\,. \tag{A10}$$

But $$\lim_{\ell\to 0} I_{T1} = \lim_{\ell\to 0}\left\{\frac{\ell D}{D^2+Z_a^2+\ell Z_a}\right\} = 0$$

$$\lim_{\ell\to 0} I_{T2} = \lim_{\ell\to 0}\left\{\frac{D}{D^2+Z_a^2+\ell Z_a} + \frac{D(Z_a+\ell)}{r_a^2+\ell^2+2\ell Z_a}\right.$$

$$\left. - \frac{DZ_a}{r_a^2}\right\} = 0$$

$$\lim_{\ell\to 0} I_{T3} = \lim_{\ell\to 0}\left\{\frac{(Z_a+\ell)^2}{r_a^2+\ell^2+2\ell Z_a} - \frac{Z_a^2}{r_a^2}\right\} = 0$$

$$\lim_{\ell\to 0} I_{T4} = \lim_{\ell\to 0} \left\{ \frac{\ell}{D^2+Z_a^2+\ell Z_a} - \frac{D(Z_a+\ell)}{r_a^2+\ell^2+2\ell Z_a} + \frac{DZ_a}{r_a^2} \right\} = 0$$

$$\lim_{\ell\to 0} I_{T5} = \lim_{\ell\to 0} \left\{ \frac{\log(1+\ell^2/r^2+2\ell Z_a/r_a^2)}{2} \right\} = 0$$

Substituting these limits into equation (A10) yields

$$\lim_{\ell\to 0} \Delta T_{ij} = 0. \tag{B4}$$

Recalling expression (A11)

$$\begin{aligned}\Delta T_{ij} = {} & C_3C_4\delta_{ij} \frac{(I_{T6}-I_{T11})}{\ell} + C_3e_{1i}e_{1j} \frac{(I_{T7}-T_{T12})}{\ell} \\ & + C_3(e_{1i}e_{2j}+e_{2i}e_{1j}) \frac{(I_{T8}-I_{T13})}{\ell} + C_3e_{2i}e_{2j}\frac{(I_{T9}-I_{T14})}{\ell} \\ & - C_3C_4(e_{2i}e_{1j}-e_{1i}e_{2j})\frac{(I_{T10}-I_{T15})}{\ell} .\end{aligned} \tag{A11}$$

But $$\lim_{\ell\to 0}\left(\frac{I_{T6}}{\ell}\right) = \lim_{\ell\to 0}\left\{ \frac{D}{2\ell} \log\,(1 + \ell^2/r_a^2 + 2\ell Z_a/r_a^2) \right\}$$

$$= Z_aD/r_a^2$$

$$\lim_{\ell\to 0}\left(\frac{I_{T7}}{\ell}\right) = \lim_{\ell\to 0}\left\{ \frac{D(Z_a+\ell)^2}{\ell(r_a^2+\ell^2+2\ell Z_a)} - \frac{DZ_a^2}{\ell r_a^2} \right\}$$

$$= \frac{2Z_aD}{r_a^2} - \frac{2Z_a^3D}{r_a^4}$$

$$\lim_{\ell\to 0}\left(\frac{I_{T8}}{\ell}\right) = \lim_{\ell\to 0}\left\{\frac{D^2}{(D^2+Z_a^2+\ell Z_a)} - \frac{D^2(Z_a+\ell)}{\ell(r_a^2+\ell^2+2\ell Z_a)} + \frac{D^2 Z_a}{\ell r_a^2}\right\} = 2Z_a^2 D^2/r_a^4$$

$$\lim_{\ell\to 0}\left(\frac{I_{T9}}{\ell}\right) = \lim_{\ell\to 0}\left\{\frac{D}{\ell}\left[\frac{D^2}{r_a^2+\ell^2+2\ell Z_a} - \frac{D^2}{r_a^2} + \log\left(1+\frac{\ell^2}{r_a^2}+\frac{2\ell Z_a}{r_a}\right)\right]\right.$$

$$= \frac{2Z_a D}{r_a^2} - \frac{2Z_a D^3}{r_a^4}$$

$$\lim_{\ell\to 0}\left(\frac{I_{T10}}{\ell}\right) = \lim_{\ell\to 0}\left\{1 - \frac{D^2}{D^2+Z_a^2+Z_a\ell}\right\}$$

$$= 1 - D^2/r_a^2$$

$$\lim_{\ell\to 0}\left(\frac{I_{T11}}{\ell}\right) = \lim_{\ell\to 0}\left\{\frac{Z_a D}{D^2+Z_a^2+\ell Z_a}\right\} = \frac{Z_a D}{r_a^2}$$

$$\lim_{\ell\to 0}\left(\frac{I_{T12}}{\ell}\right) = \lim_{\ell\to 0}\left\{\frac{Z_a D}{D^2+Z_a^2+\ell Z_a} + \frac{Z_a D(Z_a+\ell)}{\ell(r_a^2+\ell^2+2\ell Z_a)} - \frac{DZ_a^2}{\ell r_a^2}\right\}$$

$$= \frac{2Z_a D}{r_a^2} - \frac{2Z_a^3 D}{r_a^4}$$

$$\lim_{\ell\to 0}\left(\frac{I_{T13}}{\ell}\right) = \lim_{\ell\to 0}\left\{\frac{Z_a(Z_a+\ell)^2}{\ell(r_a^2+\ell^2+2\ell Z_a)} - \frac{Z_a^3}{\ell r_a^2}\right\} = \frac{2Z_a^2}{r_a^2} - \frac{2Z_a^4}{r_a^4}$$

$$\lim_{\ell\to 0}\left(\frac{I_{T14}}{\ell}\right)=\lim_{\ell\to 0}\left\{\frac{Z_a D}{D^2+Z_a^2+\ell Z_a}-\frac{Z_a D(Z_a+\ell)}{(r_a^2+\ell^2+2\ell Z_a)}\right.$$

$$\left.+\frac{DZ_a^2}{\ell r_a^2}\right\}=\frac{2Z_a^3 D}{r_a^4}$$

$$\lim_{\ell\to 0}\left(\frac{I_{T15}}{\ell}\right)=\lim_{\ell\to 0}\left\{\frac{Z_a \log\left(1+\ell^2/r_a^2+2\ell Z_a/r_a^2\right)}{2\ell}\right\}=Z_a^2/r_a^2.$$

Substituting these limits back into equation (A11), and again noting that $(D^2+Z_a^2=r_a^2)$ yields

$$\lim_{\ell\to 0}\ \Delta T_{ij}=0. \tag{B5}$$

The same limiting procedure must be carried out for the special case of $(D=0)$. For this special case we can use the following expression to transform the integrals into explicit dependence upon segment length

$$r_b=r_a+(SGN)(\ell),$$

where, as before

$$SGN=\begin{cases}+1 \text{ for node behind segment } (\theta=+\pi/2)\\ -1 \text{ for node in front of segment } (\theta=-\pi/2)\end{cases}.$$

Recalling expression (A16)

$$\Delta U_{ij}=C_1C_2\delta_{ij}I_{U13}-C_1e_{2i}e_{2j}I_{U14}. \tag{A16}$$

But $$\lim_{\ell\to 0} I_{U13} = \lim_{\ell\to 0} \left\{ (r_a + SGN\cdot\ell)\,[\log(r_a+SGN\cdot\ell)-1] - r_a(\log r_a - 1) \right\} \cdot SGN = 0$$

$$\lim_{\ell\to 0} I_{U14} = \lim_{\ell\to 0} \left\{ SGN\cdot[(r_a+SGN\cdot\ell)-r_a] \right\} = 0.$$

Substituting these limits back into equation (A16) yields

$$\lim_{\ell\to 0} \Delta U_{ij} = 0 \quad (\text{for } D = 0). \tag{B6}$$

Recalling expression (A17)

$$\Delta U_{ij} = C_1 C_2 \delta_{ij} \frac{(I_{U15} - I_{U17})}{\ell} - C_1 e_{2i} e_{2j} \frac{(I_{U16} - I_{U18})}{\ell} . \tag{A17}$$

But $$\lim_{\ell\to 0}\left(\frac{I_{U15}}{\ell}\right) = \lim_{\ell\to 0} \left\{ \frac{(r_a+SGN\cdot\ell)^2}{4\ell}\,[2\log(r_a+SGN\cdot\ell)-1] - (r_a^2/4\ell)(2\log r_a - 1) \right\} = Z_a \log r_a$$

$$\lim_{\ell\to 0}\left(\frac{I_{U16}}{\ell}\right) = \lim_{\ell\to 0} \left\{ \frac{(r_a+SGN\cdot\ell)^2 - r_a^2}{\ell} \right\}$$

$$= Z_a$$

$$\lim_{\ell\to 0}\left(\frac{I_{U17}}{\ell}\right) = \lim_{\ell\to 0}\left\{\frac{r_a(r_a+SGN\cdot\ell)}{\ell}\ [\log(r_a+SGN\cdot\ell)-1]\right.$$

$$\left. - \frac{Z_a r_a}{\ell}\ (\log r_a - 1)\right\}\cdot SGN = Z_a \log r_a$$

$$\lim_{\ell\to 0}\left(\frac{I_{U18}}{\ell}\right) = \lim_{\ell\to 0}\left\{Z_a\cdot SGN\cdot\left[\frac{r_a+SGN\cdot\ell}{\ell} - \frac{r_a}{\ell}\right]\right\}$$

$$= Z_a .$$

Substituting these limits back into equation (A17) yields

$$\lim_{\ell\to 0}\Delta u_{ij} = 0 \qquad (\text{For } D = 0) . \tag{B7}$$

Recalling expression (A18)

$$\Delta T_{ij} = - C_3C_4\ (e_{2i}e_{1j} - e_{1i}e_{2j})I_{T16} . \tag{A18}$$

But $$\lim_{\ell\to 0} I_{T16} = \lim_{\ell\to 0}\left\{\log\left(1 + \frac{SGN\cdot\ell}{r_a}\right)\right\} = 0 .$$

Therefore

$$\lim_{\ell\to 0}\Delta T_{ij} = 0 \qquad (\text{For } D = 0) . \tag{B8}$$

Finally, recalling expression (A19)

$$\Delta T_{ij} = - C_3C_4\ (e_{2i}e_{ij} - e_{1i}e_{2j})\ \frac{(I_{T17} - I_{T18})}{\ell} . \tag{A19}$$

But $$\lim_{\ell \to 0} \left(\frac{I_{T17}}{\ell} \right) = \lim_{\ell \to 0} \left\{ \frac{(r_a + SGN \cdot \ell) - r_a}{\ell} \right\} \cdot SGN = 1$$

$$\lim_{\ell \to 0} \left(\frac{I_{T18}}{\ell} \right) = \lim_{\ell \to 0} \left\{ \frac{Z_a \log(1 + \frac{SGN \cdot \ell}{r_a})}{\ell} \right\} = 1 .$$

and substituting these limits back into equation (A19) yields

$$\lim_{\ell \to 0} \Delta T_{ij} = 0 \qquad (\text{For } D = 0). \tag{B9}$$

In summary, it has been formally demonstrated in this Appendix that the net contribution to the matrices A(M,N) and B(M,N) due to an element of zero length is zero, term by term.

APPENDIX C - COMPUTER PROGRAM BITE

The following are input instructions for use of the computer program BITE, which is capable of solving two dimensional (plane stress or plane strain) elasticity problems with mixed displacement and traction type boundary conditions using the boundary-integral technique with linear variation of displacements and tractions on the boundary segments. A full listing of the computer program BITE is not included in this report because of the tremendous bulk which would be required to do so. However, a Fortran deck will be provided by the author upon request.

Input Instructions:

Card A - Title
(18A4)

Card B - (14I5)

- NNOD - number of nodes (MAX = 80)
- NSEG - number of segments (MAX = 80)
- NSYM - number of degrees of symmetry (MAX = 2)
- NBC - number of specified boundary conditions (zero traction assumed for boundary conditions which are not specified)

Card C (14I5)

- K1 { 0 - plane strain; 1 - plane stress
- K2 { 0 - stop after this problem; 1 - continue to next problem
- K3 { 0 - normal; 1 - debug printing of matrices
- K4 { 0 - default; 1 - multiple connectivity (input NODE(I,J))
- K5 { 0 - default; 1 - boundary stress solution
- K6 { 0 - default; 1 - internal displacement solution

K7 { 0 - default
1 - internal stress solution

K8 { 0 - default
1 - generate uniform pressure on all nodes { SIG1 in x_1-direction
SIG2 in x_2-direction

Card D - YOUNG - Young's Modulus
(7F 10.0) PR - Poisson's ratio
SIG - Constant for normalizing stress results (default value = 1.0)
SIG1 - Uniform tension in x_1-direction (used only if K8 = 1)
SIG2 - Uniform tension in x_2-direction (used only if K8 = 1)
SC - Scale factor (default value = 10^7)

Cards E - Node Coordinates: $(x_1(I), x_2(I))$, I = 1, NNOD

Cards F - Segment Definitions: (NA(J), NB(J)), J = 1, NSEG
(1415) (Used only if K4 = 1)

Cards G - Boundary Condition Data*: (NOD, ITYPEI, BCI, XBCI, ITYPE2,
(I5, 5X, 2(I5, 5X, 2F10.0)) BC2, XBC2)

Cards H - Boundary Stress Solution Data: (used only if K5 = 1)

Card H_1(I5) - NSSG - Number of segments for which boundary stress solution desired (If NSSG is zero, all segments are used, and cards H_2 are not read).

Cards H_2(1415) - N1, N2, ... NNSSG
List of segments for which boundary stress solution is desired.

Cards I - Interior Displacement Solution Data: (used only if K6 = 1)

Card I_1(I5) - NPTS - Number of interior displacement points.

Cards I_2 (7F10.0) - $(x_1(N), x_2(N), N = 1, NPTS)$ - coordinates of interior displacement points.

Cards J - Interior Stress Solution Data: (used only if K7 = 1)

Card J_1(I5) - NPTS - Number of interior stress points.

Cards J_2 (7F10.0) - $(x_1(N), x_2(N), N = 1, NPTS)$ - coordinates of interior stress points.

---

*See Table C1 for definition of terms.

TABLE C1 - BOUNDARY CONDITION DEFINITIONS

I TYPE	MEANING
0	TRACTION = 0 (Default Value)
1	TRACTION = BC
2	DISPLACEMENT = 0
3	DISPLACEMENT = BC
4	STEP FROM TRACTION = BC to TRACTION = XBC
5	STEP FROM TRACTION = BC to DISPLACEMENT = XBC
6	STEP FROM DISPLACEMENT = BC to TRACTION = XBC

A flow chart for the computer program BITE is given in Figure C1, and the format of the input instructions is illustrated in Figure C2.

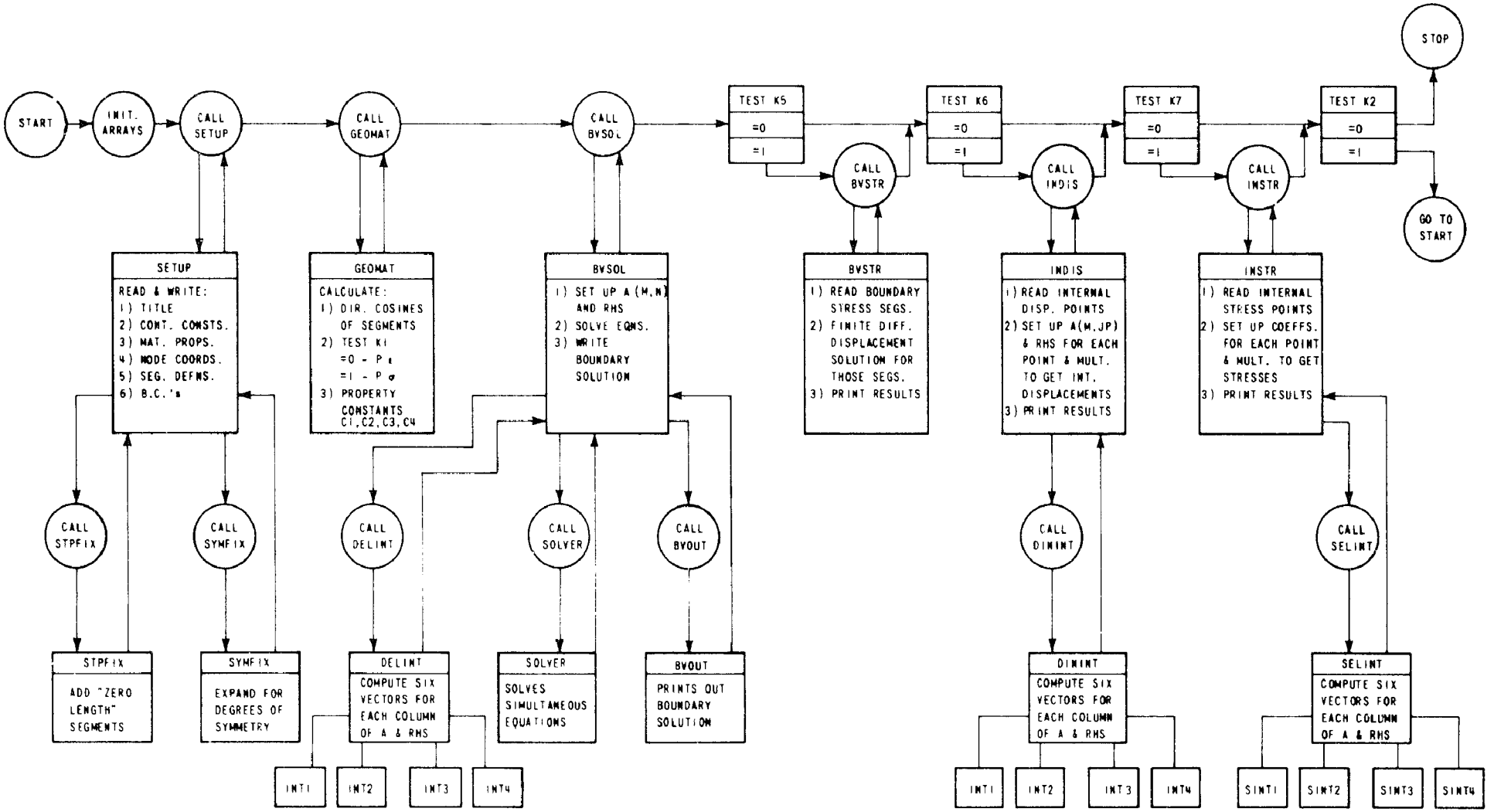

Figure C-1. Flow Chart for Computer Program BITE

COLUMNS:	10		20		30		40		50		60		70	
CARD A	←						TITLE							→
CARD B	NNOD	NSEG	NSYM	NBC										
CARD C	K1	K2	K3	K4	K5	K6	K7	K8						
CARD D	YOUNG.		PR.		SIG.		SIG1.		SIG2.		SC.			
CARDS E	X1(1). X1(2). ↓ X1(NNOD).		X2(1). X2(2). ↓ X2(NNOD).											
CARDS F	NA(1) ~	NB(1) ~	NA(2) ~	NB(2) ~	~ ~	~ ~	~ NA(NSEG)	~ NB(NSEG)	~	~	~	~	~	~
CARDS G	NOD ↓	⊠	ITYPE1 ↓	⊠	BC1. ↓		XBC1. ↓		ITYPE2 ↓	⊠	BC2. ↓		XBC2. ↓	
CARD H_1	NSSG													
CARDS H_2	N1 ~	N2 ~	N3 ~	N4 ~	~ ~	~ ~	~ NNSSG	~	~	~	~	~	~	~
CARD I_1	NPTS													
CARDS I_2	X1(1). ~		X2(1). ~		X1(2). ~		X2(2). X1(NPTS).		~ X2(NPTS).		~		~	
CARD J_1	NPTS													
CARDS J_2	X1(1). ~		X2(1). ~		X1(2). ~		X2(2). X1(NPTS).		~ X2(NPTS).		~		~	

Figure C-2. Illustrated Input Instructions for Computer Program Bite

APPENDIX D - VOLUME INTEGRATION SCHEME

Two types of volume integrals are required for the elasto-plastic implementation of Chapter III. Using the shorthand notation introduced in equations (3-10) and (3-12), the required integrals can be written as summations of the following integrals over constant plastic strain internal elements

$$\Delta\Sigma_{ijk}(M,JP) = \int_{V_{IP}} \Sigma_{ijk}(z_M, x_{JP}) dV_{JP} \tag{3-10}$$

$$\Delta E_{\ell ijk}(IP,JP) = \frac{\partial}{\partial \xi_\ell} \int_{V_{IP}} \Sigma_{ijk}(\xi_{IP}, x_{JP}) dV_{JP}, \tag{3-12}$$

where M refers to boundary nodes and IP and JP refer to internal elements (Figure 3-1). Σ_{ijk} for two-dimensions (plane strain) is given by equation (3-5)

$$\Sigma_{ijk}(r) = \frac{C_3}{r} \left[C_4(\delta_{ij}r,_k + \delta_{ik}r,_j - \delta_{jk}r,_i) + 2r,_i r,_j r,_k\right] \tag{3-5}$$

where:

$$C_3 = -1/4\pi(1-\nu)$$
$$C_4 = (1-2\nu)$$
$$r_i = (x_i - \xi_i)$$
$$r,_i = \partial r/\partial x_i \ .$$

(Figure 2-1)

Once again the case of plane stress is handled through the use of an effective Poisson's ratio.

Consider the internal element to be a general straight-sided multi-laterial of unit thickness as shown in Figure D-1. (The element can have any number of sides; four sides are shown in Figure D-1 for illustration only.) A volume integral over the element can be represented as the algebraic sum of the volume integrals over the four triangles $\overline{A}$, $\overline{B}$, $\overline{C}$, and $\overline{D}$ in this figure, regardless of whether the base point ξ is internal to or external to the element. In both cases a small circular region (radius ε) around the base point ξ is excluded because of the singular nature of the kernel Σ_{ijk} at that point.

The volume integration is now carried out for one triangle at a time as follows. Introducing the cylindrical coordinate system (r,ϕ) based at the point ξ as shown in Figure D-2, we can write

$$\Sigma_{ijk}(\xi,\overline{A}) = \int_{\overline{A}} \Sigma_{ijk}(r)dV_{\overline{A}} = \int_{\phi_a}^{\phi_b}\int_{\varepsilon}^{R(\phi)} \Sigma_{ijk}(r,\phi)rdrd\phi. \qquad (D1)$$

In the (r,ϕ) coordinate system

$$\frac{\partial r}{\partial x_1} = \cos\phi$$

$$\frac{\partial r}{\partial x_2} = \sin\phi$$

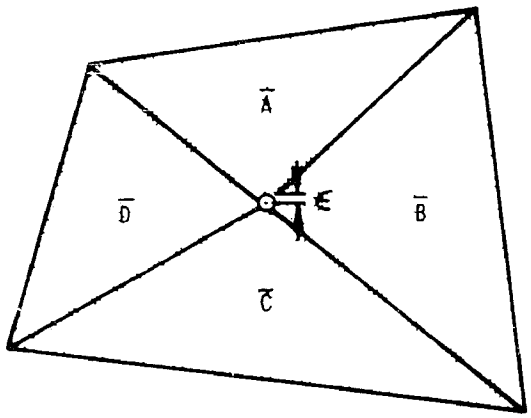

a) BASE POINT ξ INTERNAL TO ELEMENT IP

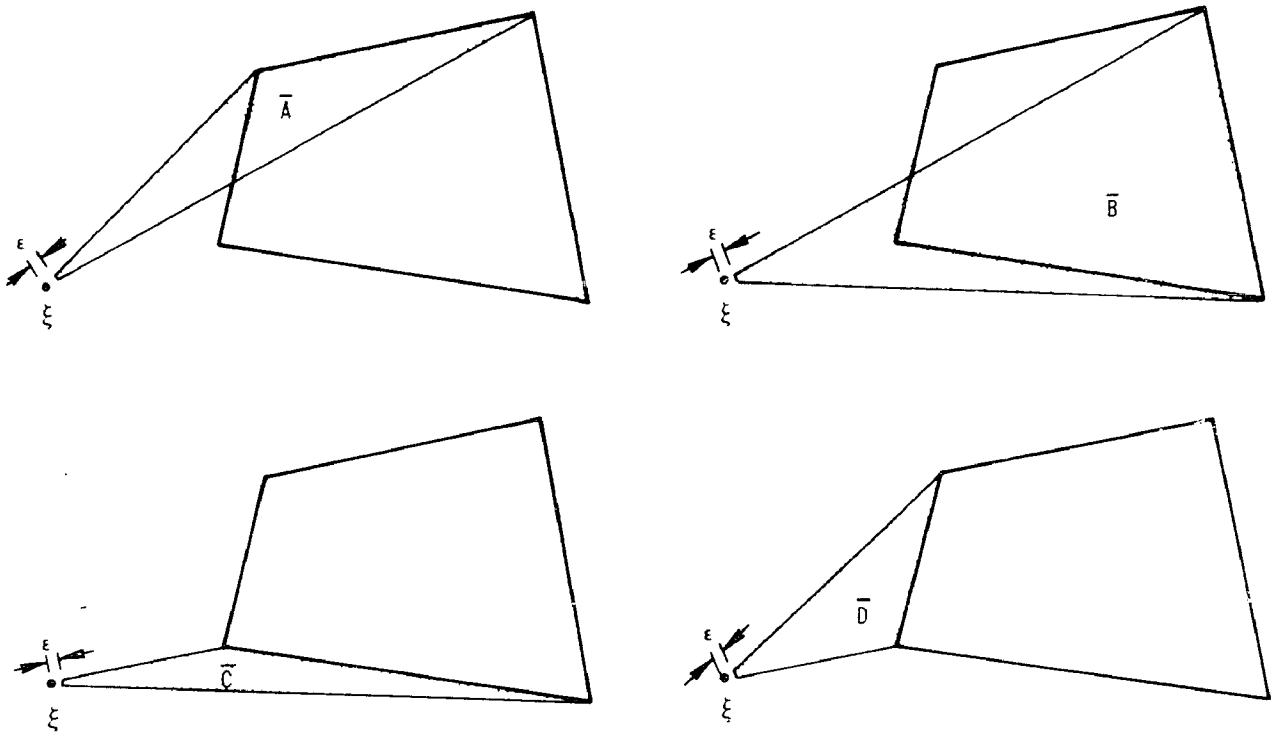

b) BASE POINT ξ EXTERNAL TO ELEMENT IP

Figure D-1 Volume Integration Scheme for Multi-Lateral Internal Element IP

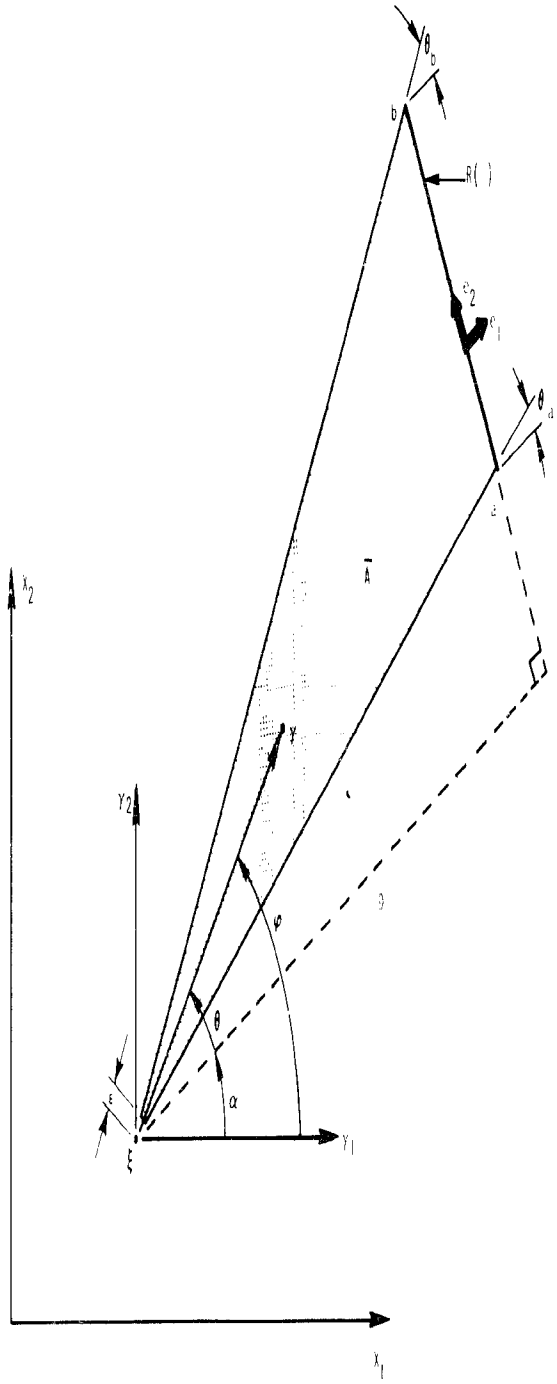

Figure D-2 Notation Used in Evaluation of Volume Integrals

Therefore $$\Sigma_{ijk}(r,\phi) = \frac{C_3}{r}\,\Psi_{ijk}(\phi), \tag{D2}$$

where $\Psi_{ijk}(\phi)$ is a function of ϕ only. Substituting equation (D2) into (D1), and integrating with respect to r yields

$$\Delta\Sigma_{ijk}(\xi,\bar{A}) = \int_{\phi_a}^{\phi_b}\int_{\varepsilon}^{R(\phi)} \frac{C_3}{r}\,\Psi_{ijk}(\phi)\,r\,dr\,d\phi \tag{D3}$$

$$= \int_{\phi_a}^{\phi_b} [C_3\Psi_{ijk}(\phi)r]_{\varepsilon}^{R(\phi)}\,d\phi .$$

Evaluating, and taking the limit as ε goes to zero yields

$$\Delta\Sigma_{ijk}(\xi,\bar{A}) = \int_{\phi_a}^{\phi_b} C_3\Psi_{ijk}(\phi)R(\phi)\,d\phi. \tag{D4}$$

It is now convenient to introduce the notation developed in Appendix A, and cast the integral in terms of the perpendicular distance (D) from the base point ξ to the line segment $\bar{ab}$, and the angle θ between D and the vector r (see Figure D-2). In terms of D and θ

$$\phi = \theta + \alpha$$

$$d\phi = d\theta$$

$$R(\phi) = D/\cos\theta\,,$$

so that
$$\Psi_{ijk}(\phi) = \frac{C_3C4D}{\cos\theta}\,[\cos\theta(\delta_{ij}e_{1k}+\delta_{ik}e_{1j}-\delta_{jk}e_{1i})$$

$$+ \sin\theta(\delta_{ij}e_{2k}+\delta_{ik}e_{2j}-\delta_{jk}e_{2i})$$

$$+ 2C_3[e_{1i}e_{1j}e_{1k}\cos^3\theta + (e_{1i}e_{1j}e_{2k}$$

$$+ e_{2i}e_{1j}e_{1k})\cos^2\theta\sin\theta \qquad (D5)$$

$$+ (e_{ei}e_{2j}e_{1k}+e_{2i}e_{1j}e_{2k}+e_{1k}e_{2j}e_{2k})\sin^2\theta\cos\theta$$

$$+ e_{2i}e_{2j}e_{2k}\sin^3\theta]\,.$$

Substituting equation (D5) into (D4) and integrating yields

$$\Delta\Sigma_{ijk}(\xi,\bar{A}) = C_3C_4D(\delta_{ij}e_{1k}+\delta_{ik}e_{1j}-\delta_{jk}e_{1i})I_{\Sigma1}$$

$$+ C_3C_4D(\delta_{ij}e_{2k}+\delta_{ik}e_{2j}e_{2i})I_{\Sigma2} + C_3De_{1i}e_{1j}e_{1k}I_{\Sigma3}$$

$$+ C_3D(e_{1i}e_{1j}e_{2k}+e_{1i}e_{2j}e_{1k}+e_{2i}e_{1j}e_{1k})I_{\Sigma4} \qquad (D6)$$

$$+ C_3D(e_{2i}e_{2j}e_{1k}+e_{2i}e_{1j}e_{2k}+e_{1i}e_{2j\ 2k})I_{\Sigma5}$$

$$+ C_3De_{2i}e_{2j}e_{2k}I_{\Sigma6}\,,$$

where $I_{\Sigma 1} = (\theta_b - \theta_a)$

$$I_{\Sigma 2} = \log (r_b/r_a)$$

$$I_{\Sigma 3} = (\theta_b - \theta_a) + \sin \theta_b \cos \theta_b - \sin \theta_a \cos \theta_a$$

$$I_{\Sigma 4} = \sin^2\theta_b - \sin^2\theta_a \qquad \text{(D7)}$$

$$I_{\Sigma 5} = (\theta_b - \theta_a) - \sin \theta_b \cos \theta_b + \sin \theta_a \cos \theta_a$$

$$I_{\Sigma 6} = \cos^2\theta_b - \cos^2\theta_a + 2 \log (r_b/r_a) .$$

Finally, the integrated kernel $\Delta\Sigma_{ijk}(N,IP)$ from the boundary node N to the internal element IP is obtained by summation of the integrals (D6) over all four triangles

$$\Delta\Sigma_{ijk}(N,IP) = \Delta\Sigma_{ijk}(\xi_N,\bar{A}) + \Delta\Sigma_{ijk}(\xi_N,\bar{B}) + \Delta\Sigma_{ijk}(\xi_N,\bar{C}) + \Delta\Sigma_{ijk}(\xi_N,\bar{D}) . \qquad \text{(D8)}$$

The most direct means of obtaining the kernel $\Delta E_{\ell ijk}(IP,JP)$ given in equation (3-12) is through term by term differentiation of equation (D6), as follows

$$\Delta E_{\ell ijk}(\xi,\bar{A}) = \frac{\partial}{\partial \xi_\ell} \Delta\Sigma_{ijk}(\xi,\bar{A}) \qquad \text{(D9)}$$

Noting that C_3, C_4, and the direction cosines in (D6) remain constant with respect to ξ, equation (D9) can be written as follows

$$\Delta E_{\ell ijk}(\xi,A) = C_3C_4(\delta_{ij}e_{1k}+\delta_{ik}e_{1j}-\delta_{jk}e_{1i})I_{E1}$$

$$+ C_3C_4(\delta_{ij}e_{2k}+\delta_{ik}e_{2j}-\delta_{jk}e_{2i})I_{E2} + C_3e_{1i}e_{1j}e_{1j}I_{E3}$$

$$+ C_3(e_{1i}e_{1j}e_{2k}+e_{1i}e_{2j}e_{1k}+e_{2k}e_{1j}e_{1k})I_{E4} \qquad \text{(D10)}$$

$$+ C_3(e_{2i}e_{2j}e_{1k}+e_{2i}e_{ij}e_{2k}+e_{1i}e_{2j}e_{2k})I_{E5}$$

$$+ C_3e_{2i}e_{2j}e_{2k}I_{E6} ,$$

where
$$I_{E1} = (\partial D/\partial \xi_\ell)I_{\Sigma 1} + D(\partial I_{\Sigma 1}/\partial \xi_\ell)$$

$$I_{E2} = (\partial D/\partial \xi_\ell)I_{\Sigma 2} + D(\partial I_{\Sigma 2}/\partial \xi_\ell)$$

$$I_{E3} = (\partial D/\partial \xi_\ell)I_{\Sigma 3} + D(\partial I_{\Sigma 3}/\partial \xi_\ell) \qquad \text{(D11)}$$

$$I_{E4} = (\partial D/\partial \xi_\ell)I_{\Sigma 4} + D(\partial I_{\Sigma 4}/\partial \xi_\ell)$$

$$I_{E5} = (\partial D/\partial \xi_\ell)I_{\Sigma 5} + D(\partial I_{\Sigma 5}/\partial \xi_\ell)$$

$$I_{E6} = (\partial D/\partial \xi_\ell)I_{\Sigma 6} + D(\partial I_{\Sigma 6}/\partial \xi_\ell) .$$

Noting that

$$\frac{\partial D}{\partial \xi_\ell} = - e_{1\ell}$$

$$\frac{\partial \theta}{\partial \xi_\ell} \equiv \eta = \frac{\sin\theta\, e_{1\ell} - \cos\theta\, e_{2\ell}}{r} , \qquad \text{(D12)}$$

the derivatives in equations (D11) can be carried out yielding

$$
\begin{aligned}
I_{E1} &= - e_{1\ell}(\theta_b-\theta_a) + (\eta_b-\eta_a) \\
I_{E2} &= - e_{1\ell} \log (r_b/r_a) + \eta_b \tan \eta_b = \eta_a \tan \theta_a \\
I_{E3} &= - e_{1\ell}(\theta_b-\theta_a) - e_{1\ell} \sin \theta_b \cos \theta_b + e_{1\ell} \sin \theta_a \cos \theta_a \\
&\quad + 2\eta_b \cos^2\theta_b = 2\eta_a \cos^2\theta_b \\
I_{E4} &= - e_{1\ell}(\sin^2\theta_b - \sin^2\theta_a) + 2\eta_b \sin \theta_b \cos \theta_b \\
&\quad - 2\eta_a \sin \theta_a \cos \theta_a \\
I_{E5} &= - e_{1\ell}(\theta_b-\theta_a) + e_{1\ell} \sin \theta_b \cos \theta_b - e_{1\ell} \sin \theta_a \cos \theta \\
&\quad + 2\eta_b \sin^2\theta_b - 2\eta_a \sin^2\theta_a \\
I_{E6} &= - e_{1\ell}(\cos^2\theta_b - \cos^2\theta_a) - 2e_{1\ell} \log(r_b/r_a) \\
&\quad + 2\eta_b \sin^2\theta_b \tan \theta_b - 2\eta_a \sin^2\theta_a \tan \theta_a .
\end{aligned}
\tag{D13}
$$

Finally the integrated kernel $\Delta E_{\ell ijk}(IP,JP)$ from the centroid of the internal element IP to the internal element JP can be obtained by summation of the integrals (D10) over all four triangles

$$
\begin{aligned}
\Delta E_{\ell ijk}(IP,JP) &= \Delta E_{\ell ijk}(\xi_{IP},\overline{A}) + \Delta E_{\ell ijk}(\xi_{IP},\overline{B}) \\
&\quad + \Delta E_{\ell ijk}(\xi_{IP},\overline{C}) + \Delta E_{\ell ijk}(\xi_{IP},\overline{D}) .
\end{aligned}
\tag{D14}
$$

APPENDIX E - ELASTO-PLASTIC FLOW RULE

The equations which describe elasto-plastic behavior of the material are developed first in a very general manner following the procedure of [33], and then specific assumptions are made to facilitate the implementation of the approach into a numerical procedure [35]. Basically, the flow rule represents a constitutive relationship between stress and strain which varies as a function of the stress state in the body, but which is assumed to be independent of the time scale of these variations (quasi-static).

Consider a yield function of the form

$$\Phi(\sigma_{ij}) = \kappa(W^p), \tag{E1}$$

where W^p is the plastic work defined by

$$W^p = \int_0^{\varepsilon^p_{ij}} \sigma_{ij} d\varepsilon^p_{ij} , \tag{E2}$$

and σ_{ij} and ε^p_{ij} are the stress and plastic strain tensors. In order for plastic straining to occur

$$\Phi - \kappa = 0,$$

and therefore

$$\frac{d}{dt}(\Phi-\kappa) = \frac{\partial\Phi}{\partial\sigma_{ij}} \dot{\sigma}_{ij} - \frac{d\kappa}{dW^p} \dot{W}^p = 0. \tag{E3}$$

From equation (E2)

$$\dot{W}^p = \sigma_{ij}\dot{\varepsilon}^p_{ij}, \tag{E4}$$

and thus equation (E3) becomes

$$\frac{\partial \Phi}{\partial \sigma_{ij}}\,\sigma_{ij} = \frac{d\kappa}{dW^{(p)}}\,\dot{\sigma}_{ij}\dot{\varepsilon}^p_{ij}\ . \tag{E5}$$

Drucker [37] has hypothesized that the net work performed on a body by an external agent during the application and removal of a set of stresses is zero or positive. The following can be shown to be a consequence of this hypothesis

$$\dot{\varepsilon}^p_{ij} = \lambda\,\frac{\partial \Phi}{\partial \sigma_{ij}}\ , \tag{E6}$$

and introducing the notation

$$\frac{d\kappa}{dW^p} = \kappa'\,, \tag{E7}$$

equation (E5) can be written as follows

$$\frac{\partial \Phi}{\partial \sigma_{ij}}\,\dot{\sigma}_{ij} = \kappa'\sigma_{k\ell}\,\lambda\,\frac{\partial \Phi}{\partial \sigma_{k\ell}}$$

$$\lambda = \frac{\dfrac{\partial \Phi}{\partial \sigma_{ij}}\,\dot{\sigma}_{ij}}{\kappa'\sigma_{k\ell}\dfrac{\partial \Phi}{\partial \sigma_{k\ell}}}\ . \tag{E8}$$

Finally, substituting back into equation (E6) yields a general form of the elasto-plastic flow rule

$$\dot{\varepsilon}_{ij}^{(P)} = \left(\frac{\frac{\partial \Phi}{\partial \sigma_{ij}} \frac{\partial \Phi}{\partial \sigma_{mn}}}{\kappa' \sigma_{k\ell} \frac{\partial \Phi}{\partial \sigma_{k\ell}}} \right) \dot{\sigma}_{mn} . \tag{E9}$$

In order to facilitate the application of equation (E9), assumptions of von Mises yielding and isotropic work hardening can be made as follows

$$\Phi = \sigma_{eq} , \tag{E10}$$

where σ_{eq} is the von Mises equivalent srress given by

$$\sigma_{eq} = \sqrt{3/2 \; S_{ij} S_{ij}} . \tag{E11}$$

S_{ij} is the standard deviatoric stress tensor

$$S_{ij} = \sigma_{ij} - \delta_{ij}(\sigma_{kk}/3). \tag{E12}$$

In conjunction with the above assumptions, κ in equation (E1) can be interpreted as the level of von Mises equivalent stress which will cause continued yielding of the material. Further, defining a von Mises equivalent plastic strain rate

$$\dot{\varepsilon}^p_{eq} = \sqrt{2/3\ \dot{\varepsilon}^p_{ij}\ \dot{\varepsilon}^p_{ij}}\quad , \tag{E13}$$

the plastic work rate can be written as

$$\dot{W}^p = \sigma_{eq}\ \dot{\varepsilon}^p_{eq}, \tag{E14}$$

and substitution into equation (E3) yields

$$\sigma_{eq}\ \dot{\varepsilon}^p_{eq} = \frac{\dot{\sigma}_{ij}\ \partial\Phi/\partial\sigma_{ij}}{\kappa'}\quad . \tag{E15}$$

But $\dot{\sigma}_{ij}\ \partial\Phi/\partial\sigma_{ij} = \dot{\Phi} = \dot{\sigma}_{eq}$, and therefore

$$\kappa' = \frac{1}{\sigma_{eq}}\left(\frac{\dot{\sigma}_{eq}}{\dot{\varepsilon}^p_{eq}}\right) = \left(\frac{1}{\sigma_{eq}}\right) P, \tag{E16}$$

where P is the local plastic modulus or slope of the equivalent stress versus equivalent plastic strain curve. The coefficients in the definitions of equivalent stress and plastic strain (E11 and E13) are conveniently chosen so that P is also the local slope of the uniaxial stress versus uniaxial plastic strain curve from a standard tensile test.

It is easily demonstrated that under the assumption of equation (E10)

$$\frac{\partial \Phi}{\partial \sigma_{ij}} = \frac{3}{2} \frac{S_{ij}}{\sigma_{eq}} , \tag{E17}$$

and substituting equations (E16) and (E17) into the general flow rule (E9) gives a specific form of the flow rule for von Mises yielding and isotropic work hardening

$$\dot{\varepsilon}^{p}_{ij} = \frac{9}{4} \frac{S_{ij} S_{mn}}{P \sigma^2_{eq}} \dot{\sigma}_{mn} . \tag{E18}$$

Noting that the total strain rate is given by the sum of the elastic and plastic strain rates, and applying Hooke's law yields

$$\dot{\varepsilon}_{ij} = \dot{\varepsilon}^{e}_{ij} + \dot{\varepsilon}^{p}_{ij}$$

$$\dot{\varepsilon}_{ij} = \frac{1}{2\mu} \left[\dot{\sigma}_{ij} - \left(\frac{\nu}{1+\nu} \right) \delta_{ij} \dot{\sigma}_{kk} \right] + \frac{9}{4} \frac{S_{ij} S_{mn}}{P \sigma^2_{eq}} \dot{\sigma}_{mn} . \tag{E19}$$

With some manipulation, equation (E19) can be inverted for $\dot{\sigma}_{ij}$ explicitly in terms of $\dot{\varepsilon}_{ij}$

$$\dot{\sigma}_{ij} = 2\mu \left[\dot{\varepsilon}_{ij} + \delta_{ij} \left(\frac{\nu}{1-2\nu} \right) \dot{\varepsilon}_{kk} \right] - \frac{3\mu \, S_{ij} \, S_{mn} \, \dot{\varepsilon}_{mn}}{\sigma^2_{eq} (1+P/3\mu)} , \tag{E20}$$

and finally, substituting equation (E20) back into equation (E18) gives the form of the flow rule desired

$$\dot{\varepsilon}^{p}_{ij} = \frac{3}{2} \frac{S_{ij} \, S_{k\ell} \, \dot{\varepsilon}_{k\ell}}{\sigma^2_{eq} (1+P/3\mu)} . \tag{E21}$$

APPENDIX F - COMPUTER PROGRAM BITEP

The following are input instructions for use of the computer program BITEP, which is capable of solving two dimensional (plane stress or plane strain) elasto-plastic problems using the boundary-integral technique. Many similarities to the elastic program BITE exist, however, there are also some major differences in the input to the two programs. Once again, a full listing of the program is not included for reasons of bulk, but will be provided by the author upon request.

Input Instructions:

Card A - Title
(18A4)

Card B - (14I5)

NNOD	- number of boundary nodes	(MAX = 36)
NSEG	- number of boundary segments	(MAX = 36)
NIPT	- number of internal nodes	(MAX = 100)
NELM	- number of internal elements	(MAX = 36)
NSYM	- number of degress of symmetry	(MAX = 2)
NBC	- number of specified boundary conditions (zero traction assumed for boundary conditions which are not specified)	

Card C - (14I5)

K1
- 0 - plane strain
- 1 - plane stress*

K2
- 0 - stop after this problem
- 1 - continue to next problem

K3
- 0 - default
- 1 - multiple connectivity (input NODE(I,J))

---

* The plane stress option is not yet operational.

K4 { 0 - default
   { 1 - debug printing of matrices

K5 - not used

K6 - not used

K7 - not used

K8 { 0 - default
   { 1 - generate uniform pressure on nodes K9 through K10 { SIG1 in x_1 direction
                                                           { SIG2 in x_2 direction

K9 - node at which pressure generation begins

K10 - node at which pressure generation ends

Card D - (1F10.0)
- Young - Young's Modulus
- PR - Poisson's Ratio
- SIG - not used
- SIG1 - uniform tension in x_1-direction (used only if K8 = 1).
- SIG2 - uniform tension in x_2-direction (used only if K8 = 1).

Cards E - Stress Strain Curve

Card E_1(I5) - NSS - Number of data points

Card E_2(2F10.0) - ((SS(I,J),J=1,2),I=1,NSS)
Stress and corresponding strain from uniaxial stress-strain curve

Cards F - (2F10.0) Node Coordinates: $(x_1(N),x_2(N), N=1,NNOD)$

Cards G - (14I5) Segment Definitions: (NA(M),NB(M),M=1,NSEG)
(used only if K4 = 1).

Cards H - 2F10.0) Internal Node Coords: $(x_{p1}(IP),x_{p2}(IP),IP=1,NIPT)$

Cards I - (14I5) Internal Element Defns: ((NIP(IP,J),J=1,NSGS),IP=1,NELM)
(NSGS is the number of segments used to define each element and must be less than seven)

Cards J - Boundary Conditions: (one set per load step)

Card J_1 - ISTP - load step number
(14I5)[1] NBC - number of boundary conditions for this load step
PCT1 - percentage increase in generated traction in x_1-direction (used only if K8 = 1)
PCT2 - percentage increase in generated traction in x_2 direction (used only if K8 = 1)

Cards J_2- (NOD,(ITYPE(I),BC(I),I=1,3),J=1,NBC)*
(I10,3(I10,F10.0))

TABLE F1 - BOUNDARY CONDITION DEFINITIONS

ITYPE	MEANING
0	TRACTION = 0
1	TRACTION = BC
2	DISPLACEMENT = 0
3	DISPLACEMENT = BC

A flow chart for the computer program BITEP is given in Figure F-1, and the format of the input instructions is illustrated in Figure F-2.

*See Table F1 for definition of terms.

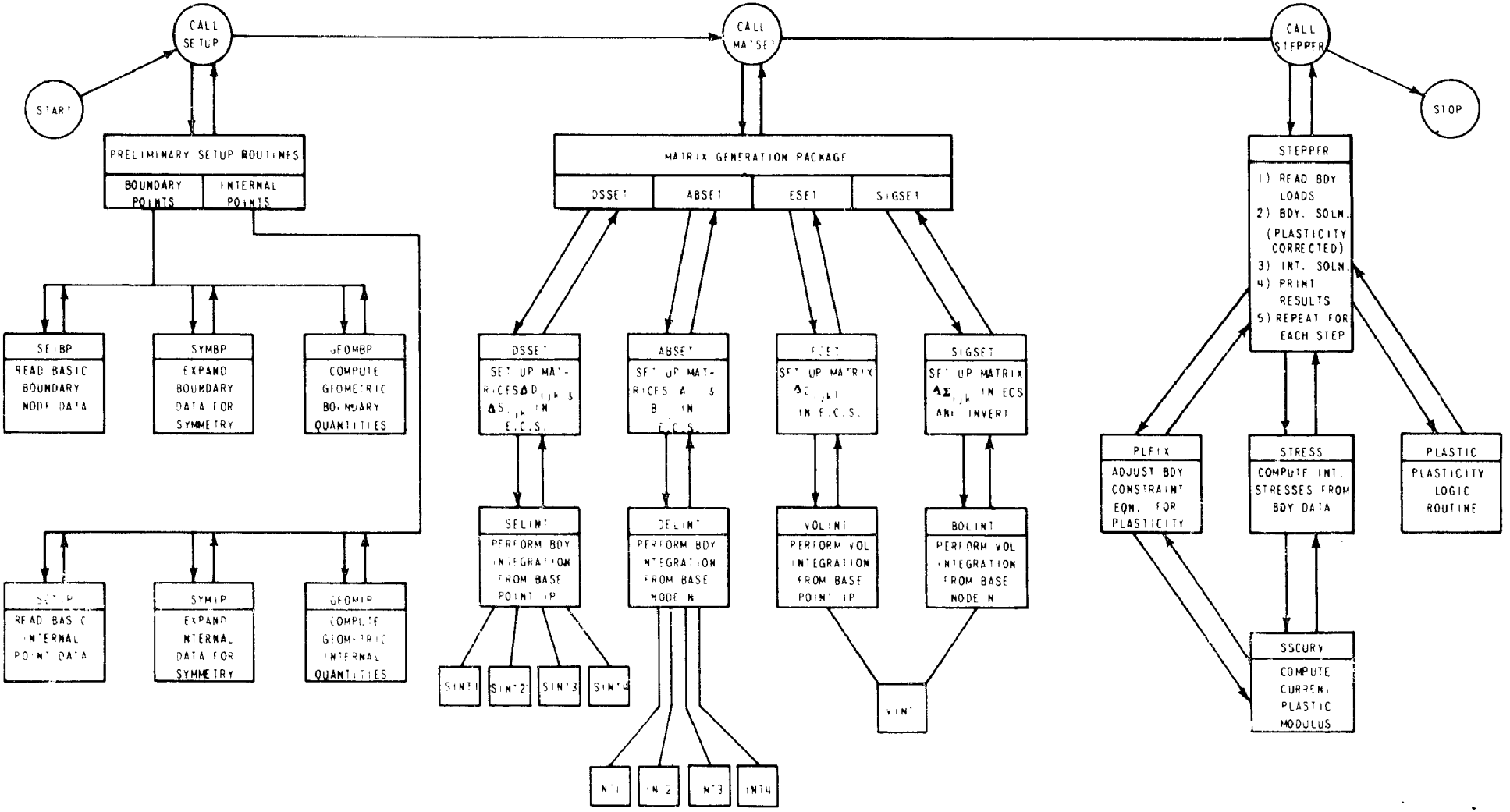

Figure F-1 Flow Chart for Computer Program BITEP

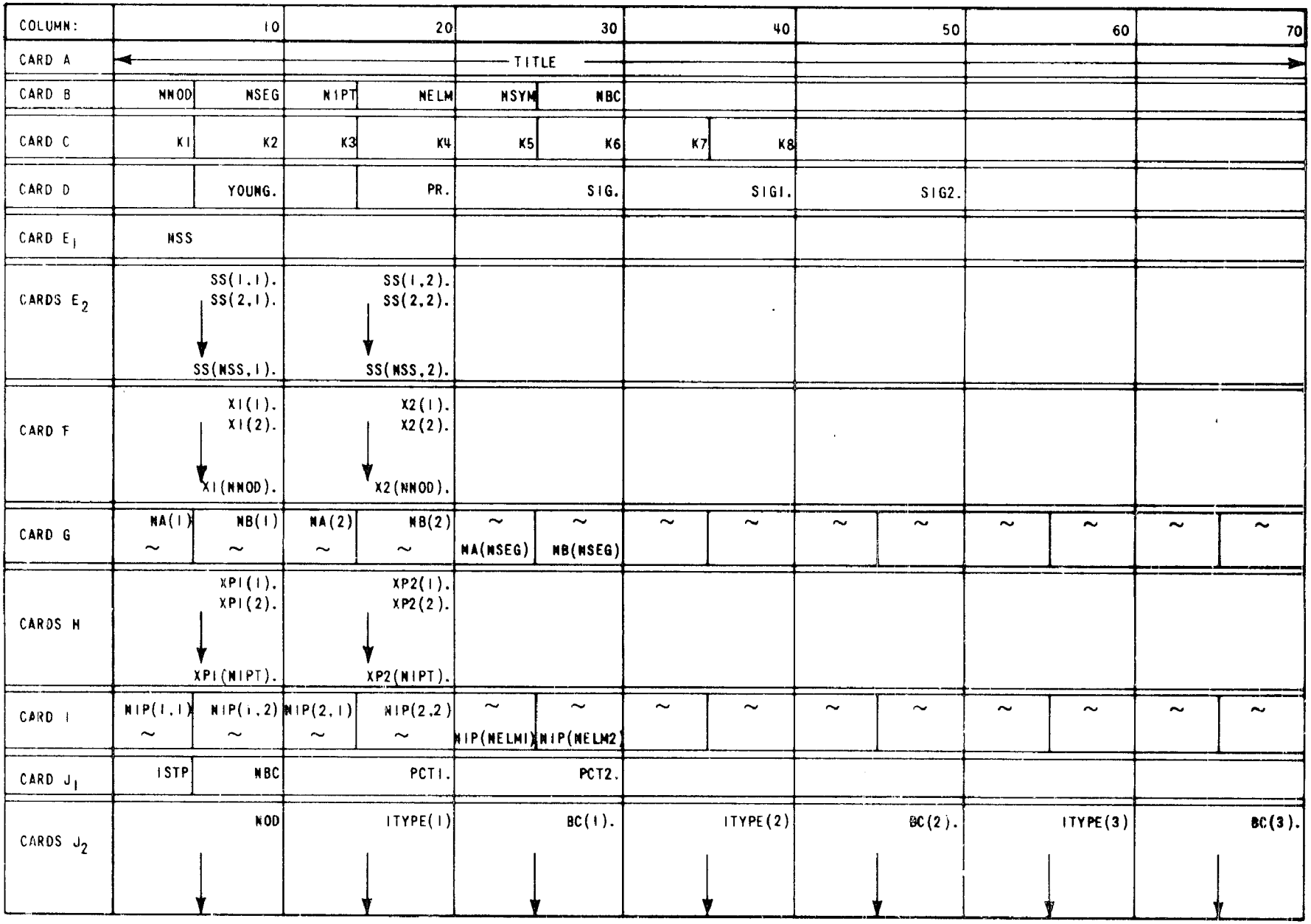

Figure F-2. Illustrated Input Instructions for Computer Program BITEP